

HARI P.N. NAGARAJAN

Development of a Graph-based Metamodelling Framework for Additive Manufacturing and Its Simulation Using Machine Learning

HARI P.N. NAGARAJAN

Development of a Graph-based Metamodelling
Framework for Additive Manufacturing
and Its Simulation Using Machine Learning

ACADEMIC DISSERTATION

To be presented, with the permission of
the Faculty of Engineering and Natural Sciences
of Tampere University,
for public discussion in the Pieni sali 1
of the Festia Building, Korkeakoulunkatu 8, Tampere,
on 1 December 2022, at 8:30 o'clock.

ACADEMIC DISSERTATION

Tampere University, Faculty of Engineering and Natural Sciences
Finland

<i>Responsible supervisor and Custos</i>	Professor Eric Coatanéa Tampere University Finland	
<i>Supervisor</i>	Associate Professor Karl R. Haapala Oregon State University USA	
<i>Pre-examiners</i>	Professor Ian Gibson University of Twente Netherlands	Professor Ola Isaksson Chalmers University Sweden
<i>Opponents</i>	Associate Professor Tom Vaneker University of Twente Netherlands	Professor Ola Isaksson Chalmers University Sweden

The originality of this thesis has been checked using the Turnitin OriginalityCheck service.

Copyright ©2022 Hari Nagarajan

Cover design: Roihu Inc.

ISBN 978-952-03-2675-3 (print)
ISBN 978-952-03-2676-0 (pdf)
ISSN 2489-9860 (print)
ISSN 2490-0028 (pdf)
<http://urn.fi/URN:ISBN:978-952-03-2676-0>



Carbon dioxide emissions from printing Tampere University dissertations have been compensated.

PunaMusta Oy – Yliopistopaino
Joensuu 2022

ACKNOWLEDGEMENTS

I would express my sincere gratitude to my supervisors, Professor Eric Coatanéa and Professor Karl R. Haapala for their support, instruction, supervision, and patience throughout my doctoral studies. Their supervision and encouragement have served as an inspiration in my personal and professional growth.

I would also like to acknowledge my colleagues at the manufacturing laboratory in Finland. Special thanks to Jari Tuominen and Jorma Vihinen for the technical advice. I would also like to forward my deepest gratitude to the administrative officer: Anna Nykänen for their unfailing support and assistance during my doctoral research.

I would like to acknowledge the preliminary examiners Dr. Ian Gibson from Twente University and Professor Ola Isaksson from Chalmers University of Technology for their time and effort they put to provide feedback to improve the manuscript quality.

Finally, yet importantly, my deepest gratitude goes to my parents (R. Rajeswari and N. Nagarajan) and my sister (Mithuna Nagarajan) for their unconditional, limitless love and care from miles away. My warmest thanks go to my close friends for their emotional support: Suraj Panicker, Saigopal Vasudevan, Ahalya Ganesh, Hossein Mokhtarian, Shahriar Bakrani, and Romaric Prod'hon.

Tampere 27. 10. 2022
Hari Nagarajan

ABSTRACT

Modelling and simulation can play a significant role in enhancing the understanding of a complex manufacturing system and its operation. With the advent of Industry 4.0, there is a need to integrate advanced manufacturing processes, e.g., using industrial internet of things (IIoT) technologies, to create manufacturing systems that are not only interconnected, but communicate better and can analyse and use information to drive intelligent action into the physical world. Such progress requires traditional manufacturing paradigms of mass production to move into more complex and diverse production technology domains of mass customization and enhanced product differentiation, modification, and innovation. Additive manufacturing has emerged as a reliable alternative to conventional manufacturing, including subtractive processes, often attributed to its claim for unprecedented design freedom and versatility for the production of highly customized products. However, for successful adoption of additive technologies into mainstream production, modelling and simulation of the manufacturing system in the entirety of its complexity is required to simulate and optimize its design, operation, and use, while achieving desirable production outcomes. At present, models developed to characterize the various activities in an additive manufacturing process take different forms (e.g., analytical, empirical, physics-based, and machine learning models) at varying levels of granularity. Thus, holistic system modelling requires an array of heterogeneous models for characterizing a single additive manufacturing technology. However, the inclusion of different process activities, geometries, and materials makes it a challenge to compose the necessary subsystem-level heterogeneous models into a holistic system model. To address this gap, this research aims to develop a graph-based metamodeling framework for digitally integrating the product design and manufacturing strategies to develop holistic and simulatable multi-domain metamodels. The developed framework supports 1) integration of different forms of knowledge to develop multi-domain metamodels, 2) application of deterministic and probabilistic machine learning approaches to enable simulation of developed metamodels, and 3) predictive analysis and optimization through simulation of the developed metamodels to enable design and manufacturing decision making. This research enables systemic characterization of additive manufacturing process inputs

and outputs using pre-existing knowledge and experimental data. Additive manufacturing process modelling was driven by product design and process data/information, and supported by simulation for decision making. Underpinning models within the research encompass two commercially available additive manufacturing processes. This research demonstrates that the use of data-driven and other approaches that utilize both collected data and pre-existing knowledge can enable the development of accurate and explainable metamodels for close monitoring and control of additive manufacturing to ensure desirable product quality.

TIIVISTELMÄ

Mallinnuksella ja simuloinnilla voi olla merkittävä rooli monimutkaisen valmistusjärjestelmän ja sen toiminnan ymmärtämisen lisäämisessä. Teollisuus 4.0:n myötä on tarpeen integroida kehittyneitä valmistusprosesseja, esimerkiksi käyttämällä esineiden internetin (IIoT) -teknologioita, jotta voidaan luoda valmistusjärjestelmiä, jotka eivät ole vain yhteydessä toisiinsa, mutta kommunikoivat keskenään paremmin sekä pystyvät analysoimaan ja käyttämään informaatiota fyysisen maailmaan sijoittuviin älykkäisiin ohjaus menetelmiin. Tällainen edistys edellyttää perinteisten massatuotannon valmistus paradigmojen siirtymistä monimutkaisempiin ja monipuolisempiin tuotantoteknologia-alueisiin, jotka koskevat massaräätälöintiä ja tehostettua tuotteiden eriyttämistä, modifiointia ja innovaatioita. Ainetta lisäävät valmistus menetelmät ovat nousseet esiin luotettavana vaihtoehdona tavanomaisille tuotantomenetelmille, mukaan lukien ainetta vähentävät menetelmät, johtuen usein kyseisten menetelmien ennennäkemättömistä muotoilun vapauksista ja monipuolisuudesta pitkälle räätälöityjen tuotteiden valmistuksessa. Lisäainevalmistusteknologioiden onnistunut ottaminen käyttöön valtavirran tuotannossa edellyttää kuitenkin lisäaine valmistusjärjestelmän mallintamista ja simulointia kokonaisuudessaan sen muotoilun, toiminnan ja käytön simuloimiseksi ja optimoimiseksi, samalla kun saavutetaan halutut tuotantotulokset. Tällä hetkellä mallit, jotka on kehitetty karakterisoimaan eri toimintoja additiivisessa valmistusprosessissa, saavat eri muotoja (esim. analyttisiä, empiirisiä, fysiikkapohjaisia ja koneoppimismalleja) vaihtelevalla tarkkuudella. Täten, kokonaisvaltainen järjestelmän mallinnus vaatii joukon mallinuksia yksittäisistä lisäainevalmistus teknologioiden karakterisoinneista. Erilaisten prosessitoimintojen, geometrioiden ja materiaalien yhdistäminen tekee kuitenkin haasteelliseksi tarvittavien osajärjestelmätasojen heterogeenisten mallien kokoamisen kokonaisvaltaiseksi järjestelmämalliksi. Tämän puutteen korjaamiseksi, tämän tutkimuksen tavoitteena on kehittää graafipohjainen metamallinnuskehys tuotesuunnittelun ja valmistusstrategioiden integroimiseksi digitaalisesti kokonaisvaltaisten ja simuloitavien monialaisten metamallien kehittämiseksi. Kehitetty viitekehys tukee 1) eri tiedon muotojen integrointia monialaisten metamallien kehittämiseen, 2) determinististen ja todennäköisyyspohjaisten

koneoppimislähestymistapojen soveltamista kehitettyjen metamallien simuloinnin mahdollistamiseksi ja 3) ennustavaa analyysiä ja optimointia simuloimalla kehitettyjä metamalleja, jotta voidaan mahdollistaa suunnittelun ja valmistuksen päätöksenteko. Tämä tutkimus mahdollistaa lisäainevalmistusprosessin syöttö arvojen ja tulosten systeemisen karakterisoinnin olemassa olevan tiedon ja kokeellisen tiedon avulla. Lisäainevalmistusprosessin mallintamista ohjasivat tuotesuunnittelu- ja prosessitiedot, ja sitä tuettiin simulaatiolla päätöksentekoa varten. Tutkimuksen taustalla olevat mallit kattavat kaksi kaupallisesti saatavilla olevaa lisäainevalmistusprosessia. Tämä tutkimus osoittaa, että datalähtöisten ja muiden lähestymistapojen käyttö, joissa hyödynnetään sekä kerättyä dataa että olemassa olevaa tietoa, voi mahdollistaa tarkkojen ja selitettävissä olevien metamallien kehittämisen lisäainevalmistuksen tarkkaan seurantaan ja valvontaan halutun tuotteen laadun varmistamiseksi.

CONTENTS

1	Introduction	17
1.1	Motivation.....	17
1.2	Problem Statement and Research Objective.....	18
1.3	Dissertation Structure	19
2	Background	21
2.1	Additive Manufacturing.....	21
2.2	Relevance of Additive Manufacturing for Functional Part Production	22
2.3	Adoption of Additive Manufacturing for Mainstream Production.....	23
2.3.1	Fused Deposition Modelling.....	24
2.3.1.1	Polymer Extrusion Technology	24
2.3.2	Wire and Arc Additive Manufacturing	26
2.3.2.1	Cold Metal Transfer Welding Technology.....	27
2.3.2.2	Effects of Welding Parameters during Layer-by-Layer Deposition	29
2.4	Process Modelling and Simulation.....	31
2.4.1	Metamodelling Approaches.....	32
2.4.2	Graph-based Visualization to Support Manufacturing Metamodelling	33
2.4.3	Empirical Learning Using Artificial Neural Networks	33
2.4.4	Manufacturing Process Modelling using Artificial Neural Networks	35
2.4.5	Bayesian Networks as a Meta-modelling Strategy	36
2.5	Discussion.....	38
3	Methodology	40
3.1	Graph-Based Metamodelling	40
3.1.1	Graph-based Metamodelling Framework.....	41
3.1.2	Framework Implementation.....	42
3.2	Graph-based Metamodelling Case Studies	49
3.2.1	Application of Graph-based Metamodelling for a Material Extrusion Process	49
3.2.2	Application of Graph-based Modelling for Direct Energy Deposition Processes	51
3.2.2.1	Evaluating Worker Health and Safety in WAAM.....	51
3.2.2.2	Evaluating Dimensional Quality in WAAM	52

	3.2.2.3	Characterizing Microstructure and Mechanical Properties in WAAM	53
	3.2.2.4	Multi-Domain Metamodel for WAAM Product Quality	53
3.3	Discussion		54
	3.3.1	Characteristics and Bounds of the Graph-based Metamodelling Framework.....	55
4	Results and Thesis contribution.....		57
	4.1	Graph-based Metamodelling for a Material Extrusion Process	57
	4.2	Graph-based Metamodelling for a Direct Energy Deposition Process	63
	4.2.1	Worker Health and Safety Impacts in WAAM	63
	4.2.2	Dimensional Quality in WAAM-CMT	66
	4.2.2.1	Experimental Results for Single Bead Geometry in CMT.....	68
	4.2.2.2	Experimental Evaluation of Multi Bead Geometry in CMT.....	70
	4.2.2.3	Discussion.....	73
	4.2.3	Thermal Influence on Microstructure and Mechanical Properties in WAAM-CMT	74
	4.2.4	Holistic Metamodelling of Geometrical and Mechanical Responses in WAAM-CMT	81
	4.3	Usability of the Developed Framework.....	83
5	Conclusions and Future Work		86
6	References.....		89

List of Figures

Figure 1. Dissertation Structure.....	22
Figure 2. Additive Manufacturing Technologies.....	24
Figure 3. FDM Equipment Setup.....	27
Figure 4. WAAM Equipment Setup	28
Figure 5. A function model of a typical WAAM-CMT process	30
Figure 6. Graph-based Metamodelling Framework.....	45
Figure 7. Algorithm for Composing Equations into a Generic Function Representation.....	47
Figure 8. Algorithm for Causal Rule Extraction from Functional Model	50
Figure 9. A Modular KB-ANN Topology of the FDM Process using Graph based Metamodelling Framework	62
Figure 10. A Simplified Modular KB-ANN Topology for the FDM Process using Causal Graph Developed	63
Figure 11. Validation Error Comparison of Fully Connected Classical ANN and KB-ANN.....	64
Figure 12. Graph Model of Operator Health Impacts in WAAM.....	66
Figure 13. Causal Graph Model Summarizing Literature on Single Bead Wire Additive Manufacturing	68
Figure 14. Causal Graph Model Summarizing Literature on Multi-Bead Wire Additive Manufacturing	69
Figure 15. Effect of Input Variables on the Mean Height for a Single Bead Geometry	71
Figure 16. Visualization of the Bayesian Inference for Backward Simulation	74

Figure 17. Schematic of the Deposited Wall with Locations of Temperature Measurement and Mechanical Samples Marked Along Build Direction77

Figure 18. Optical micrographs (25 μm scale) of WAAM built parts using G4Si1 welding wire for M1E1. Micrographs reported along wall height from top to bottom (sample A1, A2, and B). Phases identified: AF – Acicular ferrite, ALF – Allotriomorphic ferrite, WF – Widmanstätten ferrite, and F – Equiaxed ferrite.....78

Figure 19. Optical micrographs (25 μm scale) of WAAM built parts using AM70 welding wire for M2E1. Micrographs reported along wall height from top to bottom (samples A1, A2, and B). Phases identified: AF – Acicular ferrite, and B – Bainite.79

Figure 20. Composite Graph-Based Metamodel Integrating Models for Geometry, Thermal profile, and Microhardness84

Figure 21. a) Model Prediction and Design Space for Microhardness, dash-line represents the region and point of the validation experiments, b) Model Prediction and Design Space for Weld Height, dash-line represents the region and point of the validation experiments, and c) Experimental Validation Results for Microhardness and Weld Height.....84

List of Tables

Table 1. Fundamental Categories of Variables.....	46
Table 2. Colour Coding in Graph Model.....	48
Table 3. Causality for Generic Functions and Bond Graph Organs (Paynter, 1961).....	49
Table 4. Contributions of the Author’s Publications and their Associated Research Tasks	60
Table 5. Weld Parameter Settings, Consumables, and Equipment for Single Bead and Multi-Bead Geometries	70
Table 6. Two-way ANOVA for Single Bead Experiments	72
Table 7. Quality Metrics for the Regression Equation.....	73
Table 8. MREM and AREM Values for the Regression Model.....	75
Table 9. MREM and AREM Values for the Backward Bayesian Model	75
Table 10. Microstructure and Mechanical Property Results for G4Si1 and AM70 Deposits	80

ORIGINAL PUBLICATIONS

- Publication I **H.P.N. Nagarajan**, H. Mokhtarian, H. Jafarian, S. Dimassi, S. Bakrani, A. Hamed, E. Coatanea, G. Wang, and K.R. Haapala, 2018 “Knowledge-Based Design of Artificial Neural Network Topology for Additive Manufacturing Process Modelling: A New Approach and Case Study of Fused Deposition Modelling,” *ASME Journal of Mechanical Design*, Volume 141(2), pp. 021705-12, Dec 2018. <https://doi.org/10.1115/1.4042084>
- Publication II **H.P.N. Nagarajan**, S. Panicker, H. Mokhtarian, E. Coatanea, and K.R. Haapala, “Improving Worker Health and Safety in Wire Arc Additive Manufacturing: A Graph-based Approach,” *Procedia CIRP*, 2020, Proceedings of the 27th CIRP International Conference on Life Cycle Engineering (LCE2020), May 13-15, Grenoble, France. <https://doi.org/10.1016/j.procir.2020.01.116>
- Publication III **H.P.N. Nagarajan**, S. Panicker, H. Mokhtarian, T. Remy-Lorit, E. Coatanea, R. Prod’hon, H. Jafarian, K.R. Haapala, and A. Chakraborti, 2019 “Graph based Meta-modelling to Characterize Cold Metal Transfer Process Performance,” *Smart and Sustainable Manufacturing Systems* 3, no. 2 (2019): 169-189. doi:10.1520/SSMS20190026
- Publication IV S. Panicker, **H.P.N. Nagarajan**, J. Tuominen, M. Patnamsetty, E. Coatanea, and K.R. Haapala, 2022, “Investigation of Thermal Influence on Microstructure and Mechanical Properties in Wire Arc Additive Manufacturing of Steels, *Material Science and Engineering A*, 853 (2022): 143690. <https://doi.org/10.1016/j.msea.2022.143690>

Publication V

H.P.N. Nagarajan, S. Panicker, D. Wu, S. Bakrani, E. Coatanea, and K.R. Haapala, “Modelling the Geometrical and Mechanical Responses in Wire Arc Additive Manufacturing: A Concept for Graph Metamodel based Design Space Exploration. (Prepared and Unpublished)

AUTHOR'S CONTRIBUTIONS

The dissertation includes the scientific observations and results of five (5) publications. The contributions of the author are as follows:

Publication I: The author was the main contributor to this journal article. This paper demonstrates the development of a graph based meta-model using dimensional analysis conceptual modelling in additive manufacturing. The approach presented in the manuscript demonstrates the ability of graph-based modelling to integrate heterogenous models of the different subsystems in an additive manufacturing technology. In addition, the method also demonstrates the ability to apply machine learning approaches such as artificial neural networks to perform predictive model analysis on top of graph metamodels. The manuscript was written and revised by the author. Hossein Mokhtarian assisted in the experimental methodology. Other co-authors provided their feedback on the manuscript.

Publication II: The conference article presents the application of the graph based meta modelling approach for modelling a multi domain output variable, worker health and safety in wire and arc additive manufacturing. The manuscript demonstrated the ability to perform cross functional integration of different forms of knowledge from various science and engineering domains into an integrated system metamodel. In addition, the ability to perform rapid system wide simulation and scenario analysis of the developed meta model through the application of a probabilistic machine learning approach is presented. The manuscript was written and revised by the author. The development of the background section of the manuscript was assisted by Suraj Panicker. The other co-authors provided their feedback.

Publication III: The author was the main contributor to this journal article. This publication presents the application of graph based meta modelling approach to model the dimensional accuracy of a wire and arc additive manufacturing process using cold metal transfer technology. The manuscript demonstrates the ability of graph-based modelling to integrate heterogenous process models into a meta model.

Additionally, a probabilistic machine learning approach using Bayesian Networks is employed on the meta model to allow for fast simulation of the modeled process for process parameter tuning. The manuscript was written and revised by the author. Suraj Panicker and Romaric Prod'hon assisted in the data collection and experimental methodology. Other co-authors provided their feedback on the manuscript.

Publication IV: The journal article presents a material analysis study of wire arc additive manufacturing using steels. Weld thermal properties, microstructure, and resultant mechanical properties were characterized in this experimental study. The manuscript was jointly prepared by the author and Suraj Panicker. Jari Tuominen assisted in the experimental procedure and Madan Patnamsetty assisted in the material analysis. Other co-authors provided their feedback on the manuscript.

Publication V: This publication presents a holistic multidomain metamodel for wire and arc additive manufacturing. The author was responsible for the writing and revision of the manuscript. The validation experiments were jointly performed by Suraj Panicker and the author. Other co-authors provided their feedback on the manuscript.

1 INTRODUCTION

1.1 Motivation

In recent years, major technological advancements in manufacturing (e.g., additive manufacturing (AM), industrial internet of things (IIoT) and cloud computing, nanomanufacturing, and advanced materials) have brought about paradigm shifts in the way products are designed and manufactured. Metal-based AM, in particular, has emerged as an arena that is receiving interest from various technology domains, and from traditional and non-traditional manufacturers. Further, AM research has enabled the growth of innovative techniques and functional products, framing the technology as a feasible alternative to subtractive, forming, and consolidating manufacturing techniques (Bourell, Leu, and Rosen 2009; Abdulhameed et al. 2019).

The favourability of AM as a mainstream manufacturing option is founded on the potential advantages over traditional manufacturing technologies. AM supports design freedom enabling customizable and complex product realization, selective deposition strategies for better material utilization, elimination of tools and fixtures simplifying the product supply chain, and production on demand leading up to distributed manufacturing, cloud manufacturing, and just-in-time manufacturing. These advantages have helped drive AM processes into the mainstream and have generated enthusiasm for future economic and social development (Gibson, Rosen, and Stucker 2015; Bourell, Leu, and Rosen 2009; Altıparmak and Xiao 2021). While AM enables unprecedented versatility and flexibility in part production, industrial practice for their broad integration into production remains conservative and has progressed slowly, with primary applications in specialized industries (e.g., aeronautics/aerospace, medical device production, and custom consumer products) (Frazier 2014; Abdulhameed et al. 2019).

Research focused on the adoption of AM within industry has highlighted close monitoring and control of the production process to ensure repeatable and desirable product quality as a crucial step towards successful technology integration (Vasinonta, Beuth, and Griffith 2001; Craeghs et al. 2011; Bandyopadhyay, Zhang, and Bose 2020; Z. Chen et al. 2022; Abdulhameed et al. 2019). Application of

modelling, simulation, and optimization techniques to product design and process operation can improve reliability and repeatability in AM (Z. Chen et al. 2022). Presently, AM processes tend to function as a one-step solution to product development, wherein several functions are bundled in a single piece of equipment, resulting in a complex multi-physical-chemical-metallurgically dependent system. Thus, modelling the system in the entirety of its complexity is required to simulate and optimize its design, operation, and use, which presents a number of technical and practical challenges.

1.2 Problem Statement and Research Objective

Modelling and simulation can play a significant role in enhancing the understanding of the complex multi-physical-chemical-metallurgical nature of AM technologies. Developing models of the activities/functions of AM systems involves mapping the non-linear interrelationships between the process outputs and the influencing process variables. However, the multidisciplinary nature of the modelling and multi-objective optimization of large systems makes the development and simulation of models time-consuming and expensive. The use of surrogate modelling to develop metamodels for holistic system representation can help reduce the simulation time, but fully data-driven approaches require large volumes of data to consistently provide the level of fidelity required for monitoring and control of multi-criteria manufacturing performance measures. Models developed to represent the various activities/ functions take different forms (e.g., analytical, empirical, physics-based, and machine learning models) at varying levels of granularity. Thus, holistic system modelling requires an array of heterogenous models for a single AM technology. However, the inclusion of different AM process activities/functions, geometries, and materials makes it a challenge to compose the necessary subsystem-level heterogenous models into a holistic system model. Composability and interoperability of individual heterogenous functions becomes increasingly important with the advent of Industry 4.0 where, there is a need to integrate advanced manufacturing processes, e.g., using industrial internet of things (IIoT) technologies, to create manufacturing systems that are not only interconnected, but communicate better and can analyse and use information to drive intelligent action into the physical world. Such progress requires traditional manufacturing paradigms of mass production to move into more complex and diverse production technology

domains of mass customization and enhanced product differentiation, modification, and innovation (Khorasani et al. 2022).

Toward this future vision of advanced manufacturing, the overarching goal of this research is to develop a framework for digitally integrating the product design strategies and data structures (e.g., material data, design data, and process data) through modelling and simulation for different advanced manufacturing technologies. The metamodelling framework supports development of production solutions for enhancing the quality and efficiency of advanced manufacturing systems, with a reasonable cost of simulation and analysis.

The main objectives of this dissertation research are the following:

1. Present a holistic modelling approach that supports integration of different forms of knowledge to develop multi-domain metamodels.
2. Apply deterministic and probabilistic machine learning approaches to enable simulation of developed meta-models for inference.
3. Provide predictive analysis and optimization capabilities to developed metamodels to support design and manufacturing decision making.

The above-mentioned objectives are achieved in this research by addressing the following research questions:

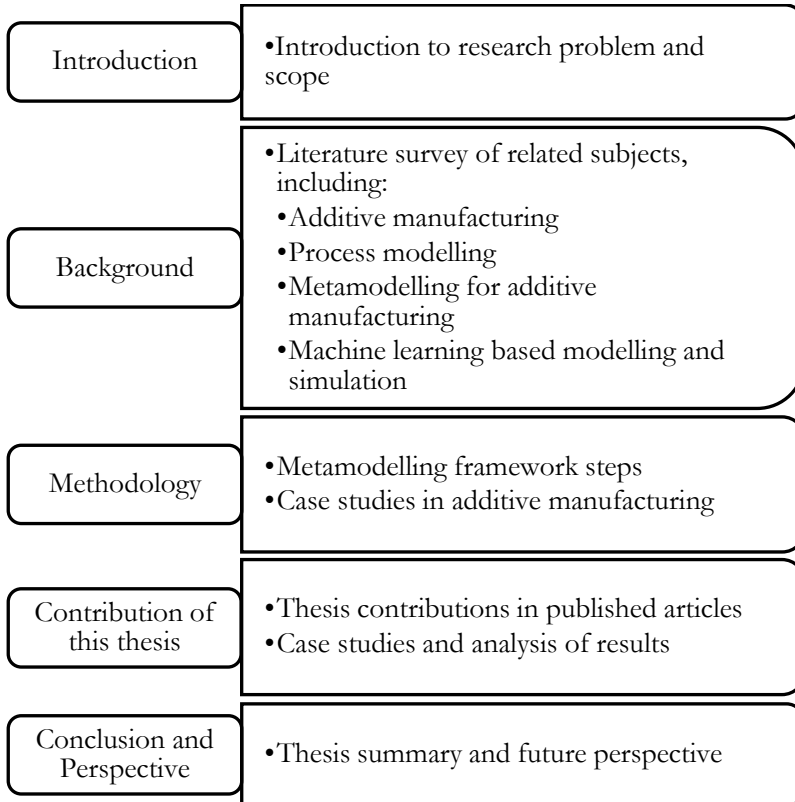
1. How can different types of knowledge at varying levels of granularity (e.g., expert knowledge, product and process data, and prior models) be integrated into a holistic metamodel?
2. How can heterogenous models be combined from different manufacturing science and engineering domains into a holistic metamodel?
3. What type of inferences can be made from the simulation of the developed metamodels?

1.3 Dissertation Structure

The research conducted as part of this dissertation is reported in manuscript format and is composed of five chapters (Figure 1). Chapter one introduces the research including motivation, background, problem statement, objectives, and tasks. Chapter 2 presents a review of existing literature and describes the background on additive manufacturing focusing on process modelling, simulation, and multi-domain multi-objective optimization. Chapter 3 presents the research methodology including modelling and simulation framework and their application to different case studies.

Chapter 4 presents the results and contributions of the dissertation from the published articles. Chapter 5 summarizes and concludes the research. Recommendations for future work are also discussed to improve on findings and carry forward the research. The publications developed as part of this research are presented as a collection at the end of this dissertation.

Figure 1. Dissertation Structure



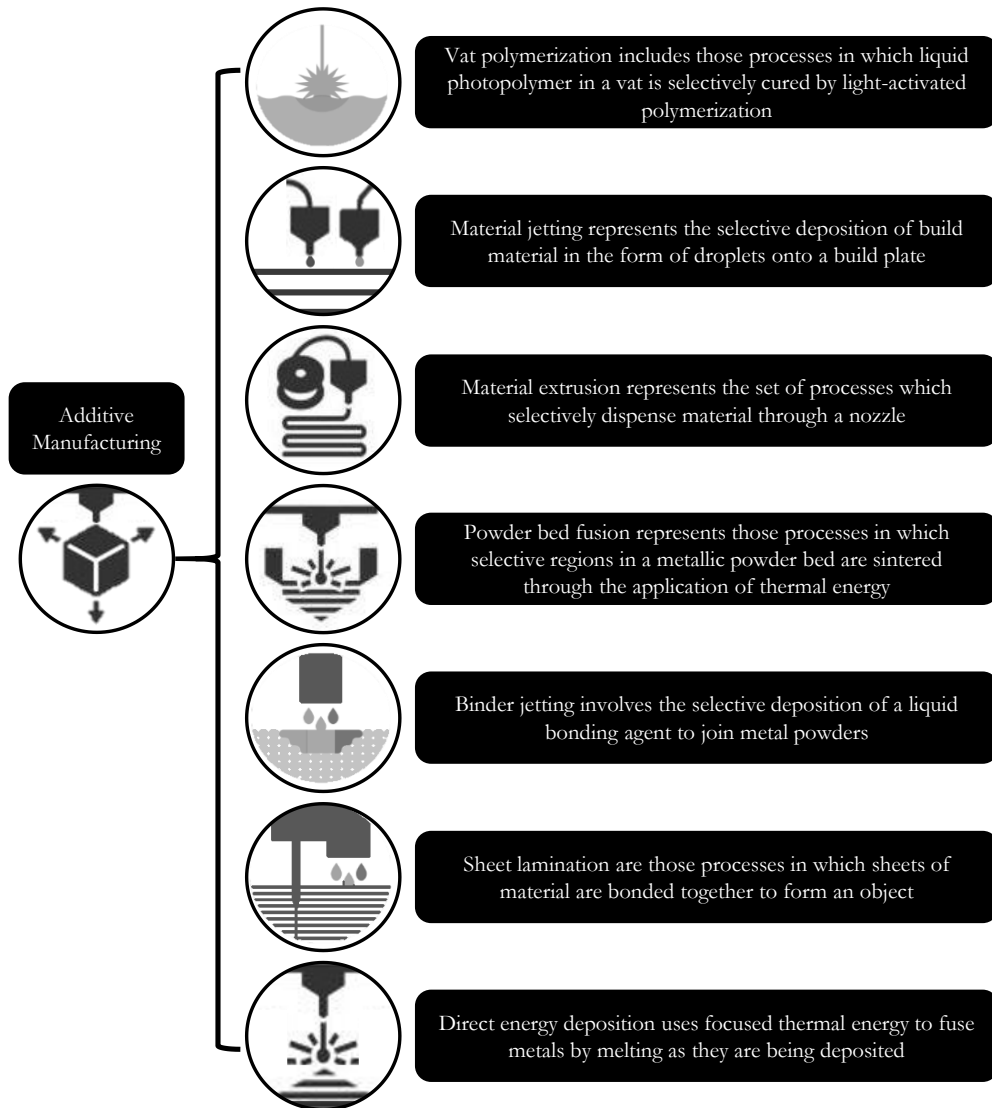
2 BACKGROUND

This chapter briefly introduces the existing literature on which this research is grounded and shows how the research in this dissertation will go beyond the existing knowledge base. This chapter draws from five manuscripts produced as part of this dissertation research.

2.1 Additive Manufacturing

AM is the process of joining materials layer-by-layer using three-dimensional model data (F42.91 Subcommittee 2012). AM systems can utilize a variety of materials such as polymers, paper, ceramic, metal, and composites. Different feedstocks and binding processes are used to form the desired geometry, layer-by-layer, usually by fusing ceramic, polymer, or metal powders through application of heat (e.g., through curing or sintering). ASTM International (F42.91 Subcommittee 2012) defines seven key process types that form the set of AM technologies (Figure 2): (1) Vat photopolymerization, including stereolithography (SL) and digital light processing (DLP); (2) Material jetting, including multi-jet modelling (MJM); (3) Material extrusion, including fused deposition modelling (FDM) and fused filament fabrication (FFF); (4) Powder bed fusion, including electron beam melting (EBM), selective laser sintering (SLS), selective heat sintering (SHS), and direct metal laser sintering (DMLS); (5) Binder jetting, including powder bed and inkjet head 3D printing (PBIH), and plaster-based 3D printing (PP); (6) Sheet lamination, including ultrasonic consolidation (UC) and laminated object manufacturing (LOM); and (7) Directed energy deposition, including wire and arc additive manufacturing (WAAM) and laser metal deposition (LMD).

Figure 2. Additive Manufacturing Technologies (F42.91 Subcommittee 2012)



2.2 Relevance of Additive Manufacturing for Functional Part Production

AM is presented in literature as a strong competitor of traditional manufacturing methods (Bourell, Leu, and Rosen 2009). The growth in popularity of AM is related

to the advantages it provides in terms of material and design freedom to produce unprecedented shapes with high geometric complexity. A key aspect of AM and its future success is its ability to quickly produce parts and components customized to application- or customer-specific needs. The layer-based process allows for the design of almost any geometry, a drastic expansion of the previously constrained design space (Frazier 2014). As introduced above, the benefits that make AM advantageous compared to traditional subtractive and formative processes are compatible with the principles of environmental responsibility, economic growth, and social prosperity (Chan, Manoharan, and Haapala 2017; S. H. Huang et al. 2013; Abdulhameed et al. 2019). These benefits include elimination of tooling, the ability to manufacture complex geometries, optimized product design, increase product functionality, and the selective placement of material only where necessary, which contribute to a reduction in waste and an increase in process efficiency (Gibson, Rosen, and Stucker 2015). It has been shown that the ability to update, repair, and remanufacture tooling presents opportunities for significant reductions in energy consumption, emissions, and costs (Kellens et al. 2017). The optimal design of products can be exploited to increase product performance and add value through embedded functionality. Furthermore, benefits to the supply chain can be realized through the displacement of inefficient and detrimental production processes, improvement of supply chain flexibility, elimination of work-in-process and stock obsolescence, compression of the supply chain, manufacturing closer to the distribution location, and implementation of on-demand (just-in-time) manufacturing (Mashhadi, Esmacilian, and Behdad 2015). AM, therefore, has the potential to impact the life cycle of products directly and indirectly by increasing affordability, longevity, and likability of products and to reduce the burden placed on the environment by manufacturing processes (Nagarajan and Haapala 2017).

2.3 Adoption of Additive Manufacturing for Mainstream Production

Research on AM processes and their integration as a mainstream manufacturing approach has been growing steadily over the years. Currently, AM is used in development of fully functional products in a range of industries such as aerospace, automobile, biomedical, electronics, and consumer product industries (Wohlers et al. 2021; Abdulhameed et al. 2019). However, despite the use of AM in niche applications, successful adoption and integration of AM into production environments is still challenging for businesses (Lavoie and Addis 2018). The

integration of the new technologies in mainstream manufacturing is often limited due to the lack of technical knowledge of AM capabilities, as well as repeatability and reliability issues, and costs incurred by the integration of AM equipment into final production (Z. Chen et al. 2022). Often, the full potential of AM technologies is not leveraged since existing design paradigms have been developed for conventional (e.g., subtractive or for forming) processes (Thompson et al. 2016). In addition, direct application of AM for products designed for existing traditional manufacturing solutions is not economically viable or cost competitive.

To elaborate on adoption and integration issues in AM, let us consider material extrusion technology, such as fused deposition modelling (FDM), and DED, such as wire and arc additive manufacturing (WAAM), which are among the most well researched and most widely used AM processes. A review of these two process technologies and their associated subsystems can provide an overview of the knowledgebase available for the processes as well as to portray the vast differences between the various AM technologies. These unique characteristics as well as differences between AM technologies need to be understood for successfully integrating AM in mainstream manufacturing.

2.3.1 Fused Deposition Modelling

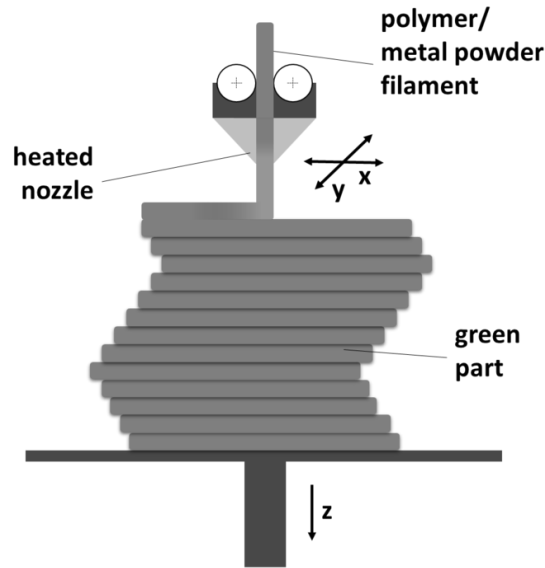
The FDM process (Figure 3) involves successive melting, extrusion, deposition, and solidification of thermoplastic polymer melts (Gibson, Rosen, and Stucker 2015). Typical FDM equipment consists of a material delivery system or extrusion system, heating system, build plate, and filament feeder. The process begins with the generation of layer profile information using a rapid prototyping (RP) software for any given 3D CAD model. The FDM equipment then deposits semiliquid molten polymer beads onto a heated build plate following the layer information provided from the RP software (F42.91 Subcommittee 2012). This process remains a source of innovation; new technologies are being developed using this approach for metal printing using a metal and polymer matrix, for example, see Refs. (X. Wang et al. 2017) and (Rabinovich 2000).

2.3.1.1 Polymer Extrusion Technology

The FDM process involves storage of thermal energy in the molten material, distribution of this energy into the part through a thermal conduction process, and

energy dissipation from the part by convection cooling. The redistribution of the thermal energy ensures the bonding between layers. Several methods exist for thermoplastic delivery in the process, namely, use of liquefiers for self-extruding filament, fluid metering rotary pumps, and high-pressure plunger systems (Batchelder et al. 1994; Hilmas et al. 1996).

Figure 3. FDM Process (“Material Extrusion-Based Additive Manufacturing” 2022)



Furthermore, for FDM parts, the cross section of a deposited layer is shaped through the direct flow of polymer melt between the previous layer and the printing nozzle. This results in shapes having the form of flattened ellipsoids. Since the 1980s, process models have been developed for understanding the complex phenomena taking place in FDM, such as thermal transfer, layer creation, and bonding processes (Bellehumeur et al. 2004; Yardimci et al. 1996). Existing research on FDM modeling has focused on the cooling of single and multiple filaments, thermal behavior of the liquefier, analysis of melt front location, degree of cooling in the nozzle and impact of its design on operational stability, temperature distribution across different part design configurations, and impact of the build file (Batchelder et al. 1994; Yardimci et al. 1996; Atif Yardimci and Güçeri 1996). The vast knowledge about the process available along with the advancements need to be mapped and utilized strategically

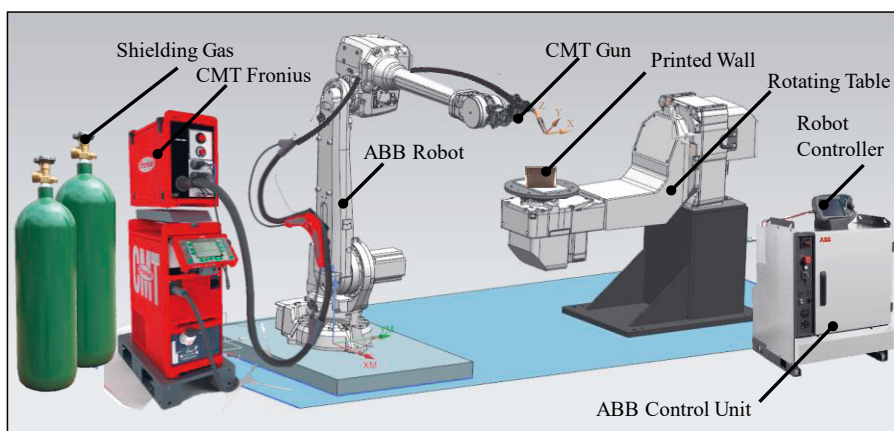
for a successful integration in a production facility to effectively use the technology for functional part production.

Additionally, switching over to a metal additive manufacturing processes can bring its own share of system complexities to untangle to make sense of the information available. For that reason, let's consider a direct energy deposition process such as wire and arc additive manufacturing.

2.3.2 Wire and Arc Additive Manufacturing

WAAM (Figure 4) has gained importance due to its ability to economically fabricate metal products, including those made of aluminium, titanium, and nickel alloys (Ding et al. 2015). WAAM is a DED process classified by ASTM (F42 Committee 2016) that utilizes an electric arc to melt and deposit metal filler wire. WAAM processes have high-energy efficiency (~90%) and high material deposition efficiency; almost 100% of the filler material wire is deposited, resulting in reduced waste and emissions. Furthermore, the process is characterized by a high material deposition rate (up to 2500 cm³/hr) and low equipment cost, making it one of the fastest and most economical metal manufacturing processes (Wu et al. 2018). However, the current capability of WAAM to produce functional metal components is limited due to the relatively low accuracy and quality of the prints.

Figure 4. WAAM Equipment Setup



The high heat input and high material deposition rate, as well as the layer-by-layer deposition of the process, induces residual stresses due to the non-uniform

expansion and contraction of the material. These thermally induced stresses produce distortions in the part that affect part accuracy and part surface quality (Ding et al. 2015; Wu et al. 2018; Sequeira Almeida 2012). To improve weld quality by reducing the high heat input in WAAM, the cold metal transfer (CMT) process was introduced by Fronius (Fronius International GbmH n.d.)

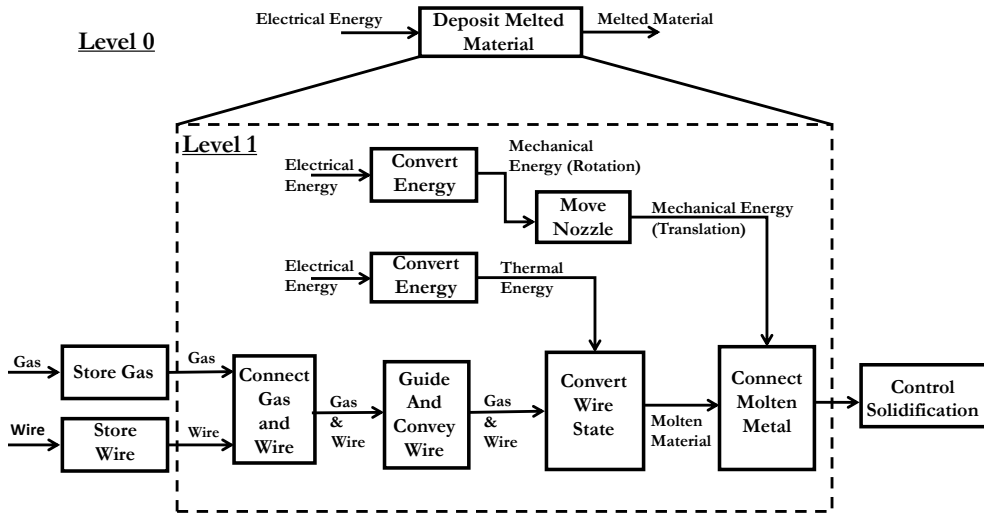
2.3.2.1 Cold Metal Transfer Welding Technology

WAAM has innovated in the metal printing industry with its high material deposition rates and printing speed. However, in WAAM using conventional arc welding, high deposition rates are often associated with very high heat input, unstable arc, and spatter. To overcome these deficiencies, the CMT process uses high-speed digital control to alter the arc length and the thermal input during welding by mechanically feeding and retracting the wire electrode, thereby controlling material transfer to the melt pool (Pickin and Young 2006). For the same amount of material deposited, CMT requires less current compared to pulsed metal inert gas (MIG) welding and generates less heat input to the workpiece. CMT makes it possible to weld certain metals and alloys, such as aluminium, titanium, nickel, steel, and bimetal alloys, which otherwise is difficult using traditional welding processes. The major advantages of CMT are the ability to weld thin-walled structures (a few millimetres in thickness) with greater accuracy, reduced spatter, lower part distortion, improved weld bead characteristics, and higher welding speeds (Välimäki 2017). The functional model of a typical WAAM-CMT process is illustrated in Figure 5.

Thermal deformation and defects in WAAM parts are commonly caused by accumulated heat energy and unstable weld pool dynamics resulting from poor process parameter settings and control (Wu et al. 2018). These defects tend to be material specific; for instance, titanium alloys are prone to oxidation and aluminium alloys often develop porosity, while severe deformations and surface roughness are common in steel alloys and cracks are common in bimetal alloys. Inherent residual stresses in WAAM result in part distortion, loss of geometric tolerance, delamination, and deterioration of fatigue performance and fracture resistance of the part (Wu et al. 2018). Improper selection of process parameters, e.g., welding current, welding voltage, wire feed rate, shielding gas flow rate, and welding temperature, gives rise to residual stresses. Thus, modelling the interrelationships between welding parameters, part mechanical properties, and part dimensional accuracy is essential for meeting the demanding product quality requirements of industry. WAAM

process models also offer an efficient way to reduce the variability induced by the complexity of the process.

Figure 5. Function model of a typical WAAM-CMT process



In CMT process technology, on/off arcing is carried out in three phases, namely, the boost, burn, and short-circuit phases, in order to reduce the overall heat input to the weld (Mezrag, Deschaux-Beaume, and Benachour 2015). The arc is on during the boost and burn phases of the welding cycle, while no current is maintained during the short-circuit phase for metal transfer using the controlled dip transfer mechanism. Metal transfer is carried out by dipping the molten droplet into the weld melt pool and retracting the wire at a specific frequency (50-130 Hz) to force the droplet to detach due to surface tension. The fast retraction movement ensures spatter free welding, since no metal transfer occurs in the gap between the wire and base material (Almeida and Williams 2010). In addition, the heat input to the weld only occurs during the arcing period and detachment of droplets occurs when the process current is switched off (Välämäki 2017).

The CMT welder functions as a closed system with only a small number of principal parameters available for tuning by the operator. The welder employs synergic lines that have been predesigned by the equipment manufacturer (Fronius) for combinations of different filler materials, filler wire diameters, and shielding gases. These synergic lines enable automated control of the voltage and current cycles during welding for the desired wire feed rates in each phase of the CMT process, while also controlling the parameters for wire retraction (Välämäki 2017;

Näkki 2018). In addition to the required wire feed rate, the operator is able to adjust two fine-tuning parameters that modify the synergic line: arc length correction (ALC) and dynamic correction (DC). ALC and DC influence the average power and deposition rate. In addition, ALC influences the bead characteristics, such as bead shape, dilution, and penetration (Sequeira Almeida 2012). Figure 4 illustrates the influencing variables in WAAM-CMT.

2.3.2.2 Effects of Welding Parameters during Layer-by-Layer Deposition

To establish process settings, the user defines the filler wire feed rate and travel speed for industrial robot movement. The wire feed rate governs the deposition rate of the filler material (wire), the working current, and the working voltage based on the synergic line to ensure heat input is sufficient for proper melting of deposited wire [13]. The travel speed also influences the weld deposition rate and is defined in the code that commands the welding robot. Hence, by tuning these parameters, the operator can control the dimensions (width and height) of the weld bead produced. Further, the combination of wire feed rate (WFR) and travel speed (TS) also defines the linear heat input and, consequently, the interpass temperature of each layer before deposition. The linear heat input (Q) is given by Eq. 1 (Näkki 2018):

$$Q = \frac{P}{TS} = k \times \frac{I \times U}{TS} \quad (1)$$

where P is the welding power, k is the process efficiency factor (0.85 for CMT (Pépe et al. 2011)), I is the average current, and U is the average voltage.

The heat input and interpass temperature have a high influence on the melt pool shape and grain structure of the solidified material (Kou 2003). Specifically, the interpass temperature plays a major role in determining the grain structure and, in turn, the mechanical properties of a part produced using WAAM. For instance, a higher interpass temperature generally provides a finer grain structure and improved toughness for high strength steel. However, this trend tends to reverse as interpass temperature exceeds a particular threshold, causing the weld pool to puddle and collapse (X. L. Wang et al. 2017). An unstable melt pool will negatively affect the geometric quality of the weld. Thus, controlling the heating and cooling during welding to maintain a desirable interpass temperature is essential for achieving a high-quality weld.

The dimensionless WFR/TS ratio plays an important role in governing heat input in WAAM; experimental process testing of different materials has shown that relatively precise operational boundaries exist for this ratio. To obtain good dimensional quality in the weld, it is necessary to model the influence of this ratio and to tune the parameters not to exceed its value limits during printing. This dimensionless ratio plays the role of a model invariant, and governs heat input, material deposition, and, ultimately, the bead shape after solidification. This invariant can be rediscovered using dimensional analysis theory [18]. Rather than undertaking a number of experiments, a suitable WFR/TS value can be more easily determined using the conservation of mass between the volume of wire added and deposited weld geometry (G. Barenblatt 1979) (Eq. 2):

$$\frac{WFR}{TS} = \frac{A_{weld}}{A_{wire}} \quad (2)$$

where A_{wire} is the wire cross-sectional area and A_{weld} is the weld cross-sectional area. This dimensionless ratio can be used as supplementary information in modelling the process. For the given wire properties and process parameters, the expected weld cross-sectional area can be determined. This information can help the manufacturing engineer in defining potential welding strategies (e.g., weaving pattern, nozzle travel direction, and wire feed direction) to best achieve the specified weld geometry and quality.

Differences in quality for different metallic materials have been reported for front feeding, back feeding, or side feeding of the wire. In the case of wire laser additive manufacturing (WLAM), (Ding et al. 2015) indicated the wire feed orientation influences droplet transfer and the quality of the deposit. Torch angle, which determines the wire feed orientation, is not well documented as a factor in prior work. Further, in WLAM, the deposition width is mainly determined by the laser power, while the height is influenced by welding speed. The deposition area is determined using the ratio of the wire feed rate to the welding speed. Increasing power for WLAM implies a decrease of the deposition height and an increase of the deposition width. These experimental results could be adopted for WAAM-CMT since power is directly controlled by the wire feed rate through the control algorithm of the predefined synergic lines for different materials.

2.4 Process Modelling and Simulation

Industries adopt new technologies to remain competitive in the marketplace. Effects of new technologies are often uncertain at the outset, and over time new information regarding their capabilities becomes better known. Modelling of new processes and systems must utilize the breadth of knowledge available at the earliest phases to develop models more quickly and efficiently. Pre-existing manufacturing knowledge is available in many different forms and spans across various science and engineering domains due to its multidisciplinary nature, especially for new process technologies (e.g., additive manufacturing). Additionally, simulation of developed models must be flexible to enable the use of new-found knowledge when making predictions.

While additive manufacturing has rapidly grown in popularity, AM systems have not been broadly adopted across manufacturing industry due to large capital (AM equipment, monitoring and control systems, and post processing equipment) and material costs as well as production challenges (Thomas and Gilbert 2014). Crucially, AM technologies function as multi-parameter-dependent processes, which require knowledge of the process physics to dynamically monitor and control the process (Huang et al. 2015; Song and Mazumder 2011; Mazumder et al. 2000). A vast amount of disparate knowledge exists about the various AM technologies as well as their individual subsystems (Witherell et al. 2014a; Pal et al. 2014; Francois et al. 2017; Almeida and Williams 2010; Batchelder et al. 1994; Yardimci and Güçeri 1996; Yardimci et al. 1996).

Though available knowledge for AM technologies provides a set of dispersed sub-models supporting the understanding of localized phenomena, it does not provide a systemic perspective or a system model. Further, the use of high-fidelity models for holistic system simulation would result in many control variables, which may not be suitable for implementation in fast control solutions. Simulation and control are challenging due to the computing requirements for processing large and complex sets of variables. Thus, surrogate modelling for development of meta-models that can integrate different forms of knowledge and models together for holistically representing the AM technology has been gaining traction for system-level simulation, optimization, and control, as discussed below.

2.4.1 Metamodelling Approaches

Several metamodelling approaches such as kriging models, polynomial models, and neural network models exist in literature for modelling complex systems. A meta-modelling approach using machine learning approaches (artificial neural networks (ANNs), Bayesian networks (BNs), etc.) can provide a number of advantages for characterizing AM processes. For example, ANNs enable the development of global predictive models that integrate a variety of parameters and support the implementation of a closed loop control system to improve part quality and process repeatability. In other meta-modelling approaches, such as kriging or Gaussian process regression, modelling is performed as black boxes built over a designed set of experiments. This surrogate approach, like most applied meta-modelling approaches, views the modelled system as a black box. However, the cost of experiments for training black box models can be very high due to the need for large experimental data sets, which can be mitigated by using pre-existing process or system knowledge. Thus, for successful integration of AM in mainstream manufacturing, current efforts must focus on using this untapped knowledge of the process or system, thus, enabling a grey or white box meta-modelling approach. Such approaches differ from classical surrogate modelling methods in the volume of data needed for training models. The need for experimental data sets can be reduced by integrating existing system knowledge available for the observed process into a machine learning model by using knowledge extraction and management (E. Coatanéa et al. 2016; Efthymiou et al. 2015). Additionally, meta-modelling approaches can enable the development of models that reduce the inaccuracies arising from incomplete knowledge. Classical meta-models are often statistical models that represent unknown systems. Meta-modelling focuses on correlating the parametric input/output values, while ignoring the nature of complex inter-relationships within the system. Hence, these approaches do not require detailed knowledge of the underlying physical phenomena (Shao 2007). In place of physical knowledge, the predictability of meta-models relies upon statistical features, such as sampling strategy and modelling algorithms, requiring experimental data.

Depending on the visibility of the internal design, structure, and implementation of the computational models, with increasing opacity they can be classified as white box, grey box, and black box models (Kroll 2000). White box models are transparent, meaning the internal relationships between inputs, physical phenomena, and outputs are known. Black box models are input/output statistical correlation models, where knowledge of internal relationships is unknown. Grey box models combine the

attributes of white box (using pre-existing knowledge to understand system structure, though physical phenomena may be unknown) and black box (statistical data correlation) models to holistically model the system. The use of pre-existing knowledge enables the characterization of the system's internal structure, which can then facilitate the design of experiments to collect only the necessary data for modelling the unknown aspects of the system. However, directly characterizing a system's structure from pre-existing knowledge can be a challenge, since knowledge such as data and models are present in multiple forms and lack interoperability (Witherell et al. 2014a). For this reason, a framework is needed to translate different forms of knowledge into a compatible, unified structure that supports simulation and optimization. This framework will help clarify the parametric relationships that describe the system, which are necessary for building a grey box modelling approach.

2.4.2 Graph-based Visualization to Support Manufacturing Metamodelling

Graph-based visualization of a system in the form of directed graphs, input-output graphs, or causal graphs unifies system knowledge (e.g., data and mathematical relationships) and provides a foundation for building metamodels of manufacturing systems at different levels of abstraction (e.g., a process or set of processes) (Borutzky 2011). These metamodels can be constructed by integrating subsystem models of varying fidelity, i.e., representing pre-existing knowledge as known physical/chemical relationships and unknown relationships using machine learning and other empirical approaches (e.g., ANNs or Bayesian networks (BNs)). A causal graph that characterizes the explainable cause-and-effect relationships within the system of interest can serve as a basis for developing a dynamic model, which can support simulation and enable prediction, monitoring, and control of the modelled system. The dynamic nature of the system can be characterized by employing empirical approaches to the unified graph-based representation. The key advantages of using graphs in this research are 1) integration and composability of pre-existing knowledge, 2) establishing a causal ordering with directed graphs, and 3) topology design for ANN and BN development as explained below in the next sections.

2.4.3 Empirical Learning Using Artificial Neural Networks

Empirical learning techniques, including machine learning methods, usually require little theoretical knowledge about the problem domain to derive generalized models

from available data. This advantage of modelling with little theoretical knowledge of the domain is offset by the need for large training data sets. For example, ANNs have proven to be equal, or superior, to other empirical learning systems over a wide range of domains, when evaluated in terms of their generalization ability (Shavlik, Mooney, and Towell 1991; Atlas et al. 1990). ANNs are usually comprised of layers (k) with nodes (j), where each node sums up i weighted outputs of the nodes from the previous layer as per Eq. 3

$$s_{j,k} = \sum_i w_{ij,k} x_{i,k-1} + w_{0,k} \quad (3)$$

Here, $s_{j,k}$ represents the weighted sum of node j at layer k , w_{ij} represents the weight of the i^{th} output at node j , $w_{0,k}$ represents the initial weight of layer k at the first node. This summation of $s_{j,k}$ is then passed through a non-linear activation function, the output of which acts as input for the next layer. A common choice for the activation function is the sigmoid function, also called the continuous unit step function (Eq. 4).

$$h(s_{j,k}) = \frac{1}{1 + \exp(-s_{j,k})} \quad (4)$$

The computational power attributed to ANNs originates from the non-linear functions of the weighted sums, $h(s_{j,k})$. However, the non-linearity also makes it difficult to mathematically analyze these networks and requires a large set of training data to capture the desired relationship. In ANNs, a state p_i of a neural network can be uniquely described by $\{w_1 \dots w_n\}_p$, where w_i represents a weight within the network. During the training process, the network iteratively traverses a subset of the state space p , continuously improving the model performance. The total number of states p and the total number of weights n of an ANN can be reduced by incorporating prior knowledge about the system, which can increase the efficiency of the model while reducing the computational cost (Tu 1996).

The initial weights allocated to the network nodes impacts the learning efficiency of ANNs (Ahmad and Tesauro 1989), and is the central source of the well-known vanishing gradient problem associated with ANNs (Hochreiter et al. 2001). This problem is present when training ANNs with gradient-based learning methods and backpropagation. According to (Hochreiter et al. 2001), in such methods, each of the ANN's weights receives an update proportional to the gradient of the error function with respect to the current weight, in each iteration of training. In some cases, the gradient will be vanishingly small, preventing the weight from changing its value. In the worst case, this may completely stop the ANN from training. This

problem is more probable when too many hidden layers of neurons are used in an ANN. Heuristic rule can be used to constrain the potential size of an ANN (Panchal et al. 2011). However, this implies the design of ANNs must reduce the number of inputs, number of outputs, size of hidden layers, and number of hidden layers.

2.4.4 Manufacturing Process Modelling using Artificial Neural Networks

ANNs as a modelling strategy have been widely used to approximate complex functions. In this context, they can be considered a metamodeling approach (Papadrakakis, Lagaros, and Tsompanakis 1998; Varadarajan, Chen, and Pelka 2000; Atashkari et al. 2007; Magnier and Haghghat 2010). ANNs are utilized in numerous domains and form the backbone of deep learning algorithms. ANNs are utilized in process modelling for forecasting output variables using numerous architectures and training algorithms. ANNs, with the assistance of data standardization, data pre-processing, and model performance optimization, have become a key enabler in modelling different manufacturing processes. The main advantages of ANNs compared to other process modelling approaches have been reported as: (i) the ability to handle noisy and ambiguous data, (ii) a lower difficulty of implementation than other approaches, (iii) the suitability for accurate representation of dynamic problems, and (iv) the ability to provide novel solutions for complex systems inputs-outputs (Dawson and Wilby 2001). However, it is only possible to perform black box modelling using classical ANNs. Hence, limited information about the hidden layers and relations between the layers is known. Such empirical modelling can result in model overfitting as explained in the previous section (Tu 1996). In addition, ANNs require large number of experimental tests for training, which demands high computational costs to reach an acceptable model fit. Thus, in addition to model compactness, research must be focused on designing ANN architectures that are more transparent and require less computation to improve cost-effectiveness.

The architecture of an ANN is problem-dependent, and requires extra training to explore and progressively generate a suitable architecture via the weights allocated to each of the nodes within an ANN. ANN models tend to be difficult to interpret, which has led the technique to lose its lustre as a metamodeling approach (G. G. Wang and Shan 2006). The reliability of ANNs for process modelling can be challenged when there is limited training data available or if the training data is subject to large variability due to the complexity of the modelled system. Deep learning approaches can overcome the challenges of modelling large, complex

systems, but the duration of training can be extremely long (up to several years) and costly (G. G. Wang and Shan 2006; Schmidhuber 2015; Bengio, Goodfellow, and Courville 2015). In addition, the topology (architecture) of an ANN must be specified before the training; thus, available system knowledge can be considered in the design of a network's topology.

ANNs are an effective empirical method for characterizing the non-linear interactions between variables of a complex manufacturing system as explained above. However, for large modelling problems (number of variables to model > 20), the deterministic nature of the approach may lead to poor model accuracy (lack of ANN generalization due to overfitting for small datasets) and low model transparency (black box nature of ANNs) especially in a complex manufacturing setting with competing performance objectives. Thus, probabilistic machine learning was investigated to overcome model size limitation and improve model transparency. Specifically, the use of Bayesian networks are investigated as explained next.

2.4.5 Bayesian Networks as a Meta-modelling Strategy

Bayes' theorem describes the probability of occurrence of an event based on the prior knowledge of conditions that might have some relation to the event (Nielsen and Jensen 2009). A BN uses this Bayesian inference (Eq. 6) to assign and update probabilities for a hypothesis as it is exposed to more evidence or information.

$$P(U) = \prod_i P(V_i | pa(V_i)) \quad (6)$$

In Eq. 6, $P(U)$ represents the joint probability of the network, and $pa(V_i)$ is the set of parent nodes for variable V_i .

A BN is often used as an inference tool, which can use available information from a subset of variables in a system to predict the behaviour of other parts of the same system (Nielsen and Jensen 2009). In recent times, BNs have been employed in various disciplines such as engineering, natural sciences, medicine, sports, and economics, largely due to their advantages, as explained by Heckerman (Heckerman, Geiger, and Chickering 1995): 1) ability to handle incomplete datasets by encoding statistical dependencies between the variables, 2) ability to learn causal relationships between the variables within a system to perform interventions and investigate

predicted results, and 3) ability to model domain knowledge and data simultaneously, making it a sophisticated package for data analysis.

A BN uses directed acyclic graphs (DAGs) to represent the dependencies within a system (comprising all the variables). Each variable is represented as a node in the BN. The type of node (e.g., parent, child, or constraint node) to be used is determined based on the type of variable to be modelled. The dependency between variables are represented by arcs (unidirectional arrows) connecting the respective nodes. Parent nodes feed dependencies into the dependent child nodes, forming a hierarchy of decisions. Based on the dependencies between different variables, their joint probability distribution can be factorized into a set of conditional and marginal probability tables. The network uses these probability tables at each node to make inferences during simulations (Koller et al. 2007).

The use of BNs to model and simulate solutions can enable fast design exploration opportunities with good data visualization for engineers. BNs can provide an accurate representation of the design space with limited computational expense by learning representative network structures from data and pre-existing knowledge. In comparison to function-oriented methods and resampling methods, BN modelling is progressive, i.e., the graph-based approach to develop the network enables the combination of multi-disciplinary models, knowledge, and data by providing a global and intuitive view of dependencies. Thus, the user can model the system using both quantitative and qualitative data. Data can be directly used to identify interrelationships between nodes in a BN during the graph generation using supervised and unsupervised learning algorithms such as Tabu, Maximum Spanning Tree, Naïve Bayes, Markov Blanket, to name a few (Aliferis et al. 2010; Tsamardinos et al. 2003; S. Chen et al. 2020; Monma et al. 1990; Asano et al. 1988; de Werra and Hertz 1989). Alternately, knowing the interactions between variables from expert knowledge or the literature, this information can be fed to the network in the form of connections (arcs) between nodes, as well as the conditional probabilities between variables. Furthermore, any new data or knowledge can be seamlessly integrated into the model at any stage of model development without difficulty. It is important to note that any existing data or knowledge can be excluded from the model without affecting the other elements of the model. BNs intrinsically enable the integration of data- or knowledge-related uncertainty to the model. This allows for the determination of confidence levels linked to the feasibility of identified solutions. Thus, product/process performance estimations and filtering of solutions based on thresholds can be performed easily. The above-mentioned advantages of BN have made it an attractive option for complex manufacturing process modelling and

simulation (Pradhan et al. 2007; Jing et al. 2021; Jones et al. 2010; Lewis and Ransing 1997).

2.5 Discussion

Many of the products we use every day are multi-component integrations that require an array of multi-disciplinary and multi-granular approaches during product development to combine and compare multiple numerical solutions. For such complex problems, engineering intuition cannot always be relied upon for making accurate design and manufacturing decisions. Thus, characterizing product and process performance through modelling is warranted. However, the multidisciplinary nature of the modelling and multi-objective optimization of large systems make the development and simulation of models time-consuming and expensive. The continuous advancement of information technology is increasing the efficiency and accuracy of computational tools such as finite element analysis (FEA) and computational fluid dynamics (CFD) to run complex simulations. Currently, high fidelity simulation results also serve as accurate data for development of surrogate and graph models. Depending on the length-scale (micro, meso- or macro scale) as well as type of finite element model (multi-physics, pure conduction model, thermo-mechanical, and thermo-metallurgical), the accuracy and computation time might vary (Bayat et al. 2021). However, despite these advancements, simulating large, complex system models with high precision remain highly time-consuming, and iteration of simulations becomes difficult (Schoinochoritis, Chantzis, and Salonitis 2017; G. G. Wang and Shan 2006).

The use of surrogate modelling to develop metamodels for holistic system representation can help reduce the simulation time, but fully data-driven approaches do not consistently provide the level of fidelity required for monitoring and control of multi-criteria manufacturing performance measures. In addition, during conceptual design, product/process engineers tend to rely on their experience and knowledge, as quantitative data about the product is either unknown or uncertain. Such design problems present multifunctional, multidimensional, and multimodal responses at different levels of scale, which make it difficult for traditional optimization algorithms to effectively search the design space. Thus, there is a need for modelling frameworks to incorporate a variety of data driven and other

approaches which utilize both collected data and pre-existing knowledge to build accurate and explainable metamodels.

The review of existing literature on AM process modelling approaches presented above forms the basis for the graph-based metamodeling framework developed in this research. The developed framework utilizes pre-existing knowledge and data to develop graph-based representations, which act as a pre-cursor for machine learning approaches to build a holistic metamodel for simulation. A detailed description of the developed framework and its functional elements are next documented in the methodology section of this dissertation next.

3 METHODOLOGY

This chapter introduces the graph-based metamodelling approach developed in this research. The theoretical backgrounds of the processes, methods, tools, and techniques used in the research have been presented in the background section. The use of graph models in simulation for parameter prediction, design space exploration, and optimization are presented. The capabilities of graph modelling and simulation are demonstrated for two additive manufacturing processes: fused deposition modelling, and wire and arc additive manufacturing.

3.1 Graph-Based Metamodelling

The graph-based metamodelling approach presented in this section focusses on the development of input-output causal graphs or knowledge graphs representing the interactions between the different variables of a system of interest. At its core, the knowledge or causal graph only models the input-output relationship and does not explain on the inner workings of the system of interest. Thus, the graphical model can be envisioned as a type of surrogate modelling approach. The main attribute of this approach is determining the directional causality between the variables of the system. Causality in the physical world can be explained as the mechanisms that result in phenomena. For example, let us consider the stem of a bicycle as a mechanism; the phenomena are then the movements of objects connected to this mechanism (i.e., the handlebar and the front wheel). The stem serves as the linkage that transfers the movement of the handlebar (input action) to the movement of the front wheel (output phenomenon). However, it is important to note that causal relations are in fact not symmetric and do not correspond to linkage of moving bodies alone (Filippo et al. 1991). For example, let us consider an example of a part printed using WAAM. The phenomena are the heating and cooling of the part and the resultant mechanical properties. The link that connects these phenomena is the mechanism of microstructural evolution of the printed material. In mathematical terms, these two phenomena are represented as the variables and their related

equations that the mechanism links. However, the mathematical function representing the microstructural evolution defines a symmetrical linkage between the phenomena (variables) and mechanism (function) wherein any one of the variables can be represented as dependent, while the others are independent. Such a representation is a functional linkage as opposed to a causal linkage; hence, additional assumptions must be made to assign a causal ordering (Iwasaki and Simon 1994; A. Simon and Iwasaki 1988).

Intuitively, we can assign a temporal order to these events in WAAM, wherein the temperature profile of the part results in microstructural evolution, which jointly affect the resultant mechanical properties. Such a temporal representation allows for defining the order and, in turn, the direction in which the dependency between variables flow in the system. Simultaneously, when representing an input-output relationship for surrogate modelling, a predefined directional dependency of the variables is established in the training dataset. Here, the performance variables, or outputs of the system, and the inputs that influence these outputs are clearly defined. Though the relationships between the variables cannot be directly linked to causality in its traditional meaning, the directional flow of variable dependencies provides a strong basis for a causal relationship in the direction of the flow determined by the modeler. Thus, graphical models present a promising avenue for characterizing the linkages between a mechanism and resultant phenomena and provide more model transparency than data-driven surrogate modelling approaches.

3.1.1 Graph-based Metamodelling Framework

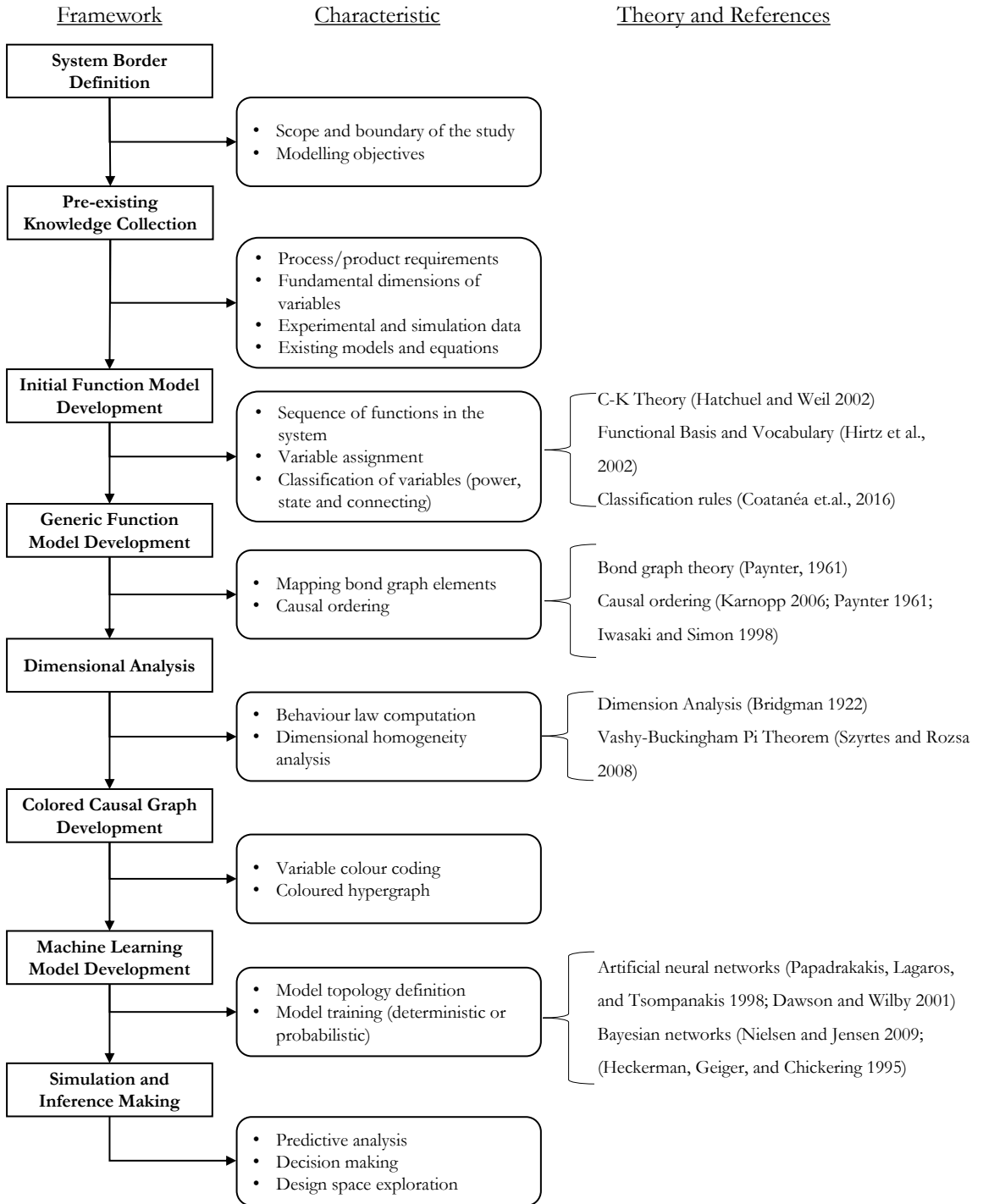
The graph-based metamodelling framework developed in this research uses knowledge in the form of functional and non-functional design requirements and collected data to model the system of interest in the form of a directed knowledge graph. The directed knowledge graph represents the relationships between the variables of the system and enables qualitative and quantitative design/system analysis using simulation. The approach starts with the definition of a system boundary and modelling objectives followed by the collection of available knowledge about the system of interest. A functional model is developed for the system of interest based on the available knowledge, which is then translated into graphical elements to build the graph metamodel. A detailed description of the framework implementation is presented next, and summarized graphically in Figure 6.

3.1.2 Framework Implementation

The metamodelling framework developed in this research enables the extraction and encoding of knowledge associated with system architectures, equations, data, and units of measure. Figure 6 visualizes the sequential steps in the metamodelling framework; this iterative process ends when a computable model of the system of interest is available with the required level of detail. As noted above, modelling starts with the definition of a system boundary and modelling objectives. Next, the available knowledge about the system of interest is documented and collected from various sources. For example, market research provides an enterprise with the information of essential and non-essential requirements of a new design. This information combined with expert knowledge about the design helps designers to determine the functional requirements of the system of interest. The architectural knowledge of a system in the form of a functional decomposition can be further broken down into the units of measurements used for the variables, and their decomposition into fundamental dimensional blocks (mass, length, and time) to be used as initial knowledge. Similarly, experiments and computational studies are often key sources of process and product data which can be used to fit equations. Product use and service data collected through observation, manual measurement, and/or automated sensing technology may also be used to compliment the process and product data from experiments/computations. Thus, in the developed framework, the functional requirements of the design as well as the collected data/equations are termed as available knowledge and are used for system modelling.

After aggregating the available knowledge, it is synthesized into a functional representation/model, i.e., the sequence of functions that describe the behaviour of the observed system. Depending on the available knowledge, two types of functional models can be developed namely, an initial function model or a generic function model. The initial function model development is followed when the available knowledge about a system is in the form of design requirements or data. A generic function model is developed when the available knowledge is in the form of existing models or equations describing the performance of the system of interest. Functions present abstractions of a system's activities by relating the inputs and outputs for an intended purpose. They enable analysis of complex systems through the decomposition of a system into its components performing the functions. Development of a functional model requires defining the purpose of the model, required detail and availability of the knowledge and equations prior to the modeling process.

Figure 6. Graph-based metamodeling framework



For developing a function model, the overall functionality of the system is decomposed into the sequence of functions interacting with each other. Functions are represented with verbs of actions in boxes and are connected to each other with arrows that indicate the sequence of occurrence. Function model development is followed by assignment of variables associated with the function, guided by the fundamental categories presented in Table 1. The power variables (including flow and effort) are attributed to the arrows that connect functions and the state variables are assigned inside function boxes. Following the development of a functional representation/model, the dimensional analysis conceptual modelling (DACM) framework is used to transform the initial functional model into a generic functional model formed around a limited set of fundamental functions using the causal rules extracted from bond graph theory (Hirtz et al. 2002; Karnopp, Margolis, and Rosemberg 2000; Shim 2002). It is important to note that the generic function model is directly developed when the knowledge about a system is available as equations. Figure 7 presents an algorithm to compose equations into a generic function model. Next, dimensional analysis (DA) is applied to each node of the graph to form behavioural equations (G. I. Barenblatt 1987). A colour pattern is applied to different variables to highlight their design nature as shown in Table 2.

Table 1. Fundamental categories of variables

Fundamental variable category	Secondary variable category
System variable	Energy
	Efficiency rate
Power variable	Generalized effort
	Generalized flow
State variable	Generalized displacement
	Generalized momentum
	Connecting variables

Generic functions represented by Bond graph organs (elements) are used as intermediates between the initial functional models and the final graph model (Shim

2002; Karnopp, Margolis, and Rosemberg 2000). To facilitate the systematic assignment of variables to the generic functional representation, all variables are classified into five generalized categories, namely, flow, effort, momentum, displacement, and connecting (Eric Coatanéa 2005). While the connections between input and output variables may be known, the causal nature of these connections must be represented mathematically. The sequence of functions in the functional model provides initial insight into the global causality. Mapping these functions to the generic bond graph organs enables the evaluation of the causality among the variables characterizing those functions. The causal relationship among variables for generic functional models is built upon the existing validated causal rules in Bond graph theory (Paynter 1961).

Figure 7. Algorithm for composing equations into a generic function representation

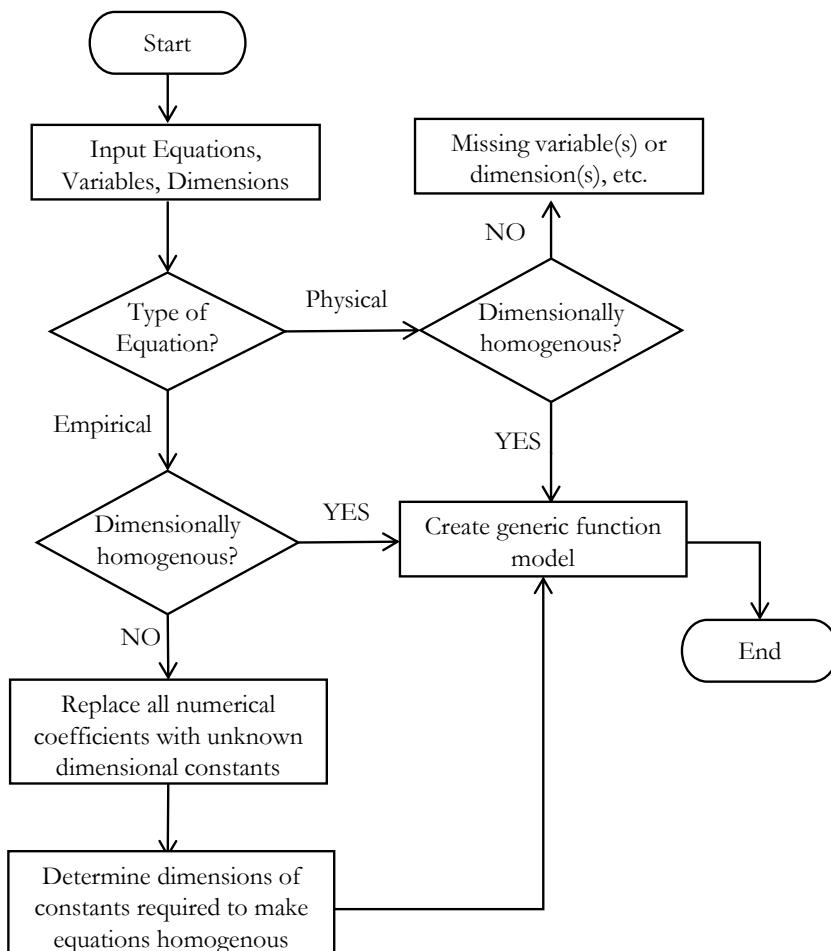


Table 3 summarizes the causal rules (bond graph organs) used in the modelling approach. The cause-effect relationship is not only dependent on the sequence of functions, but also dependent on the nature of the bond graph organ and the type of the assigned variables.

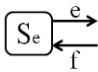
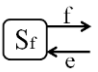
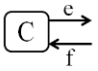
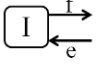
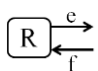
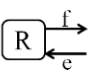
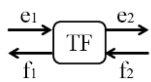
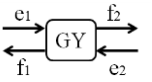
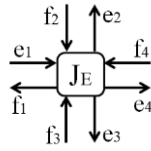
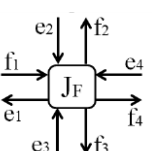
Table 2. Colour coding in graph models

Type of variable	Description and colour coding
Exogenous variables	Grey/Black – Variables associated with the system’s environment. These are imposed on the modeller and have fixed values.
Independent variables	Green – Variables of the system that are not influenced by other variables. Values are not fixed.
Dependent variables	Blue – Variables of the system that are influenced by other exogenous and independent variables. Values are determined based on their interrelationship with other variables of the system.
Performance/output variables	Red – Dependent variables that characterize different performance attributes of the system. These variables are defined by the modeller based on their objectives.

Figure 8 represents a causal extraction algorithm used to automate the modelling process. First, the algorithm checks if a generic functional organ is defined for each functional box. Then, the algorithm explores each functional box of the model from start to end, to verify that there is no conflict in the coherence of the generic functional representation in terms of causality. Finally, according to categories of assigned variables and using the causal rules (Table 3), the cause–effect relationships between variables are established (Paynter 1961; E. Coatanéa et al. 2016). The causal ordering process follows the established mapping of bond graph elements and

functions following the order from variables \rightarrow equations \rightarrow architecture \rightarrow causality.

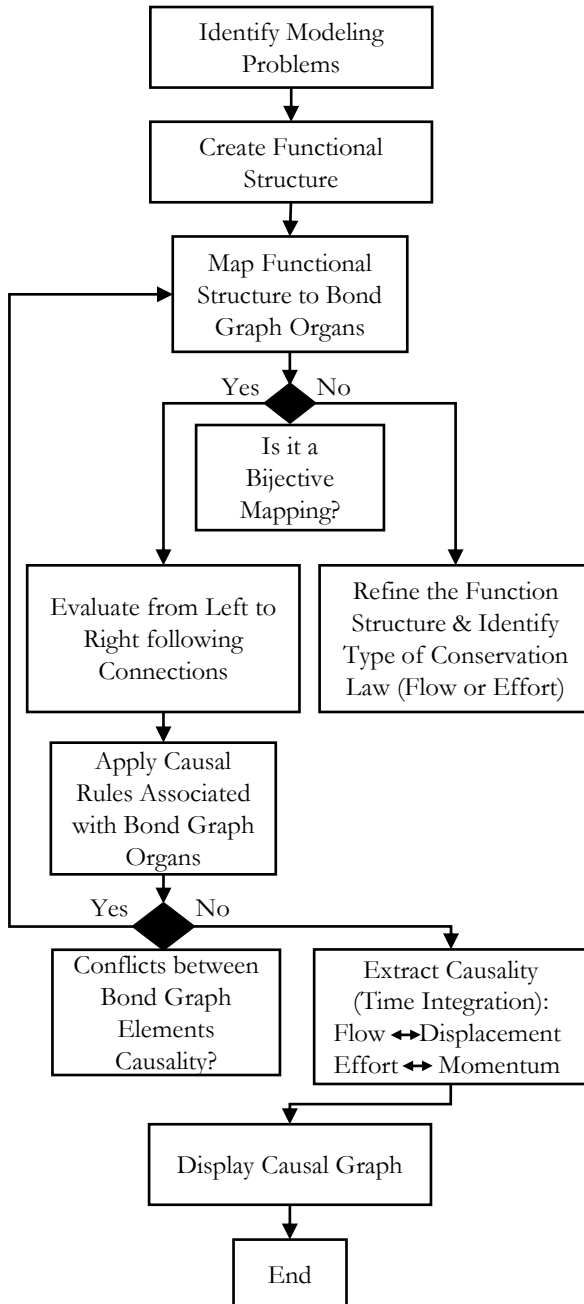
Table 3. Causality for generic functions and bond graph organs (Paynter 1961).

Bond Graph Element	Schematic view	Bond Graph Element	Schematic view
Source of effort (Se) Fixed effort-out causality		Source of flow (Sf) Fixed flow-out causality	
Capacitor (C) Fixed effort-out causality		Inertia (I) Fixed flow-out causality	
Resistor (R) Preferable effort-out causality (Resistive)		Resistor (R) Preferable flow-out causality (Conductive)	
Transformer (TF) Maintain incoming causality (two-port element)		Transformer (TF) Switch incoming causality (two-port element)	
Effort Junction (JE) or (0) (Multi-port element) Only one incoming effort $e_1 = e_2 = e_3 = e_4$ $f_1 + f_2 + f_3 + f_4 = 0$		Flow Junction (JF) or (1) (Multi-port element) Only one incoming flow $f_1 = f_2 = f_3 = f_4$ $e_1 + e_2 + e_3 + e_4 = 0$	

Once the relationships between all the variables of the system are assigned and colour coded, the final graph model can be obtained. The primary result of this modelling is a coloured hypergraph with a list of governing equations for the system of interest. In the research reported here, the coloured graph model is then used as precursor to build two type of machine learning models. First, the causal graph is used in combination with ANNs to build a predictive model for system performance evaluation and process parameter prediction. The causal graph developed using a combination of different knowledge archetypes can be used to guide the topology definition and optimization in an ANN. Second, the developed graph model is composed into a directed acyclic graph (DAG) to be used for probabilistic modelling using BN. The BN model can then be used for qualitative or quantitative simulations

to perform design and manufacturing decision making through prediction analysis, multi-domain optimization, and design space exploration.

Figure 8. Algorithm for causal rule extraction from functional model



The usability of the developed modelling framework is demonstrated in this research with the help of additive manufacturing modelling case studies. Each case study has been presented as a part of peer-reviewed, published research articles, and provided in the publications section of this dissertation. Next, a summary of the methods applied for each case study is presented.

3.2 Graph-based Metamodelling Case Studies

The graph metamodelling framework developed as part of this research is demonstrated for modelling and simulation of two additive manufacturing process technologies namely, material extrusion and direct energy deposition as presented next.

3.2.1 Application of Graph-based Metamodelling for a Material Extrusion Process

The manufacturing process evaluated in the first case study (**Publication I**) is a material extrusion process, fused deposition modelling (FDM). The process involves several steps that need to be characterized to holistically model the system. In addition, the interactions between the different processing steps also need to be presented in the form of variable interactions. The process starts with a polymer filament heated to melting temperature at the nozzle before being deposited onto a build plate in a layer-by-layer fashion. Thus, modelling of the filament feed rate, melt location within the nozzle, heat transfer to the filament and molten polymer, flowability of the molten polymer through the nozzle, and the mechanism facilitating the flow of the polymer through the nozzle need to be performed to evaluate dimensional quality and resulting manufacturing time for the FDM part. The research hypothesizes that the exploration of the manufacturing space can be effectively performed using a modelling approach combining graph-based metamodelling and machine learning to improve FDM part quality and build time, while keeping the number of required training data sets low. The mechanisms associated with the FDM process are discussed in **Section 2.3.1** and **Publication I**.

Several metamodelling approaches, including Kriging models, polynomial models, and neural network models, have been reported in literature for modelling complex systems. A metamodelling approach using causal graphs and ANNs can

provide numerous advantages as detailed in **Section 2.5** ANNs enable the development of global predictive models integrating numerous parameters. The proposed approach differs from classical surrogate methods in using existing knowledge; thus, the number of required experiments is reduced. The experiments are used to train only parts of the model, rather than the entire model. Through knowledge extraction and management, we limit the need for experimental data sets by integrating the existing system knowledge available for the observed process into the ANN (Efthymiou et al. 2015; E. Coatanéa et al. 2016). Nevertheless, existing knowledge in literature is represented in multiple forms and lacks interoperability (Witherell et al. 2014b). For this reason, the graph-based modelling framework is utilized to integrate and harmonize different types of knowledge to be coherent with each other, and to visualize the cause-effect relationships in the form of causal graphs. The conceptual modelling framework used in the study is presented in **Section 3.1** and **Publication I**.

Following the development of the causal graph, which represents the different functions (mechanisms) and associated variables of the FDM process, ANN modelling was carried out. A comparative study was conducted, wherein the outputs were first modelled using classical ANNs without using the pre-existing knowledge documented in the form of a causal graph. Next, the causal graph was used as a precursor to build a knowledge-based artificial neural network (KB-ANN) in the form of modular ANNs applied on top of the causal graph. Both models (classical ANN and KB-ANN) were experimentally validated, and conclusions were drawn based on their relative performance in terms of fit and prediction accuracy (see **Publication I**).

The findings of the study support the hypothesis that the integration of pre-existing knowledge through a graph-based modelling approach fitted with modular ANNs can provide better prediction performance when compared to classical ANNs. Though the use of pre-existing knowledge allowed for development of modular ANN models with good prediction performance, the possibility of overfitting in the ANNs was visible and generalization of the developed ANN models could not be verified for the small number of experimental data points available for modelling. In addition, the uncertainty involved with pre-existing knowledge included in KB-ANN models cannot easily be accounted for, which may lead to higher prediction error. Nevertheless, the case study highlights the usability of causal graphs as precursors for developing machine learning models of complex systems.

3.2.2 Application of Graph-based Modelling for Direct Energy Deposition Processes

The manufacturing process evaluated in the second set of studies is a direct energy deposition process, namely, wire and arc additive manufacturing (WAAM). Four studies were conducted for modelling this technology to demonstrate the capabilities of the developed graph-based metamodelling framework. The different case studies for WAAM are as follows: (1) multidomain modelling of worker health effects during WAAM; (2) modelling dimensional quality of parts built using WAAM-CMT; (3) characterizing the thermal effect on microstructure and mechanical properties of WAAM built parts; and (4) multidomain metamodelling of WAAM-CMT for optimization.

3.2.2.1 Evaluating Worker Health and Safety in WAAM

The disruptive nature of advanced manufacturing technologies, such as AM, requires extensive characterization of the emissions and wastes that can increase safety and health risks to operators and others. Characterizing worker health and safety requires expertise in manufacturing processes, and delves into domains such as measurement science, environmental science, and public health and safety. Currently, production risk and reliability assessments can overshadow worker health and safety evaluations due to increasing demand for quick, seamless integration of new technologies on the shop floor. To address this gap, a review of research literature was conducted focusing on the influence of welding process parameters, welding fumes, and fume exposure on worker health. The reviewed literature on WAAM worker safety and health effects are documented as part of **Publication II**.

The literature was used as pre-existing knowledge to graphically model the interrelationship between WAAM process variables (parameters), their influence on process emissions and waste, and associated worker impacts. Following the development of the graph model, implementation of a Bayesian network (BN) that integrates process knowledge (process operation, emissions, and related impacts), worker habits and exposure pathways, health and safety factors (health risks and severity of risks), and suitable safety protocols from the developed graph is discussed. The research demonstrates the use of the graph-based metamodelling framework to integrate pre-existing knowledge to hasten the development of multi-domain models which are simulatable for decision making.

3.2.2.2 Evaluating Dimensional Quality in WAAM

Achieving predictable, reliable, and cost-effective operations in WAAM is a key concern during production of complex-shaped functional metallic components for demanding applications, such as in the aerospace and automotive industries. An approach using causal graph-based modelling and Bayesian networks was proposed to develop a meta-model for a test case using WAAM-CMT. The causal graph developed for the process was used as a precursor to develop a BN model of the WAAM process for dimensional quality. The BN model was simulated to perform scenario analysis and predictive analysis. The advantages of using a probabilistic machine learning approach as opposed to a deterministic approach such as ANN are detailed in **Sections 2.5.5** and **2.5.6, Publication III**, and **Publication V**. To summarize, BNs provide an interactive and fast modelling approach for AM process and product characterization taking into account the uncertainty in the knowledge used to develop the network. BN modelling starts with the development of a directed acyclic graph (DAG), which is supported by the causal graph-based modelling approach developed in this research.

The research in **Publication III** uses the graph-based metamodeling approach to model WAAM for dimensional quality. Two experimental strategies were utilized in this research. First, single layer experiments were conducted varying nine process parameters to identify the most influential parameters on dimensional quality. Next, a multilayer part was printed using WAAM by varying three influential parameters, namely, wire feed rate (WFR), travel speed (TS), and number of layers (n). Causal graphs were developed for the single layer experiments and multilayer experiments, respectively. The two causal graphs were developed as a collection of different models. For the multi-layer experiments, the interrelationships between wire feed rate, travel speed, and interpass temperature were characterized through empirical modelling with the help of power laws. The regression equations obtained via the power law approach were then used to develop a BN model. The fundamental advantage of the BN approach used in this study is the ability to translate the causal graph directly into a BN model and to enable two-way simulation, for forward prediction (prognosis) of targets and backward prediction (diagnosis) of input parameters. The simulation of the BN allows the user to choose values for WFR, TS and n to obtain the required target values and, simultaneously, allows the user to visualize the effects of inputs on the target values. The backward prediction is useful in manufacturing since the final part dimensions are defined up front by the design requirements. In addition, the BN method provides a validated approach to generate

grey box models in which analytic knowledge in form of equations can be used together with experimental knowledge (data).

3.2.2.3 Characterizing Microstructure and Mechanical Properties in WAAM

The study in **Publication IV** was developed to characterize the influence of thermal phenomena on the resultant microstructure and mechanical properties of WAAM-built parts. The work focused on developing the required knowledge base for holistic metamodelling of the WAAM process, which was reported in **Publication V**, and integrated material- and process-related parameters, the thermal history of the parts, part microstructures, and their associated mechanical properties (Vickers hardness). Two steel alloys were used in this experimental research, namely G4Si1, a mild steel alloy, and AM70, a high-strength low-alloyed steel (HSLA). WFR and T_0 were varied at two levels for both materials to achieve a low heat input level and high heat input level, resulting in four thin wall structures for testing. Samples were taken from the deposited walls to investigate the microstructure evolution (optical microscopy specimens) and mechanical properties (tensile and microhardness specimens) under the different weld conditions explored. Microstructure and mechanical property analysis were performed for samples taken along the entire height of the wall to characterize the effect of successive heating and cooling of the layers on the microstructure. For tensile testing, horizontal samples (cut along print nozzle travel direction) and vertical samples (cut along wall build direction) were chosen to check for isotropy in the printed wall's mechanical properties. Microstructure and mechanical property analyses are presented in **Publication IV**.

3.2.2.4 Multi-Domain Metamodel for WAAM Product Quality

The study presented in **Publication V** developed a holistic metamodel for WAAM integrating dimensional quality, thermal phenomena, microstructure, and mechanical properties. A BN model was built on top of a graph model for simulation and decision making. The study integrates results of **Publication III** and **Publication IV** as pre-existing knowledge for metamodel development. A combination of existing models from previous publications, literature on process physics, and experimental data were used as pre-existing knowledge for the development of the graph model. Three categories of models and associated levels of detail exist in this

research. The first two models used to represent the geometry and the thermal profile of the weld have the highest level of fidelity owing to the significant amount of experimental data points obtained. The thermal profile of the weld is modelled in two different ways: 1) modelling the thermal profile as an average cooling rate of the weld layer using a Gaussian process regression (GPR) model and 2) modelling the thermal profile as the wait time between layers using Lasso (Least Absolute Shrinkage and Selection Operator) and ordinary least squares (OLS) regression. The third model is less granular and models microhardness using an artificial neural network with two inputs. The geometric model for the width and height of the weld was developed in **Publication III**. The geometric model was developed in the form of a power law using ordinary linear regression. The resultant graph model integrates the empirical models for WAAM part geometry from **Publication III**; the GPR and OLS models developed for thermal phenomena using process data from physical experiments (heating and cooling data); and an ANN model for mechanical properties data. The developed BN model is validated using physical experiments.

3.3 Discussion

This chapter described the graph-based modelling framework developed as part of this research for holistic metamodelling of additive manufacturing processes. The framework offers simulation capabilities with the help of machine learning to perform physics-based reasoning, systematic search for contradictions, predictive analysis of outputs and pre-tuning of process parameters, and design space exploration. The development and application of the framework as described in the foregoing addresses the three research questions presented in the introduction chapter. Specifically, the developed framework allows designers to model systems with different levels of detail and abstraction depending on the availability of knowledge associated with the different components of a system. The framework allows for transformation and integration of knowledge available into a unified graph representation. The algorithms offer a systematic approach to assign variables for describing functions, extract causality among variables, and establish governing equations among variables in the model. The framework focuses on the functionality of system using function modelling and graph representation as the fundamental modelling strategy. The graph representation acts as a precursor for facilitating the development of machine learning models. The use of pre-existing knowledge in the graph development stage reduces the need for large datasets for training a machine

learning algorithm. In this research, the graph-based metamodeling framework has been applied to several additive manufacturing process modelling case studies.

3.3.1 Characteristics and Bounds of the Graph-based Metamodeling Framework

The development of the methodology explained in this chapter has its limitations, which can be addressed by future developments. Several distinguishing characteristics of the framework are as follows:

1. The framework can represent functions at different levels of granularity.

The framework combines knowledge of different types and levels of detail as functions and bond graph elements, which are then composed into a knowledge/causal graph. Thus, representation of functions and variables, while ensuring their dimensional homogeneity influences the accuracy of the metamodel.

2. The framework results in two outputs: a graph model and a machine learning model, which combine to form a metamodel.

The framework first develops a graph model. The graph model does not provide simulation capabilities but does allow for qualitative reasoning based on its architecture. It is used as pre-cursor for developing a machine learning model, which allows for simulation and quantitative reasoning through layering of the two models into a metamodel.

3. The framework can be used for simulation and computational studies.

The type of machine learning model used can determine the scope of computational analysis that can be performed using the developed metamodel. Deterministic machine learning using ANN has only been tested for predictive analysis in this work. Probabilistic modelling using BN has been used for prediction, multi-domain optimization, and design space exploration.

4. The framework can be characterized as a metamodeling tool.

The framework is a metamodeling tool because it enables the integration of models with different purposes at different level of detail into a single composite model. However, it can be differentiated from conventional metamodeling techniques (e.g., surrogate modeling), since this approach offers more transparency into the various model elements.

5. The framework can be applied to different research domains.

The framework offers a generic modelling approach applicable to disciplines beyond the manufacturing domain presented in this research. The framework has been successfully applied to applications in systems engineering, product design, manufacturing systems modelling and optimization, and cybersecurity (in development), and network analysis. Nevertheless, future work should validate the usability of the approach for other research domains.

4 RESULTS AND THESIS CONTRIBUTION

The following chapter articulates the results and contributions of the publications presented in this research. Table 4 highlights the contribution of each published article with relation to the research objectives detailed in Chapter 1.

4.1 Graph-based Metamodelling for a Material Extrusion Process

The article presented in ASME JMD 2019 (**Publication I**) presents the graph-based modelling framework for defining the topology of a knowledge based artificial neural network (KB-ANN). The detailed analysis of the results has been presented in Publication I of this dissertation. A summary of the results is presented below.

The FDM process was initially modelled using the developed framework to develop a causal graph to be translated into an ANN topology. Three classical ANNs and a KB-ANN topology were evaluated in this study. The ANN's topology is designed for maximum compactness to maintain all the connections in the causal graph. The KB-ANN topology is developed in the form of modular ANNs as shown in the causal graph (Figure 9 and 10).

Three classical ANNs were designed to model the three outputs, namely, wall thickness (e), part height (H_t), and mass (M_t) using three inputs: layer height (h_i), travel speed (TS), and extruder temperature (T_{set}). The mean squared error (MSE) for best performance was found to be $5.43e-04$ after nine iterations, $1.15e-04$ after 10 iterations, and $2.01e-03$ after 23 iterations for wall thickness, part height, and mass respectively.

The KB-ANN was designed as four modular ANNs following the simplified causal graph shown in Figure 9. The first modular ANN is designed for one output, ratio of viscosity (μ) of molten polymer at extrusion temperature to the viscosity (μ_i) of molten polymer at a reference temperature ($175\text{ }^\circ\text{C}$). The filament feed rate (FFR) and extruder temperature (T_{set}) are used as inputs. Here, the output of the modular ANN 1 is an intermediate blue variable, which cannot be directly measured and hence has to be estimated using numerical simulations

Table 4. Contributions of author's publications and their associated research tasks

Source	Contribution of Dissertation Research	Research Objective
H.P.N. Nagarajan , H. Mokhtarian, H. Jafarian, S. Dimassi, S. Bakrani, A. Hamed, E. Coatanea, G. Wang, and K.R. Haapala, 2018 "Knowledge-Based Design of Artificial Neural Network Topology for Additive Manufacturing Process Modelling: A New Approach and Case Study of Fused Deposition Modelling," ASME Journal of Mechanical Design, Volume 141(2), pp. 021705-12, Dec 2018. https://doi.org/10.1115/1.4042084	The work demonstrates a proof of concept for knowledge reuse and integration using graph metamodelling.	1
H.P.N. Nagarajan , S. Panicker, H. Mokhtarian, E. Coatanea, and K.R. Haapala, "Improving Worker Health and Safety in Wire Arc Additive Manufacturing: A Graph-based Approach," Procedia CIRP, 2020, Proceedings of the 27th CIRP International Conference on Life Cycle Engineering (LCE2020), May 13-15, Grenoble, France. https://doi.org/10.1016/j.procir.2020.01.116	The ANN and KB-ANN modelling developed in this research allows for simulation of the developed metamodel.	2
H.P.N. Nagarajan , S. Panicker, H. Mokhtarian, E. Coatanea, and K.R. Haapala, "Improving Worker Health and Safety in Wire Arc Additive Manufacturing: A Graph-based Approach," Procedia CIRP, 2020, Proceedings of the 27th CIRP International Conference on Life Cycle Engineering (LCE2020), May 13-15, Grenoble, France. https://doi.org/10.1016/j.procir.2020.01.116	The KB-ANN modular setup allows for partial and holistic simulation of the modelled sub-systems for decision-making.	3
H.P.N. Nagarajan , S. Panicker, H. Mokhtarian, T. Remy-Lorit, E. Coatanea, R. Prod'hon, H. Jafarian, K.R. Haapala, and A. Chakraborti, 2019 "Graph based Meta-modelling to Characterize Cold Metal Transfer Process Performance," Smart and	The literature review develops the knowledge base for characterizing worker health effects in WAAM using causal graphs.	1
H.P.N. Nagarajan , S. Panicker, H. Mokhtarian, T. Remy-Lorit, E. Coatanea, R. Prod'hon, H. Jafarian, K.R. Haapala, and A. Chakraborti, 2019 "Graph based Meta-modelling to Characterize Cold Metal Transfer Process Performance," Smart and	The use of graph metamodelling demonstrates the ability to integrate multi-domain knowledge from literature.	
H.P.N. Nagarajan , S. Panicker, H. Mokhtarian, T. Remy-Lorit, E. Coatanea, R. Prod'hon, H. Jafarian, K.R. Haapala, and A. Chakraborti, 2019 "Graph based Meta-modelling to Characterize Cold Metal Transfer Process Performance," Smart and	The research demonstrated a knowledge driven experimental effort for modelling WAAM dimensional quality using causal graphs.	1

	The use of casual graphs as pre-cursors for probabilistic machine learning was developed.	2
	The work highlights the advantage of BNs over deterministic models (ANN) to perform holistic two-way simulation and decision making.	3
S. Panicker, H.P.N. Nagarajan , J. Tuominen, M. Patnamsetty, E. Coatanea, and K.R. Haapala, 2022, "Investigation of Thermal Influence on Microstructure and Mechanical Properties in Wire Arc Additive Manufacturing of Steels, Material Science and Engineering A. (Accepted for Publication)	The literature review conducted on the microstructural effects in WAAM supports the development of the knowledge base for holistic metamodelling.	1
	The experimental characterization supports identification the part-process-property structure in WAAM-CMT.	
H.P.N. Nagarajan , S. Panicker, D. Wu, S. Bakrani, E. Coatanea, and K.R. Haapala, "Modelling the Geometrical and Mechanical Responses in Wire Arc Additive Manufacturing: A Concept for Graph Metamodel based Design Space Exploration. (Prepared and Unpublished)	The holistic metamodel combines multi-domain knowledge from material, manufacturing, and product domain.	1
	Different types of knowledge (data, ANN, and regression models) are integrated into a single	

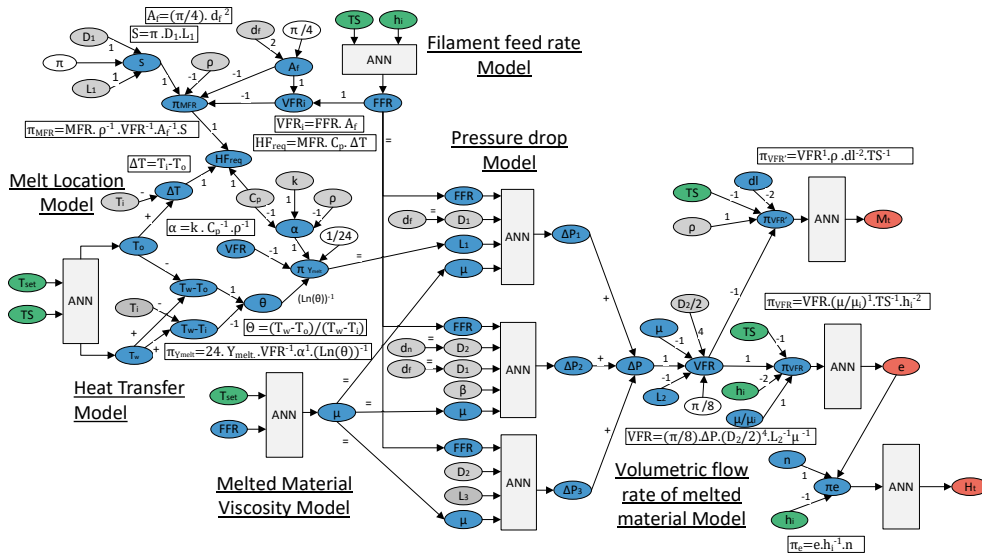
graph model using the developed framework.

The use of BN allowed for propagation of optimization objectives to perform design space exploration and decision-making.

3

The second modular ANN is designed for output wall thickness (e). To reduce the dimensionality of the ANN, the inputs to predict thickness were represented in the form of Pi numbers (dimensionless primitives) using dimensional analysis theory (DA) (Bridgman, n.d.). The third modular ANN was designed for height (H_t) as output and inputs, layer height (h_i) and number of layers (n).

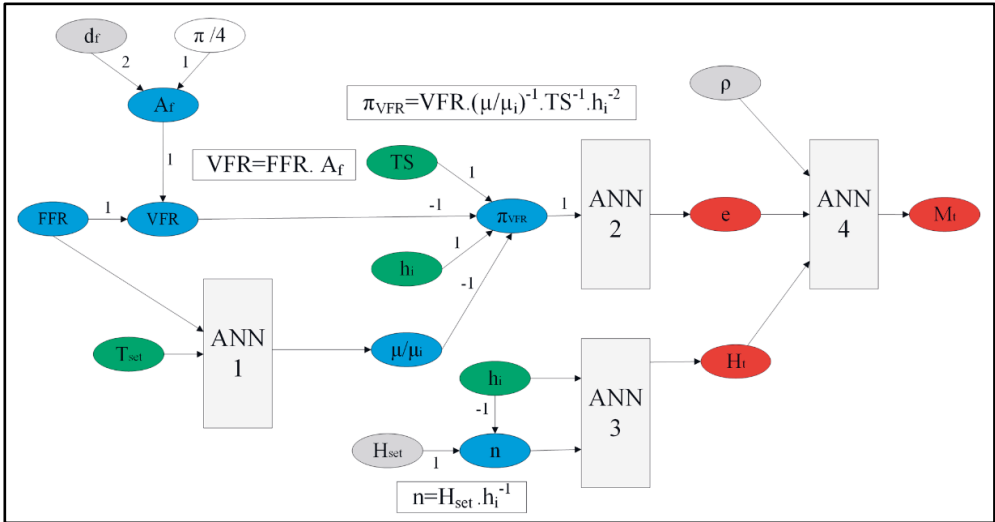
Figure 9. A modular KB-ANN topology of the FDM process using graph based metamodeling framework (Nagarajan et al., 2019)



The fourth modular ANN was designed for mass (M_t) as output with inputs, wall thickness (e), height (H_t), and density of the material (ρ) used. The results shows that the modular ANN 1 was able to obtain the best validation performance at 53rd iteration with $MSE = 7.7186e-05$. The MSE for modular ANN 2 for wall thickness

(e) was found to be $9.30e-05$ after 93 iterations. The modular ANN 3 results obtained best-fit performance with $MSE = 1.41e-04$ after four (4) iterations. The best performance at four (4) iterations indicates a mediocre fit to the training data. Finally, the results of the modular ANN 4 for mass (Mt) observed MSE of $2.54e-04$ after 23 iterations.

Figure 10. A simplified modular KB-ANN topology for the FDM process using causal graph developed (H. Nagarajan et al. 2019)

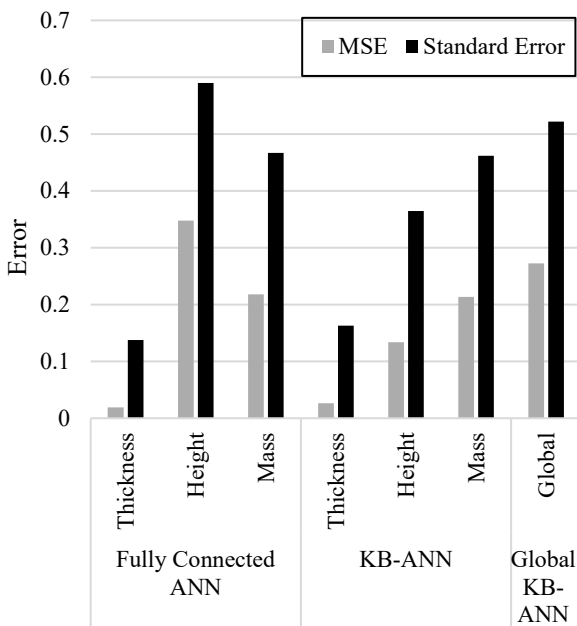


The validation of the developed models was carried out with nine (9) experimental tests. The values for the independent input variables (layer thickness, extruder temperature, and travel speed) were chosen at random. From validation, the standard prediction error for thickness, height, and mass in the KB-ANN were found to be 0.1627, 0.3647, and 0.4621 respectively. Similarly, the prediction error for the fully connected classical ANN was found to be 0.1376 (thickness), 0.5898 (height), and 0.4667 (mass). The propagated global error of the KB-ANN model was found to be 0.5220. A comparison of the MSE and standard error calculated after validation for the two types of networks are shown in Figure 11. It was seen that the errors for the KB-ANN are in the same range as the prediction error of the classical ANN.

The KB -ANN has performed better than the classical fully connected ANN in terms of fit to the provided experimental data. From validation, the prediction error of the KB-ANN was found to be almost the same for thickness and mass, while lower for height. This prediction error was largely the result of loss of information when streamlining the complete causal graph in Figure 9 to the simpler version in

Figure 10. Specifically, the regression fit for the height KB- ANN was poor, largely due to the absence of adequate knowledge or models to represent the phenomenon that can define part height. The addition of more variables to the study in the form of simulations or experimental estimation would improve the training and result in lower prediction error. The key difference between the models lies in the total number of weights that define the state space for each model. In this case, the KB-ANN had 12 fewer weights than its classical counterpart did.

Figure 11. Validation error comparison of fully connected classical ANN and KB-ANN



Furthermore, the hidden layer of the KB-ANN operates within the dimensionally homogenous space. The combination of these factors results in improved efficiency during fit and similar performance for the same number of training (27) samples. This is visible in the training and its robustness. The KB-ANN provides robust results in term of generalization compared with the classical ANN. Nevertheless, the small amount of the data set used in this effort, limit the conclusions that can be drawn from the training, validation, and test. The higher number of epochs obtained for the KB-ANN compared to its classical ANN counterpart demonstrate that the difference will increase with bigger datasets. It also indicates that KB-ANN can provide better results for smaller datasets.

The KB-ANN modelling was able to limit the number of required experiments to develop a metamodel capable of dynamically predicting control factors of FDM. The causal graph representation enabled the design of KB-ANN as modular ANNs with reduced dimensionality. The results demonstrated the superiority of the KB-ANN over classical full-connected ANN in terms of fit and regularization for the same performance and same number of training samples. The case study was limited to the prediction of three target variables using four modular ANNs using the simplified causal graph in comparison to the large number of target variables that essentially need to be modelled for a complex FDM system. In reality, more intermediate variables and phenomena (Figure 9) need to be modelled to represent the FDM process holistically. The current work addresses the first research task to allow the developed framework to combine knowledge in modular manner and to reduce dimensionality of complex problems using knowledge extraction, representation, and integration techniques such as dimensional analysis. Furthermore, the use of ANN modelling on the graph model allowed for simulation of the developed metamodel for process parameter prediction in line with research objective 3.

4.2 Graph-based Metamodelling for a Direct Energy Deposition Process

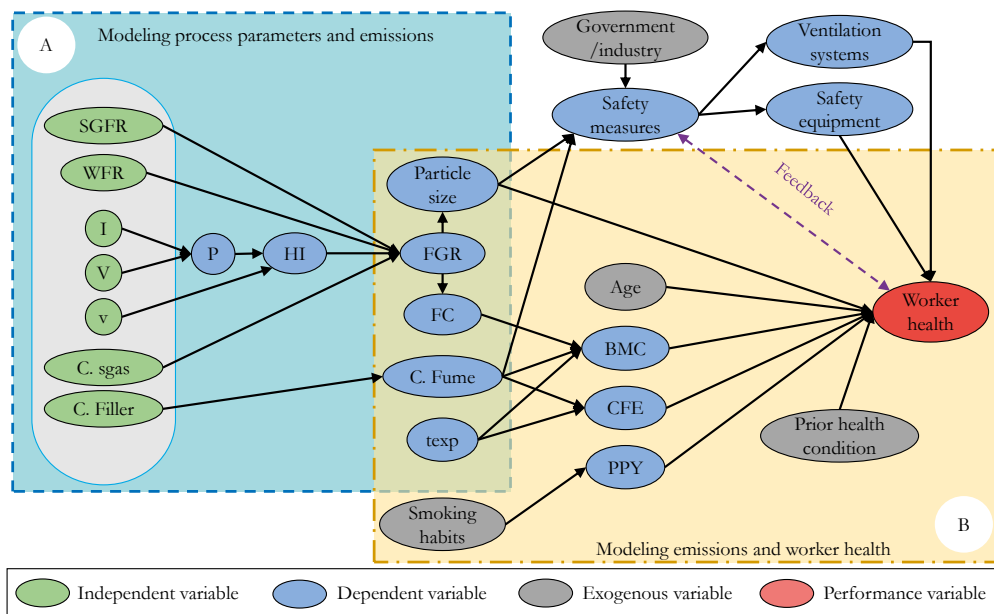
The modelling framework developed in this research was used to model the WAAM-CMT process to characterize, a) worker/operator health and safety impacts, b) dimensional quality in printed parts, and c) product quality (dimensional and mechanical).

4.2.1 Worker Health and Safety Impacts in WAAM

The body of research for modelling worker safety in welding was identified to fall into two domains namely, manufacturing technology (process) and public health. A detailed account of the literature study and model development effort has been presented in **Publication II** of this dissertation. The background study on welding emissions/wastes and public health research was used as pre-existing knowledge to graph-based model for worker health in WAAM. The developed graph-based model enables visualization of the potential cause-effect relationships and correlations

between the different variables of the system based on the referenced literature, as shown in Figure 12. At this stage, some of the relations can be considered to be causal, especially in area A, while in area B more efforts are needed to validate the causality of elements. This causal graph provides a unified structure to integrate the knowledge from the two identified domains. In the manufacturing technology domain, research has focused on characterizing the influence of the process and parameters on generation of emissions/fumes (Li et al. 2004; Sjögren and Ulfvarson 1985; Antti-Poika, Hassi, and Pyy 1977; Saito et al. 2000; Jafari and Assari 2004; I. J. Yu 2001; Cole, Epstein, and Peace 2007; Niemelä, Koskela, and Engström 2001; Balkhyour and Goknil 2010; Alfaro and Cayo 2012; Topham et al. 2010; Il Je Yu et al. 2003; Heung et al. 2007; Keane et al. 2016).

Figure 12. Graph model of operator health impacts in WAAM



The public health domain has focused on characterizing the influence of emissions and components on worker health (Koh et al. 2015; Li et al. 2004; Sjögren and Ulfvarson 1985; Antti-Poika, Hassi, and Pyy 1977; Jafari and Assari 2004; Topham et al. 2010; Gube et al. 2013; Rongo et al. 2004; Hammond et al. 2005; Chinn et al. 1995; Cotes et al. 1989; Jayawardana and Abeysena 2009; Bradshaw et al. 1998; Stănescu et al. 1967; Nakadate et al. 1998; Luo, Hsu, and Shen 2009; Sharifian et al. 2011; Z. P. Wang et al. 1994; Fogh, Frost, and Georg 1969; Storaas et al. 2015; Qin

et al. 2014; El-Zein et al. 2003; Nemery 1990; Hjortsberg, Orbaek, and Arborelius 1992; McCormick, Goddard, and Mahadeva 2008; McMILLAN and Pethybridge 1983; Barhad, Teculescu, and Crăciun 1975; Kilburn et al. 1989; Mur et al. 1985). Mathematical relationships linking process parameters to welding emissions have been documented in literature, while epidemiological studies related to health impacts are based on statistical analysis. From Figure 12, the process parameters (welding current, voltage, speed, shielding gas flow rate, shielding gas composition, and filler wire composition) function as independent variables, represented as green nodes.

Variables representing emissions, such as fume generation rate, fume composition, particle size, and cumulative exposure time, are considered as outputs which influence worker health (red target node). Intermediate variables are dependent variables whose values need to be monitored using sensors or, need to be simulated or predicted based on models. They also function as hubs within the graph model and provide a bridge for knowledge integration from the two domains. In addition to the intermediate variables, worker health is affected by exogenous variables (grey nodes), such as smoking habits, age, and prior health condition. The causal relationships between these variables can be established using experimental data, equations, and/or functional models. Here, causal relationships between variables have been established using the modelling framework.

The causal graph can be used as a precursor to the development of machine learning models, such as BNs, for simulation (H. P. N. Nagarajan et al. 2018; Mokhtarian et al. 2019). The BN will comprise multiple nodes that represent the different variables of the system of interest. These nodes will be connected in the form of direct acyclic graphs (DAGs), developed based on their causal relationships. The causal relationships shown in Figure 12 will help generate the DAG for worker health for the WAAM process. Simulation of the BN model can enable the following: 1) monitoring the effect of changes in process parameters on emissions and worker health, 2) suggesting safety equipment and procedures required based on exposure time, fume composition, and fume generation rate, and, conversely, and 3) prescribing optimal process parameters based on available safety equipment to control emissions rates and prevent adverse worker health effects. The implementation of such a model would allow engineers and managers to monitor shop floor processes and ensure the safety of workers *a priori* or as conditions change.

4.2.2 Dimensional Quality in WAAM-CMT

The metamodeling approach has been employed in this research to analyse and summarize the results of different models that currently exist in literature for WAAM. A detailed account of the results of this study has been presented in **Publication III** of this manuscript.

The selection of the papers presented in the current effort to model the WAAM process was completed using three key criteria. First, the research should support the creation of a simple model for geometry modelling and mechanical property modelling of WAAM produced parts. Second, the process reported by the research should exhibit globally similar deposition and thermal phenomena as for the WAAM process. Third, the modelled phenomena should be compatible with the modelling of the CMT WAAM used in this research. Figures 13 and 14 show the causal relationships identified and modelled graphically for single-bead and multi-bead models, respectively based on literature.

Figure 13. Causal graph model summarizing literature on single bead wire additive manufacturing (Ding et al. 2015; Girinath, Siva Shanmugam, and Sankaranarayanan 2018)

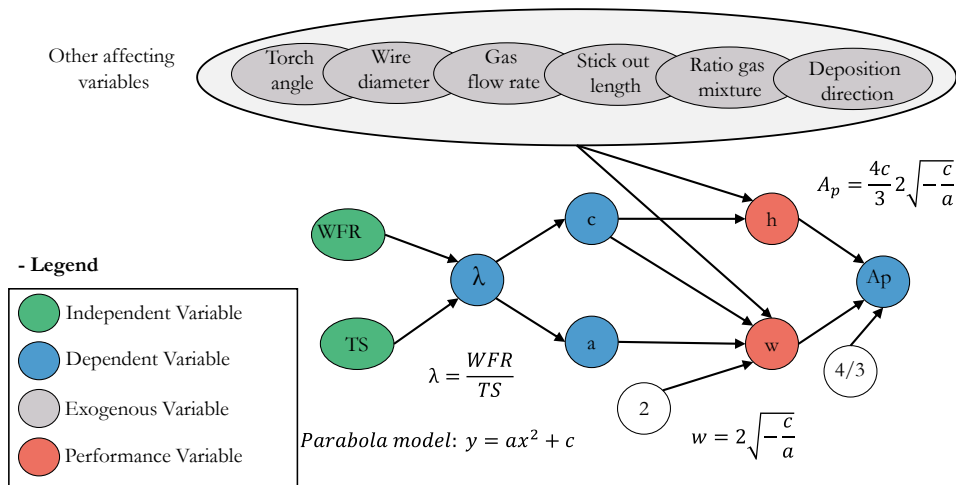
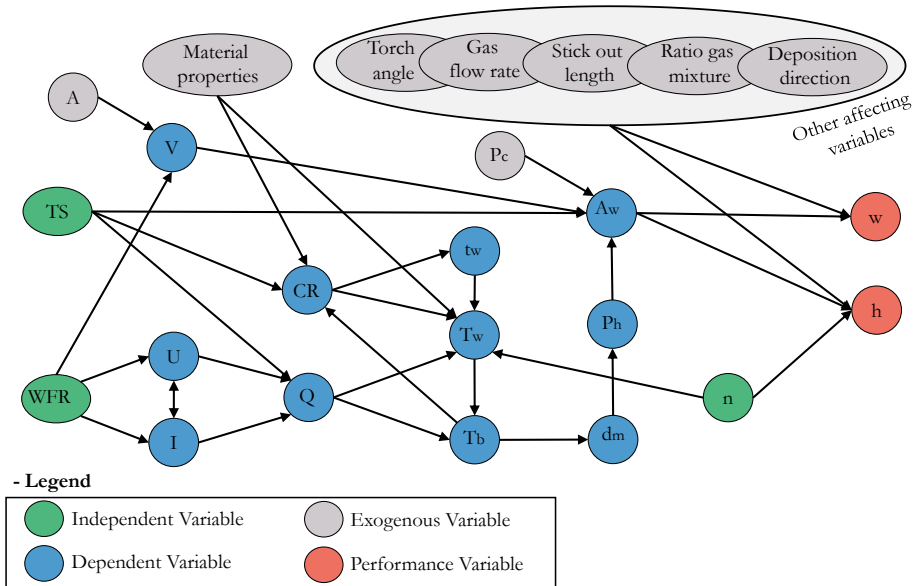


Figure 14. Causal graph summarizing literature on multi-bead wire additive manufacturing (Y. Huang et al. 2015; Rios et al. 2018; Rosenthal 1941; Nguyen 2004; Kwak and Doumanidis 2002)



From the causal graphs, it can be seen that two variables are required in the WAAM process to generate a model of the wall width and three independent variables are needed for modelling wall height. The graphs provide multiple paths from the independent variables (i.e., WFR, TS, and n) to the two variables of interest here (i.e., w and h). In future research, several parameters considered as exogenous variables here will be integrated into the set of independent variables. This modification allows for expansion of the scope of the causal models, while consequently integrating additional parameters that jointly affect bead geometry and mechanical properties.

The background study and initial causal graphs were used to develop an experimental approach to model bead width and height. The article analysed the current literature models and concluded that the bead geometry in WAAM can be modelled using a small number of independent variables. This conclusion was experimentally verified for a single bead geometry. Two experimental efforts have been carried out in this research. The first focuses on single-bead geometry by varying nine independent parameters using a Taguchi design of experiment (DOE) approach. The second effort focuses on building straight walls with stacked beads (varying the number of layers) and constant length (80 mm). A rectangular plate (300 x 200 x 20 mm) made of mild steel was used as the base plate for depositing the single-bead and multi-bead geometry. Table 5 reports the experimental welding parameters, consumables, and equipment used.

Table 5. Weld parameter settings, consumables, and equipment for single bead and multi-bead geometries

Equipment /Material/ Method	Single bead	Multi-bead
Base plate size (material)	300*200*20 mm (mild steel)	300*200*20 mm (mild steel)
Bead length (material)	50 mm (TD MAK-10S)	80 mm (TD MAK-10S)
Robot	ABB 4600 40/2.55	ABB 4600 40/2.55
Shielding gas type	MISON 8 (Ar + 8% CO ₂ + 0.03% NO)	MISON 8 (Ar + 8% CO ₂ + 0.03% NO)
DOE type (number of experiments)	Taguchi L32 (96)	Full factorial (27)
Measurement of outputs	Laser scanning	CMM, profilometer
Parameter of study (levels)		
Ignition time (t_{ign})	(100, 200, 300, 400) ms	F (400) ms
Ignition current (I_{ign})	(90, 100, 110, 120) A	F (46, 47.7, 49.2) A
Arc length correction (ALC)	(-15, -10, 0, 15) %	F (0) %
Wire feed rate (WFR)	(53.3, 58.3, 63.3, 68.3) mm/s	(33.3, 41.6, 50) mm/s
Travel speed (TS)	(6.6, 8.3, 10, 11.6) mm/s	(10, 11, 12) mm/s
Shielding gas flow rate (SGFR)	(14, 16, 18, 29) L/min	F (14) L/min
Torch angle (Φ)	(70, 90, 120) degrees	F (90) degrees
Ending time (t_{end})	(100, 200, 300, 400) ms	F (400) ms
Ending current (I_{end})	(125, 135, 145, 155) A	F (46, 47.7, 49.2) A
Number of layer (n)	F (1) layer	(9, 12, 15) layers
Wire stick out	F (15) mm	F (15) mm
Interpass temperature	N/A	150 °C
Note: F - Fixed parameter		

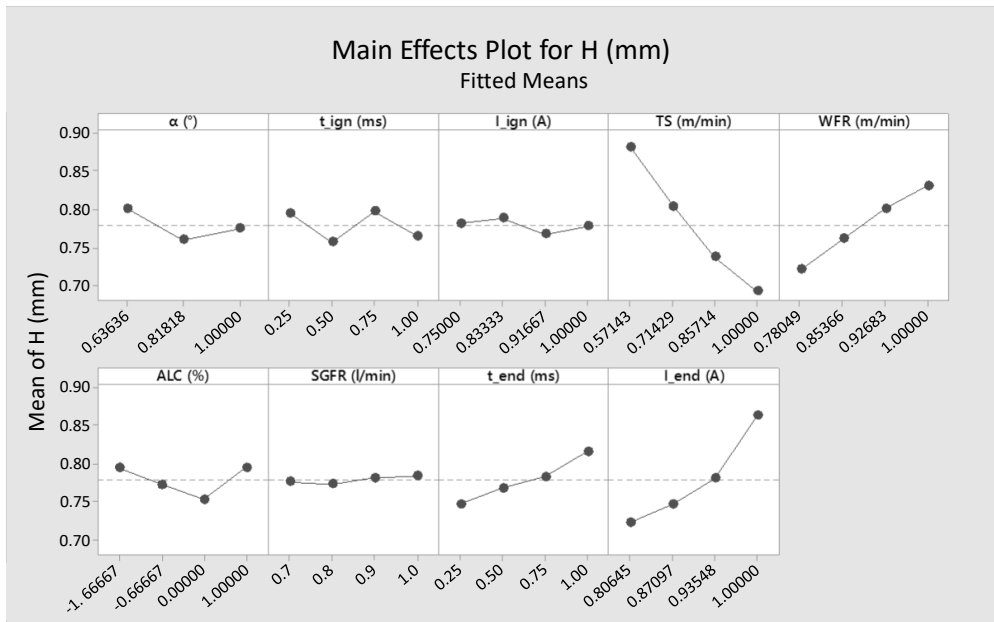
A detailed account of the experimental procedure followed in this article is presented in **Publication III** of this dissertation.

4.2.2.1 Experimental Results for Single Bead Geometry in CMT

Statistical analysis of the data collected from the single-bead experiments was used to characterize the influence of different WAAM process parameters on print quality. The recorded data was subjected to standard data cleaning. The input parameters and output data (h and w) were normalized, and a two-way analysis of

variance (ANOVA) test was conducted to identify the most influential process parameters on the height of the printed bead. The P-test associated with the ANOVA found that five out of the nine initial input parameters were statically significant in affecting the variation in height (Table 6), namely, WFR, TS, torch angle, ignition time, ending time, and ending current [37]. The effect of input variables on the mean of height (H) for the single bead geometry are shown in Figure 15.

Figure 15. Effect of input variables on the mean height for a single bead geometry



The influential parameters inferred from this initial study helped validate the high influence of WFR and TS on the weld dimensional quality as identified in the background section.

Table 6. Two-way ANOVA for single bead experiments

Source	Deg. of Freedom	Adjusted Sum of Squares	Adjusted Mean Squares	F-value	P-value
WFR	3	0.104	0.035	11.270	0.000
TS	3	0.816	0.272	88.560	0.000
α	2	0.346	0.017	5.630	0.004
t_{ign}	3	0.050	0.017	5.410	0.002
I_{ign}	3	0.009	0.003	0.950	0.421
ALC	3	0.182	0.006	1.980	0.121
SGFR	3	0.003	0.001	0.290	0.832
t_{end}	3	0.099	0.033	10.800	0.000
I_{end}	3	0.457	0.152	49.620	0.000
Error	133	0.408	0.003		
Total	159	2.151			

4.2.2.2 Experimental Evaluation of Multi Bead Geometry in CMT

The preliminary analysis conducted on the outputs of the first set of experiments for the single bead geometry and the background study, led to the identification of welding parameters that have higher impact on the quality of weld deposition. Previous experiments found that WFR, TS, heat input, and interpass temperature are the most influential parameters in CMT WAAM. A full factorial DOE was feasible for the multi-bead geometry due to the low number of input parameters chosen for this study. Two regression models were developed, one for predicting the height and the other for predicting the width of the part. Welding parameters WFR, TS, and n were considered as the independent variables. A power law was adopted to relate the independent parameters to the dependent parameters; power laws are suited for representing nonlinear relationships between variables in welding. The regression equations developed for height (h) width (w) are shown in Eq. 7 and Eq. 8, respectively:

$$w_{\pm e2} = e^{1.4978} \cdot WFR^{0.3953} \cdot n^{-0.0286} \cdot TS^{-0.6730} \quad (7)$$

$$h_{\pm e1} = e^{0.0946} \cdot WFR^{0.3539} \cdot n^{0.8608} \cdot TS^{-0.3583} \quad (8)$$

subject to

$$2.5 \leq \lambda \leq 5.0$$

$$T_o = 150 \text{ }^\circ\text{C}$$

Two quality metrics (i.e., R² and RMSE) were computed for each model with respect to the data from the 27 experiments (Table 7). The equations obtained from the regression analyses were then used to develop a BN using BayesiaLab 8 modelling software (Bayesia USA n.d.).

Table 7. Quality metrics for the regression equation

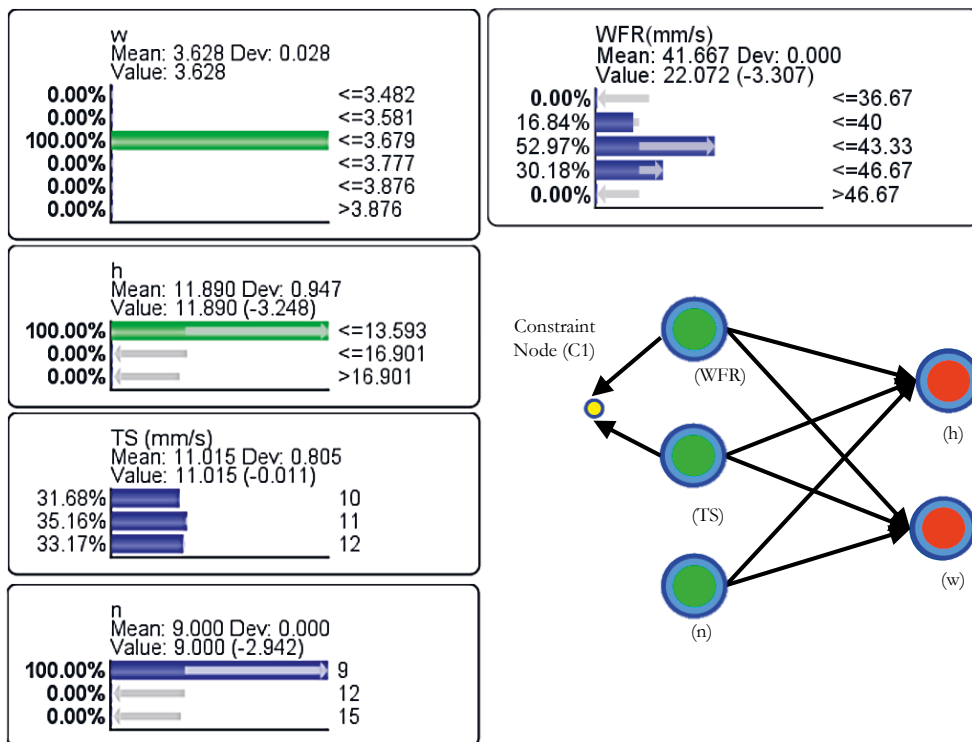
Quality metric	For w	For h
R ²	0.8562	0.9665
RMSE (root mean square error)	0.1056	0.2689

The BN model (Figure 16) for the geometrical features (height and width) for an additively manufactured wall is developed using the regression equations. Five validation experiments were performed for forward simulation, wherein the users defined the WFR, TS, and n values and the BN model was used to predict the resultant width and height values. Consequently, three experiments were performed for backward simulation, wherein the user defined height and width target values and the BN model predicted the values of input parameters to achieve the targets. During backward simulation, the user defined the target width and height of the part to be printed as 3.6 mm and 11.0 mm, respectively. The Bayesian inference engine was then used to prescribe the values for WFR (2.5 mm/min), TS (11 mm/s), and n (9 layers) to achieve the target width and height. The printed part was then measured using a CMM. The average error for the predicted wall width and height were found to be 7.72% and 8.76%, respectively.

In addition, two quality metrics were computed for the forward and backward simulation, namely, maximum relative error magnitude (MREM) and average relative error magnitude (AREM), to assess the predictability of the model. Together, these

two metrics evaluate both overall predictability and worst case predictability of the meta-model (Yang et al. 2017). Error relative to the variation range of h and w values was also computed. The MREM and AREM metrics for width and height are given in Table 8 and Table 9 for the regression models and Bayesian models, respectively. MREM, which assesses the predictable error in the worst-case scenario, was found to be 2.84% for width and 3.69% for h. AREM was found to be 1.83% for w and 1.44% for h. Finally, ϵ assesses the accuracy of the model with respect to the range of possible variation of both w and h to characterize the error magnitude better than through relative error computation. The relative error for the developed regression models was found to be slightly higher than that of the best-performing models for width of multi-bead prints from literature. Sequeira Almeida (Sequeira Almeida 2012) predicted the width for multi-bead prints with relative errors of 0.41%, 6.49%, and 5.42% for three experimental validation tests.

Figure 16. Visualization of the Bayesian inference for backward simulation



A relative error of 2.76% was observed through validation for the model in the worst case (Sequeira Almeida 2012). However, in the current work, the error computation follows a more conservative approach to characterize the magnitude of the error.

Table 8. MREM and AREM values for the regression model

Quality metric	For w	For h
MREM	2.84%	3.69%
AREM	1.83%	1.44%
Average ϵ	4.93%	2.35%

Table 9. MREM and AREM values for the backward Bayesian model

Quality metric	For w	For h
MREM	4.38%	3.62%
AREM	3.03%	3.09%
Average ϵ	8.12%	4.60%

The quality metrics presented in this study show an acceptable accuracy of the model for predicting geometrical dimensions of multilayer parts. These validation results support the hypothesis that the considered input parameters (WFR, TS, and n) are sufficient to predict geometric dimensions of multi-bead prints for the CMT WAAM process.

4.2.2.3 Discussion

This research presented a graph-based modelling approach combined with regression analysis and Bayesian networks to model the width and height of a multi-bead geometry printed using WAAM. The model performance from validation shows a good prediction capability and potential for generalization. The Bayesian network (BN) implementation enables model expansion to include more variables, such as torch angle and filler material type, with verification through future experiments. Since the BN is modular, its scope could be gradually expanded to model other targets. Modularity allows for combining analytical and experimental developments into a single model. However, to switch between different material systems, additional experiments to determine the optimal value ranges of the two constraints (λ and T_w) are required. In addition, cooling rate has been observed to have a high influence on the final mechanical properties and dimensional quality of the weld. Thus, modelling the cooling rate for different materials will allow for expansion of the BN model to include more targets such as hardness and tensile strength.

4.2.3 Thermal Influence on Microstructure and Mechanical Properties in WAAM-CMT

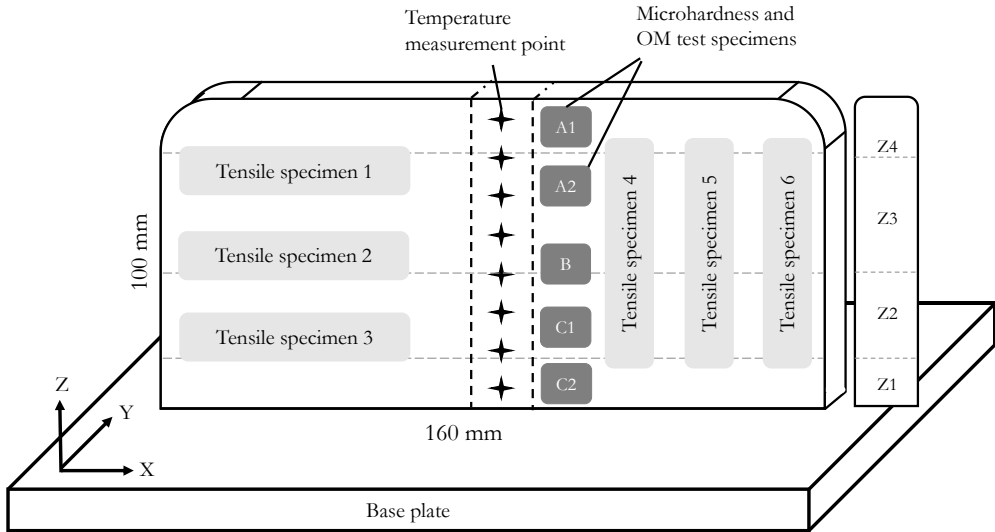
The research presented in **Publication IV** of this manuscript is an experimental characterization of the thermal phenomena observed during WAAM, and its effect on the microstructure and mechanical properties of the final printed part. The results of the study are utilized in **Publication V** of this manuscript for holistic metamodelling of the WAAM process. A detailed account of the results for the study are presented in **Publication IV** of this dissertation. The wall temperature data, hardness and tensile strength properties, and microstructure images were used to characterize the effect of different process parameters (i.e., filler wire material, WFR, TS, and T_0) on the weld properties as detailed below.

A schematic of the printed wall for microstructure and mechanical properties characterization is shown in Figure 17. Using the collected temperature data, four zones of interest from the bottom to the top of the wall, labelled Z1, Z2, Z3, and Z4 in Fig. 16 were identified. The cooling rate of the weld tends to decrease moving from zone Z1 to Z4. This trend has the effect of increasing the wait time to reach the specified interpass temperature between successive depositions. It was observed that the cooling rate reaches a steady state value as the height of the part and number of layers deposited increases; this value appears to be dependent on the material type and energy input. This phenomenon was not examined further in this study.

Image analysis was used to identify the material grain sizes and microstructure phase constituents of the printed specimens. Figure 18 shows the microstructural of the WAAM-built walls for the two parameter sets (M1E1 and M1E2) using G4Si1. The walls printed using AM70 steel alloy also exhibit distinctive microstructural variations as a result of layer-by-layer deposition (Figure 19). A summary of the mechanical property measured is presented below:

The measured YS, UTS, and % elongation values for parameter sets M1E1 and M1E2 for both materials are reported in Table 10. Lower heat input resulted in higher YS and UTS and lower uniform strain (Figure 22). YS and UTS increased by 13 % and 3.8 %, respectively, in G4Si1 steel deposits with the lower energy input parameters (M1E1) than with higher energy input parameters (M1E2). YS increased by 9 % in AM70 steel deposits with the lower energy input parameters (M2E1) than with higher energy input parameters (M2E2). However, in case of UTS the lower energy input parameters (M2E1) saw a 1 % decrease compared to high energy input parameter (M2E2).

Figure 17. Schematic of the deposited wall with locations of temperature measurement and mechanical samples marked along build direction



Percentage elongation at failure was 10 % and 3 % lower in G4Si1 and AM70 deposits respectively, for printing with lower energy input parameters (M1E1 and M2E1) than with higher energy input parameters (M1E2 and M2E2). Higher energy input parameters resulted in increased ductility and reduced hardness for both materials. Owing to a lack of significant anisotropy in G4Si1 deposits due to an equiaxed grain structure, the mechanical properties in the travel direction showed negligibly higher UTS (0.38%) than the samples taken in the build direction. A similar trend was observed for AM70 (increases of 2.7% and 0.24% in YS and UTS, respectively). Even though energy input varied for both materials for the different parameter sets, no significant microstructural changes were observed across the parameter sets for G4Si1, though energy input variation had a significant influence on the material microstructure for AM70. Prior austenite grains were equiaxed/polygonal for M2E1, while they were columnar for M2E2. Higher heat input settings normalized the columnar grains, increasing the sub-grain size. The observed microstructures for M2E1 and M2E2 were comprised of similar phases (i.e., ferrite + bainite + martensite + inclusions).

Figure 18. Optical micrographs (25 μm scale) of WAAM built parts using G4Si1 welding wire for M1E1. Micrographs reported along wall height from top to bottom (sample A1, A2, and B). Phases identified: AF – Acicular ferrite, ALF – Allotriomorphic ferrite, WF – Widmanstätten ferrite, and F – Equiaxed ferrite.

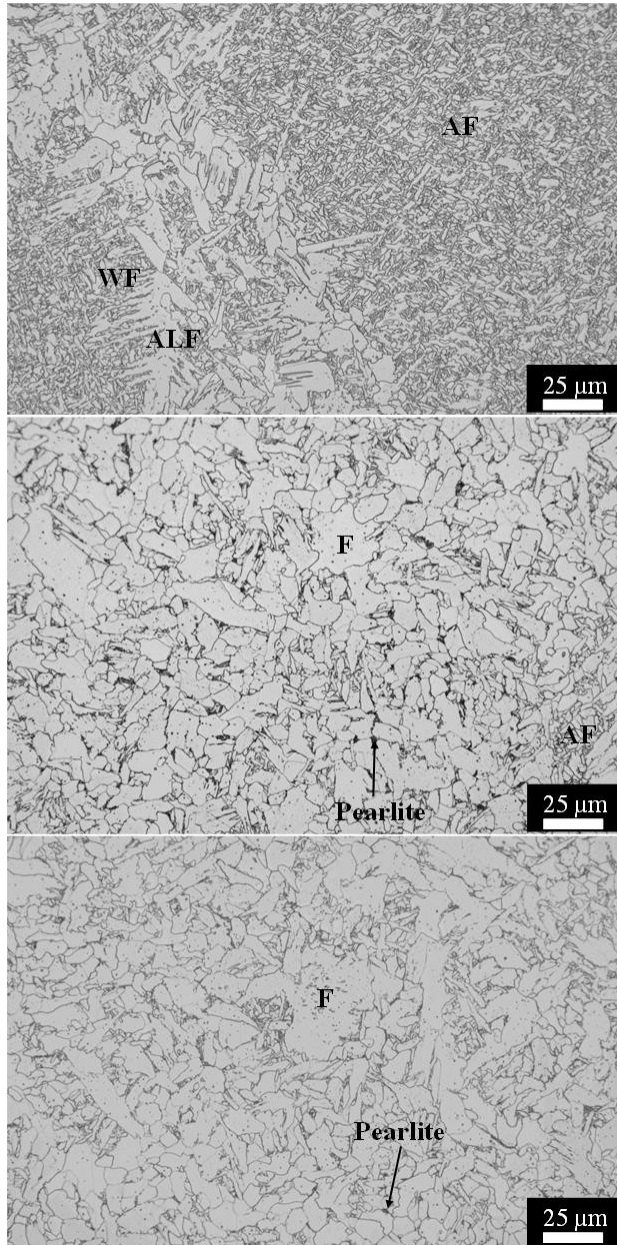
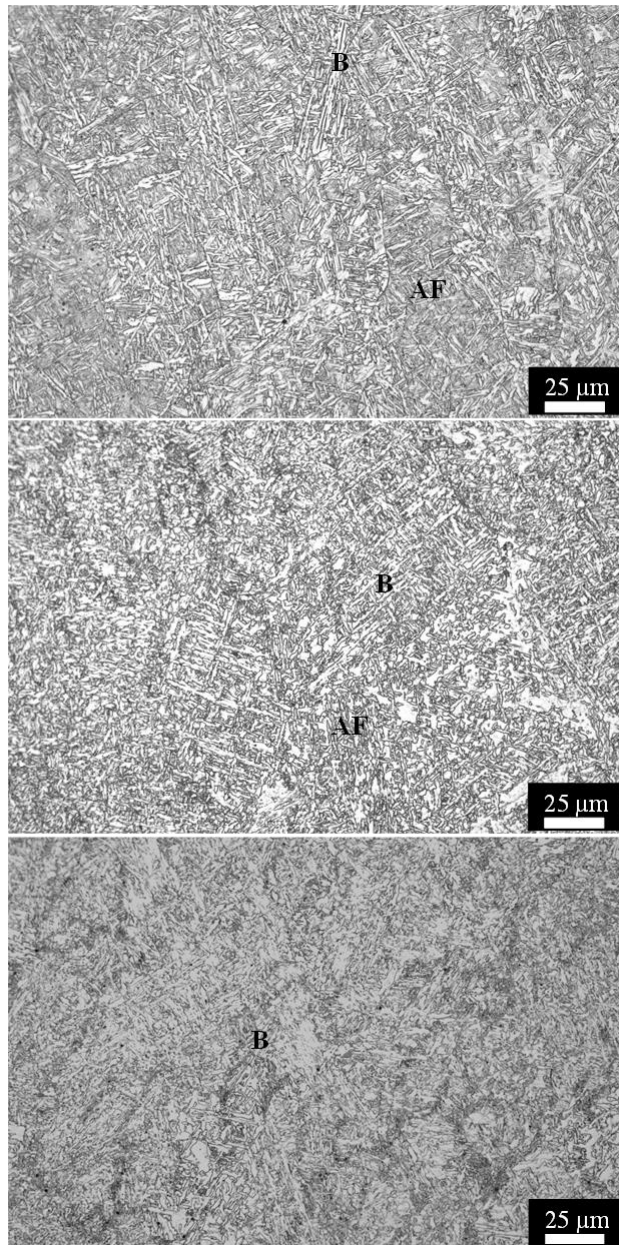


Figure 19. Optical micrographs (25 μm scale) of WAAM built parts using AM70 welding wire for M2E1. Micrographs reported along wall height from top to bottom (samples A1, A2, and B). Phases identified: AF – Acicular ferrite, and B – Bainite



Smaller grain sizes due to higher solidification rates and limited grain growth in lower energy input parameter sets (M1E1 and M2E1) resulted in higher YS and hardness

in both alloys. Since grain boundaries play an essential role in resisting dislocation movement in polycrystalline materials, the observed mechanical property trends are attributed to the presence of more grain boundaries in samples printed using lower energy input parameters.

Table 10. Microstructure and mechanical property results for G4Si1 and AM70 deposits

Tested Sample	HV1	Grain Size (μm)	YS (MPa)	UTS (MPa)	% e	Phase
M1E1-A1	191.90 \pm 9.45	3.21 \pm 2.90	447.20 \pm 0.78	628.35 \pm 17.78	31%	Acicular ferrite with traces of Widmanstätten and allotriomorphic ferrite, bainite
M1E1-A2	168.65 \pm 5.39	4.21 \pm 3.92				Equiaxed ferrite, remanent acicular ferrite, traces of pearlite and bainite
M1E1-B	168.60 \pm 4.85	4.03 \pm 4.30				Equiaxed ferrite and traces of pearlite
M1E1-C1	173.55 \pm 4.10	5.61 \pm 3.15				Equiaxed ferrite and pearlite, allotriomorphic ferrite, remanent acicular ferrite, and traces of bainite
M1E1-C2	248.25 \pm 28.27	2.46 \pm 1.95				Acicular ferrite and traces of Widmanstätten, allotriomorphic ferrite and bainite
M1E2-A1	165.25 \pm 11.92	4.55 \pm 4.83	395.55 \pm 1.62	605.00 \pm 10.60	41%	Acicular ferrite with traces of

						Widmanstätten and allotropic ferrite, bainite
M1E2-A2	155.10 ± 3.26	5.40 ± 4.78				Equiaxed ferrite, remanent acicular ferrite, traces of pearlite and bainite
M1E2-B	155.15 ± 2.16	5.38 ± 4.58				Equiaxed ferrite with trace amounts of pearlite
M1E2-C1	170.45 ± 6.00	3.92 ± 2.34				Equiaxed ferrite and pearlite, allotropic ferrite, remanent acicular ferrite, and traces of bainite
M1E2-C2	190.5 ± 10.63	2.79 ± 2.07				Bainite, acicular ferrite and traces of Widmanstätten and allotropic ferrite
M2E1-A1	311.00 ± 26.18	2*	771.82 ± 0.84	932.96 ± 28.67	25%	Acicular ferrite and bainite
M2E1-A2	271.55 ± 7.58					Bainite and acicular ferrite
M2E1-B	271.45 ± 9.56					Bainite, acicular ferrite, and martensite
M2E1-C1	286.90 ± 11.03					Bainite and acicular ferrite

M2E1-C2	339.17 ± 15.34					Bainite, martensite, acicular ferrite with trace amounts of retained austenite
M2E2-A1	305.30 ± 9.30	2-3*	707.58 ± 3.53	943.34 ± 9.98	28%	Acicular ferrite and bainite
M2E2-A2	266.50 ± 10.62					Bainite and acicular ferrite
M2E2-B	244.95 ± 7.96					Bainite, acicular ferrite, and martensite
M2E2-C1	281.95 ± 12.45					Bainite and acicular ferrite
M2E2-C2	346.25 ± 24.07					Bainite, martensite, acicular ferrite with trace amounts of retained austenite
*Obtained using manual measurement following ASTM E112.						

For printing WAAM parts with uniform microstructure, reducing or eliminating the need for stress relief heat treatment requires understanding the variation in microstructure caused by process-related thermal phenomena. Capturing data related to changes in cooling rates and wait times as a function of part height can help create better computational models which can enable process tuning and optimization. For example, cooling rate can be manipulated through forced heat transfer (conduction and convection) to attain desirable phases in different steels. The work herein will support development of models capable of characterizing the process parameter-process physics-property relationships for a family of steels in **Publication V**.

4.2.4 Holistic Metamodelling of Geometrical and Mechanical Responses in WAAM-CMT

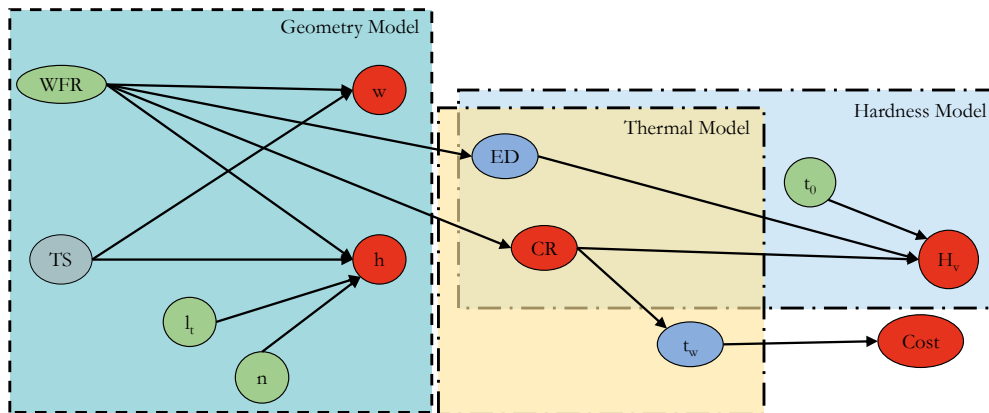
Modelling the impact of the process parameter window to predict part mechanical and geometrical response simultaneously is essential for meeting the demanding product requirements of the industry. Consequently, the specific research objective in Publication V is to model the geometrical dimensions of the weld, cooling rate of the weld and the wait time between layers, and the weld microhardness. Furthermore, the concurrent modelling, simulation, and prediction of material and geometrical response in CMT-WAAM is envisioned in the form of an integrated metamodel. This research presents the integration of the three developed models into a metamodel using the developed modelling framework for mapping the feasible design and performance space for combined process parameter tuning. A detailed account of the study is presented in Publication V of this manuscript. A summary of the modeling and results are presented below:

Three categories of models and associated levels of details exist in this research. The first two models used to represent the geometry and the thermal profile of the weld have the highest level of fidelity due to the significant amount of experimental data points obtained. The thermal profile of the weld is modelled in two different ways: 1) modeling the thermal profile as an average cooling rate of the weld layer using a gaussian process model and 2) modeling the thermal profile as the wait time between layers using Lasso (Least Absolute Shrinkage and Selection Operator) and ordinary least squares regression. The third model representing the mechanical property (microhardness) is less granular and models the microhardness using an artificial neural network with two inputs. The geometric model for the width and height of the weld has been developed by the authors in a previous work (H. P. N. Nagarajan et al. 2019). The geometric model was developed using an ordinary linear regression with the final model obtained in power-law like the thermal model.

Like the geometric model, the wait time between layers is predicted as a function of the WFR, interpass temperature (t_0), n , max temperature of later (MaxT), and the minimum temperature of the layer (MinT) using ordinary least squares (OLS) regression. Additionally, the thermal profile represented by the average cooling rate (CR) of the weld layer is developed as a Kriging model aka. Gaussian process regression (GPR).

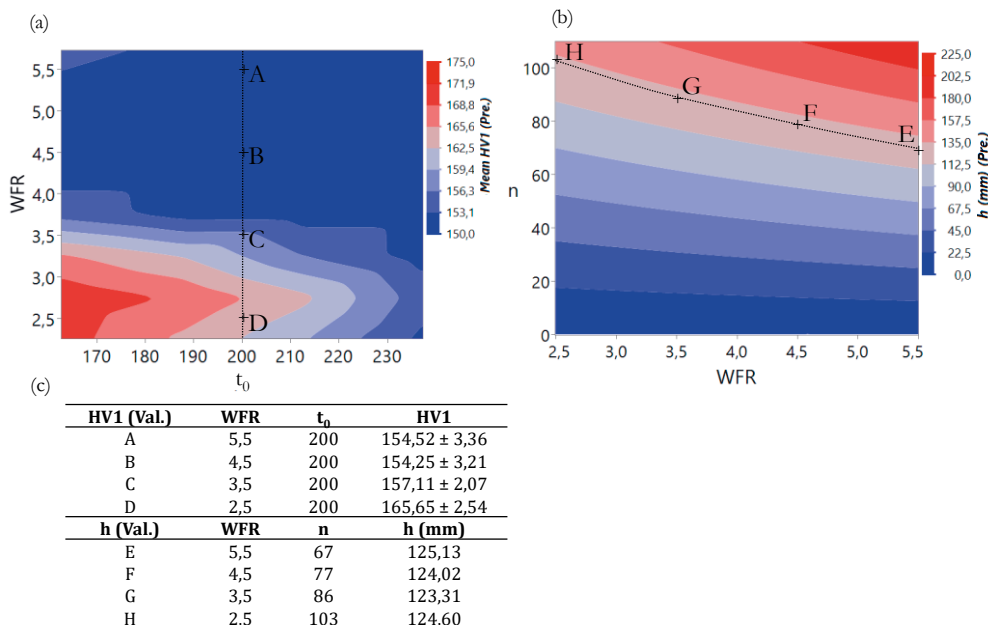
The last model is the model for the material's Vickers hardness (HV). The model in this effort focuses on correlating the WFR and t_0 with their measured HV values.

Figure 20. Composite graph-based meta model integrating models for geometry, thermal profile, and microhardness



A compact artificial neural network model with two hidden layer and six nodes in total are fit for the experimental DOE. The models are composed together using the developed modelling framework into a causal graph as shown in Figure 20.

Figure 21. a) Model prediction and design space for microhardness, dash-line represents the region and point of the validation experiments, b) Model prediction and design space for weld height, dash-line represents the region and point of the validation experiments, and c) Experimental validation results for microhardness and weld height.



The developed graph is converted into a DAG for implementing a BN for simulation. Multiple objectives can be propagated for model simulation within the probabilistic BN model and the predicted value ranges effectively present the global design space within which targeted optimization strategies can be implemented. The initial simulation of the BN was performed for design space exploration.

The simulated values of the developed Bayesian meta model were used to model the design space for HV1 and weld height in Figure 21a and 21b respectively in the form of surface response graphs. The simulated values of HV and weld height from the BN is shown in Figure 21c. The values are decomposed in two groups, (A, B, C, D) for the microhardness tests and (E, F, G, H) for the weld height validation. The dash-line in the 2D response surfaces in Figure 21 represents the region in the design space where the validation prints lie. The results of the BN metamodel simulation shows that the developed approach can support design space exploration to concurrently tune the input parameters to obtain the desired microhardness HV1 and weld height h . The metamodel is helpful in characterizing known and new materials alike for process parameter tuning to achieve desired geometric and mechanical strength characteristics.

4.3 Usability of the Developed Framework

This dissertation research presents a metamodeling framework for advanced manufacturing process and product characterization using directed graphs and machine learning. The usability of the framework has been demonstrated through modelling use cases for the FDM and WAAM processes. The development of directed graphs allowed for integration of pre-existing knowledge to develop multidomain metamodels for the two AM processes. Simulation of the developed metamodels was facilitated using machine learning approaches such as ANNs and BNs to perform in-process decision making for process parameter tuning and optimization. However, the developed metamodels are not able to holistically represent all functional aspects of the two AM processes. For example, topology optimization is an ongoing design strategy for developing low weight, low-cost functional components using AM which introduces a high level of geometrical complexity in the process. This increased geometrical complexity must be addressed in future work such that models integrate the trajectory planning of the nozzle along with precise temperature control of the polymer or molten metal. Trajectory planning plays an important role in affecting the flow of deposited material and the

temperature profile. In WAAM, multi-axis arm robots are employed for nozzle trajectory control; thus, collision detection algorithms must also be integrated to ensure defect free deposition. Thus, to support development of holistic metamodels for use in process control applications, future modelling efforts must integrate path planning with process parameter control in the form of new functions and attributes. These additional function models can be used to update existing graph models. In this manner, it can be seen that the modular nature of the developed framework allows for easy integration of new knowledge about a process or product to be introduced into an existing model.

The framework developed herein supports homogenous composition of different forms of knowledge into a simulation model at the early stages of design using only partial or incomplete knowledge about the product or process. Knowledge is composed together using functions and bond graph elements to form a homogenous graph model. However, the accuracy of the model can be affected by the completeness and level of detail included in the functions. Thus, a designer must be conscious in introducing the influencing variables associated with each function. Detailed function modelling can help alleviate accuracy issues, provided the completeness of functions can be ensured.

A challenge in the development of simulatable metamodels is the presence of looping functions in the graph. A prerequisite for the development of probabilistic machine learning models such as BN is the use of a directed acyclic graph for model fitting. Looping functions in the graph model would therefore need to be addressed to ensure that a simulation model can be developed. The TRIZ principles of *ideation* and *separation* may be applied in the functional architecture to de-loop functions and ensure one-directional dependency flow in a graph model. The process of function restructuring is not directly supported by the framework and the user is responsible for analysing and minimizing the effect of the changes on model performance.

Finally, the causality of parameters captured by the developed graph models can be affected by the type of data and models used as pre-existing knowledge. The framework suggests functional models should be mapped to BG elements to concretize the abstract functional models. The causality extraction algorithm applied is adapted from existing validated causal rules in BG theory. However, establishing the graph from existing models is also possible without mapping the functions to the BG elements, since the framework separates variables into defined categories. Though the variable relationships modelled can be verified to be causally linked (e.g., (Harding and Seefeldt 2013; Chockler 2016), the developed framework does not suggest an approach for such a validation. Thus, evaluation of the effectiveness of

the model as a causal graph is left up to the user. Nevertheless, the demonstrated framework is a generic modelling approach whose maturity can be improved through application to different process and system modelling across various domains (e.g., product design and development, supply chain management, and network cybersecurity). The addition of new attributes, methods, and tools and analysis capabilities can improve upon the framework through future research. These potential extensions are briefly presented in the next section.

5 CONCLUSIONS AND FUTURE WORK

This research was undertaken to advance technology integration efforts for AM in response to the increasing need for product and process performance improvement. In additive manufacturing, product customization enables unique product benefits, but simultaneously introduces a higher level of process complexity, which directly affect the reliability and repeatability of production. Thus, it is important for manufacturers to make informed decisions towards development of products for AM through holistic system modelling and simulation. Additionally, it is important that such decisions rely on accurate product and process data to improve production efficiency. At present, holistic system modelling requires an array of heterogeneous models for a single AM technology. However, the inclusion of different AM process activities/functions, geometries, and materials makes it a challenge to compose the necessary subsystem-level heterogeneous models into a holistic system model.

Thus, the main goal of this research is to present a digitized approach for holistically modelling AM systems for quantitative analysis (scenario analysis, decision making, design space exploration, and optimization) through simulation. This goal is pursued by addressing three primary research objectives in the five publications as shown in Table 4 of this dissertation. Thus, a graph-based metamodeling framework is developed for holistic characterization of AM systems through the following tasks:

1. Development of a modelling approach using knowledge graphs or causal graphs for characterizing AM systems. The graph-based modelling enables the integration of different forms of knowledge (functional requirements, pre-existing models/equations, and data) into a unified representation. Graphical models presented in this research characterize linkages between a mechanism and resultant phenomena and provide more model transparency than data-driven surrogate modelling approaches.
2. The developed graph metamodel is used as a precursor to train different machine learning algorithms to enable simulation analysis of the metamodel. The graph-based representation allows for training both deterministic and probabilistic machine learning approaches. The

developed approach is lean and enables faster simulation of the holistic metamodel when compared to higher fidelity simulation models.

3. The developed framework is applied for characterizing two additive manufacturing processes namely, FDM and WAAM in four modelling case studies as presented in Publication I, II, III, and V of this manuscript. The simulation of the developed case study metamodels aid in quantitative analysis of the evaluated system for prediction analysis, decision support, design space exploration, and system optimization.

Learnings from this research support adoption of AM technology for mainstream manufacturing as follows:

1. The graph-based metamodeling framework provides a uniform approach for representing the cause-effect relationships between different variables of a system. In addition, it allows for composing different forms of knowledge from different domains together into a unified representation. The use of pre-existing knowledge enables faster development of models with less demand for time-intensive experiments.
2. The graph metamodel acts as a pre-cursor for applying machine learning algorithms to enable simulation analysis. Simulations play an important role in facilitating an efficient design process through sensitivity analysis, multi-domain optimizations and at early design stages, analysis of risk and uncertainty resulting from limited knowledge. The graph metamodel enables faster computation of performance measures in comparison to high-fidelity simulation models. Faster simulation times can support development of monitoring and control systems for AM.
3. Translating product design information, manufacturing process information, and mathematical process models through holistic modelling and simulation will enable for better design and production of products for additive manufacturing through quantitative analysis. The use and development of the metamodeling framework allowed for predicting and controlling the process outputs in FDM and WAAM. This understanding can promote reliable and repeatable AM operations through informed decision making.

The future research development envisioned for the methodology have been identified as a direct result of this research, which include:

1. Automation of the developed modelling approach. The current modelling efforts implement the different steps in the framework independently. The development of a software-based solution can provide a standardized approach to modelling and accelerate the development time for graph metamodels. A dedicated software package can provide more functionality and accessibility to users for quantitative analysis of the metamodels.
2. Integration of qualitative and quantitative analysis methods into the framework for simulating the developed metamodel at different levels of fidelity. Coupling of the graph metamodeling framework with machine learning has been shown in this research to be beneficial in simulation. Similarly, principles from system dynamics can help evaluate looping functions in the graphs and constraint programming may be integrated to expand the analysis capabilities of the developed framework.
3. The use of transfer learning may be investigated for using the graph model structure and functions as pre-existing knowledge for modeling similar technologies or systems. Transfer learning can drastically reduce model development time and promote interoperability in AM.

6 REFERENCES

- A. Simon, Herbert, and Yumi Iwasaki. 1988. "Causal Ordering, Comparative Statics, and near Decomposability." *Journal of Econometrics* 39 (1): 149–73. [https://doi.org/10.1016/0304-4076\(88\)90043-7](https://doi.org/10.1016/0304-4076(88)90043-7).
- Abdulhameed, Osama, Abdulrahman Al-Ahmari, Wadea Ameen, and Syed Hammad Mian. 2019. "Additive Manufacturing: Challenges, Trends, and Applications." *Advances in Mechanical Engineering* 11 (2): 1687814018822880. <https://doi.org/10.1177/1687814018822880>.
- Ahmad, Subutai, and Gerald Tesauro. 1989. "Scaling and Generalization in Neural Networks: A Case Study." In .
- Alfaro, Sadek Crisóstomo Absi, and Eber Huanca Cayo. 2012. "Sensing Fusion Data from the Optic and Acoustic Emissions of Electric Arcs in the GMAW-S Process for Welding Quality Assessment." *Sensors* 12 (6): 6953–66.
- Aliferis, Constantin F, Alexander Statnikov, Ioannis Tsamardinos, Subramani Mani, and Xenofon D Koutsoukos. 2010. "Local Causal and Markov Blanket Induction for Causal Discovery and Feature Selection for Classification Part I: Algorithms and Empirical Evaluation." *Journal of Machine Learning Research* 11 (1).
- Almeida, PS, and S Williams. 2010. "Innovative Process Model of Ti–6Al–4V Additive Layer Manufacturing Using Cold Metal Transfer (CMT)." In *Proceedings of the Twenty-First Annual International Solid Freeform Fabrication Symposium, University of Texas at Austin, Austin, TX, USA*.
- Altıparmak, Sadettin Cem, and Bowen Xiao. 2021. "A Market Assessment of Additive Manufacturing Potential for the Aerospace Industry." *Journal of Manufacturing Processes* 68 (August): 728–38. <https://doi.org/10.1016/j.jmapro.2021.05.072>.
- Antti-Poika, Mari, Juhani Hassi, and Lauri Pyy. 1977. "Respiratory Diseases in Arc Welders." *International Archives of Occupational and Environmental Health* 40 (3): 225–30. <https://doi.org/10.1007/BF01842087>.

- Asano, Tetsuo, Binay Bhattacharya, Mark Keil, and Frances Yao. 1988. "Clustering Algorithms Based on Minimum and Maximum Spanning Trees." In , 252–57.
- Atashkari, K, N Nariman-Zadeh, M Gölcü, A Khalkhali, and A Jamali. 2007. "Modelling and Multi-Objective Optimization of a Variable Valve-Timing Spark-Ignition Engine Using Polynomial Neural Networks and Evolutionary Algorithms." *Energy Conversion and Management* 48 (3): 1029–41.
- Atif Yardimci, M, and Selçuk Güçeri. 1996. "Conceptual Framework for the Thermal Process Modelling of Fused Deposition." *Rapid Prototyping Journal* 2 (2): 26–31.
- Atlas, L., R. Cole, Y. Muthusamy, A. Lippman, J. Connor, D. Park, M. El-Sharkawai, and R. J. Marks. 1990. "A Performance Comparison of Trained Multilayer Perceptrons and Trained Classification Trees." *Proceedings of the IEEE* 78 (10): 1614–19. <https://doi.org/10.1109/5.58347>.
- Balkhyour, Mansour Ahmed, and Mohammad Khalid Goknil. 2010. "Total Fume and Metal Concentrations during Welding in Selected Factories in Jeddah, Saudi Arabia." *International Journal of Environmental Research and Public Health* 7 (7): 2978–87. <https://doi.org/10.3390/ijerph7072978>.
- Bandyopadhyay, Amit, Yanning Zhang, and Susmita Bose. 2020. "Recent Developments in Metal Additive Manufacturing." *Current Opinion in Chemical Engineering, Materials Engineering • Separations Engineering*, 28 (June): 96–104. <https://doi.org/10.1016/j.coche.2020.03.001>.
- Barenblatt, GI. 1979. "Similarity, Self-Similarity, and Intermediate Asymptotics." *Consultants Bureau, New York*.
- Barenblatt, Grigory Isaakovich. 1987. *Dimensional Analysis*. CRC Press.
- Barhad, B, D Teculescu, and O Crăciun. 1975. "Respiratory Symptoms, Chronic Bronchitis, and Ventilatory Function in Shipyard Welders." *International Archives of Occupational and Environmental Health* 36 (2): 137–50.
- Batchelder, John S, Huntington W Curtis, Douglas S Goodman, Franklin Gracer, Robert R Jackson, George M Koppelman, and John D Mackay. 1994. "Model Generation System Having Closed-Loop Extrusion Nozzle Positioning," April.

- Bayat, Mohamad, Wen Dong, Jesper Thorborg, Albert C. To, and Jesper H. Hattel. 2021. "A Review of Multi-Scale and Multi-Physics Simulations of Metal Additive Manufacturing Processes with Focus on Modeling Strategies." *Additive Manufacturing* 47 (November): 102278. <https://doi.org/10.1016/j.addma.2021.102278>.
- Bayesia USA. n.d. "BayesiaLab 8 - Bayesian Networks for Research and Analytics." Accessed December 28, 2018. <https://www.bayesiab.com>.
- Bellehumeur, Céline, Longmei Li, Qian Sun, and Peihua Gu. 2004. "Modeling of Bond Formation between Polymer Filaments in the Fused Deposition Modeling Process." *Journal of Manufacturing Processes* 6 (2): 170–78.
- Bengio, Yoshua, Ian J. Goodfellow, and Aaron Courville. 2015. "Deep Learning." *Nature* 521: 436–44.
- Borutzky, Wolfgang. 2011. *Bond Graph Modelling of Engineering Systems*. Vol. 103. Springer.
- Bourell, D. L., M.C. Leu, and D.W. Rosen. 2009. "Roadmap for Additive Manufacturing: Identifying the Future of Freeform Processing." *The University of Texas at Austin Laboratory for Freeform Fabrication Advanced Manufacturing Center*.
- Bradshaw, Lisa M, David Fishwick, Tania Slater, and Neil Pearce. 1998. "Chronic Bronchitis, Work Related Respiratory Symptoms, and Pulmonary Function in Welders in New Zealand." *Occupational and Environmental Medicine* 55 (3): 150–54.
- Bridgman, PW. n.d. "Dimensional Analysis, 1922." *Phil. Mag* 2 (12): 1263–66.
- Chan, Rothanak, Sriram Manoharan, and Karl R. Haapala. 2017. "Comparing the Sustainability Performance of Metal-Based Additive Manufacturing Processes." *ASME. International Design Engineering Technical Conferences and Computers and Information in Engineering Conference* 4 (2nd Design for Manufacturing and the Life Cycle Conference): V004T05A039. <https://doi.org/10.1115/DETC2017-68262>.
- Chen, Shenglei, Geoffrey I Webb, Linyuan Liu, and Xin Ma. 2020. "A Novel Selective Naïve Bayes Algorithm." *Knowledge-Based Systems* 192: 105361.

- Chen, Ze, Changjun Han, Ming Gao, Sastry Yagnanna Kandukuri, and Kun Zhou. 2022. "A Review on Qualification and Certification for Metal Additive Manufacturing." *Virtual and Physical Prototyping* 17 (2): 382–405. <https://doi.org/10.1080/17452759.2021.2018938>.
- Chinn, DJ, JE Cotes, FM El Gamal, and JF Wollaston. 1995. "Respiratory Health of Young Shipyard Welders and Other Tradesmen Studied Cross Sectionally and Longitudinally." *Occupational and Environmental Medicine* 52 (1): 33–42.
- Chockler, Hana. 2016. "Causality and Responsibility for Formal Verification and Beyond." *ArXiv Preprint ArXiv:1608.07879*.
- Coatanéa, E., R. Roca, H. Mokhtarian, F. Mokammel, and K. Ikkala. 2016. "A Conceptual Modeling and Simulation Framework for System Design." *Computing in Science Engineering* 18 (4): 42–52. <https://doi.org/10.1109/MCSE.2016.75>.
- Coatanéa, Eric. 2005. *Conceptual Modelling of Life Cycle Design: A Modelling and Evaluation Method Based on Analogies and Dimensionless Numbers*. Helsinki University of Technology.
- Cole, Homer, Seymour Epstein, and Jon Peace. 2007. "Particulate and Gaseous Emissions When Welding Aluminum Alloys." *Journal of Occupational and Environmental Hygiene* 4 (9): 678–87.
- Cotes, JE, EL Feinmann, VJ Male, FS Rennie, and CA Wickham. 1989. "Respiratory Symptoms and Impairment in Shipyard Welders and Caulker/Burners." *Occupational and Environmental Medicine* 46 (5): 292–301.
- Craeghs, Tom, Stijn Clijsters, Evren Yasa, and Jean-Pierre Kruth. 2011. "Online Quality Control of Selective Laser Melting." In *Proceedings of the Solid Freeform Fabrication Symposium, Austin, TX*, 212–26. <http://sffsymposium.engr.utexas.edu/Manuscripts/2011/2011-17-Craeghs.pdf>.
- Dawson, CW, and RL Wilby. 2001. "Hydrological Modelling Using Artificial Neural Networks." *Progress in Physical Geography* 25 (1): 80–108.
- Ding, Donghong, Zengxi Pan, Dominic Cuiuri, and Huijun Li. 2015. "Wire-Feed Additive Manufacturing of Metal Components: Technologies, Developments and Future Interests." *The International Journal of Advanced*

Manufacturing Technology 81 (1–4): 465–81. <https://doi.org/10.1007/s00170-015-7077-3>.

Efthymiou, Konstantinos, Konstantinos Sipsas, Dimitris Mourtzis, and George Chryssolouris. 2015. “On Knowledge Reuse for Manufacturing Systems Design and Planning: A Semantic Technology Approach.” *CIRP Journal of Manufacturing Science and Technology* 8: 1–11.

El-Zein, M, JL Malo, C Infante-Rivard, and D Gautrin. 2003. “Prevalence and Association of Welding Related Systemic and Respiratory Symptoms in Welders.” *Occupational and Environmental Medicine* 60 (9): 655–61.

F42 Committee. 2016. “Standard Guide for Directed Energy Deposition of Metals.” ASTM International. <https://doi.org/10.1520/F3187-16>.

F42.91 Subcommittee. 2012. “Terminology for Additive Manufacturing Technologies (ASTM F2792-12a).” ASTM International, Conshohocken, PA. <http://www.astm.org/Standards/F2792.htm>.

Filippo, Jenny Montbrun-Di, Marisol Delgado, Claude Brie, and Henry M. Paynter. 1991. “A Survey of Bond Graphs : Theory, Applications and Programs.” *Journal of the Franklin Institute* 328 (5): 565–606. [https://doi.org/10.1016/0016-0032\(91\)90044-4](https://doi.org/10.1016/0016-0032(91)90044-4).

Fogh, Anne, Jørgen Frost, and Johan Georg. 1969. “Respiratory Symptoms and Pulmonary Function in Welders.” *Annals of Occupational Hygiene* 12 (4): 213–18.

Francois, Marianne M, Amy Sun, Wayne E King, Neil Jon Henson, Damien Tourret, Ccut Allan Bronkhorst, Neil N Carlson, Christopher Kyle Newman, T Haut, and Jozsef Bakosi. 2017. “Modeling of Additive Manufacturing Processes for Metals: Challenges and Opportunities.” *Current Opinion in Solid State and Materials Science* 21 (4): 198–206.

Frazier, William E. 2014. “Metal Additive Manufacturing: A Review.” *Journal of Materials Engineering and Performance* 23 (6): 1917–28. <https://doi.org/10.1007/s11665-014-0958-z>.

Fronius International GbmH. n.d. “TransPuls Synergic 5000 CMT.” TransPuls Synergic 5000 CMT. Accessed July 31, 2018. <http://www.fronius.com/en/welding-technology/products/manual->

welding/mig/transpuls-synergic/transpuls-synergic-cmt/transpuls-synergic-5000-cmt.

- Gibson, Ian, David Rosen, and Brent Stucker. 2015. *Additive Manufacturing Technologies: 3D Printing, Rapid Prototyping, and Direct Digital Manufacturing*. 2nd ed. New York: Springer-Verlag. <https://www.springer.com/us/book/9781493921126>.
- Girinath, B, N Siva Shanmugam, and K Sankaranarayananasamy. 2018. "Weld Bead Graphical Prediction of Cold Metal Transfer Weldment Using ANFIS and MRA Model on Matlab Platform." *SIMULATION: Transactions of the Society for Modeling and Simulation International* 95 (8): 725–36. <https://doi.org/10.1177/0037549718809162>.
- Gube, Monika, Peter Brand, Thomas Schettgen, Jens Bertram, Kerstin Gerards, Uwe Reisingen, and Thomas Kraus. 2013. "Experimental Exposure of Healthy Subjects with Emissions from a Gas Metal Arc Welding Process—Part II: Biomonitoring of Chromium and Nickel." *International Archives of Occupational and Environmental Health* 86 (1): 31–37. <https://doi.org/10.1007/s00420-012-0738-8>.
- Hammond, S Katharine, Ellen Gold, Robin Baker, Patricia Quinlan, William Smith, Robert Pandya, and John Balmes. 2005. "Respiratory Health Effects Related to Occupational Spray Painting and Welding." *Journal of Occupational and Environmental Medicine* 47 (7): 728–39.
- Harding, David J, and Kristin S Seefeldt. 2013. "Mixed Methods and Causal Analysis." In *Handbook of Causal Analysis for Social Research*, 91–110. Springer.
- Heckerman, David, Dan Geiger, and David M. Chickering. 1995. "Learning Bayesian Networks: The Combination of Knowledge and Statistical Data." *Machine Learning* 20.
- Heung, William, Myoung-Jin Yun, Daniel PY Chang, Peter G Green, and Chris Halm. 2007. "Emissions of Chromium (VI) from Arc Welding." *Journal of the Air & Waste Management Association* 57 (2): 252–60.
- Hilmas, Greg E, John L Lombardi, Robert A Hoffman, and Kevin Stuffle. 1996. "Recent Developments in Extrusion Freeform Fabrication (EFF) Utilizing Non-Aqueous Gel Casting Formulations." In , 443–50.

- Hirtz, Julie, Robert B Stone, Daniel A McAdams, Simon Szykman, and Kristin L Wood. 2002. "A Functional Basis for Engineering Design: Reconciling and Evolving Previous Efforts." *Research in Engineering Design* 13 (2): 65–82.
- Hjortsberg, Ulf, P Orbaek, and Måns Arborelius. 1992. "Small Airways Dysfunction among Non-Smoking Shipyard Arc Welders." *Occupational and Environmental Medicine* 49 (6): 441–44.
- Hochreiter, Sepp, Yoshua Bengio, Paolo Frasconi, and Jürgen Schmidhuber. 2001. *Gradient Flow in Recurrent Nets: The Difficulty of Learning Long-Term Dependencies*. A field guide to dynamical recurrent neural networks. IEEE Press.
- Huang, Samuel H., Peng Liu, Abhiram Mokasdar, and Liang Hou. 2013. "Additive Manufacturing and Its Societal Impact: A Literature Review." *The International Journal of Advanced Manufacturing Technology* 67 (5): 1191–1203. <https://doi.org/10.1007/s00170-012-4558-5>.
- Huang, Yong, Ming C. Leu, Jyoti Mazumder, and Alkan Donmez. 2015. "Additive Manufacturing: Current State, Future Potential, Gaps and Needs, and Recommendations." *Journal of Manufacturing Science and Engineering* 137 (1): 014001.
- Iwasaki, Yumi, and Herbert A. Simon. 1994. "Causality and Model Abstraction." *Artificial Intelligence* 67 (1): 143–94. [https://doi.org/10.1016/0004-3702\(94\)90014-0](https://doi.org/10.1016/0004-3702(94)90014-0).
- Jafari, Ahmad J., and Mohammad J. Assari. 2004. "Respiratory Effects from Work-Related Exposure to Welding Fumes in Hamadan, Iran." *Archives of Environmental Health: An International Journal* 59 (3): 116–20. <https://doi.org/10.3200/AEOH.59.3.116-120>.
- Jayawardana, Pushpa, and Chrisantha Abeyseena. 2009. "Respiratory Health of Welders in a Container Yard, Sri Lanka." *Occupational Medicine* 59 (4): 226–29.
- Jing, Liting, Bowen Tan, Shaofei Jiang, and Junfeng Ma. 2021. "Additive Manufacturing Industrial Adaptability Analysis Using Fuzzy Bayesian Network." *Computers & Industrial Engineering* 155: 107216.
- Jones, B, Ian Jenkinson, Zaili Yang, and Jin Wang. 2010. "The Use of Bayesian Network Modelling for Maintenance Planning in a Manufacturing Industry." *Reliability Engineering & System Safety* 95 (3): 267–77.

- Karnopp, D, D Margolis, and R Rosemberg. 2000. "Analysis and Design of Engineering Systems."
- Keane, Michael, Arlen Siert, Samuel Stone, and Bean T. Chen. 2016. "Profiling Stainless Steel Welding Processes to Reduce Fume Emissions, Hexavalent Chromium Emissions and Operating Costs in the Workplace." *Journal of Occupational and Environmental Hygiene* 13 (1): 1–8. <https://doi.org/10.1080/15459624.2015.1072634>.
- Kellens, Karel, Raya Mertens, Dimos Paraskevas, Wim Dewulf, and Joost R. Duflou. 2017. "Environmental Impact of Additive Manufacturing Processes: Does AM Contribute to a More Sustainable Way of Part Manufacturing?" In *Proceedings of the 24th CIRP Conference on Life Cycle Engineering*, 61:582–87. Kamakura, Japan: Elsevier. <https://doi.org/10.1016/j.procir.2016.11.153>.
- Khorasani, Mahyar, Jennifer Loy, Amir Hossein Ghasemi, Elmira Sharabian, Martin Leary, Hamed Mirafzal, Peter Cochrane, Bernard Rolfe, and Ian Gibson. 2022. "A Review of Industry 4.0 and Additive Manufacturing Synergy." *Rapid Prototyping Journal* ahead-of-print (ahead-of-print). <https://doi.org/10.1108/RPJ-08-2021-0194>.
- Kilburn, Kaye H, Raphael H Warshaw, C Thomas Boylen, and John C Thornton. 1989. "Respiratory Symptoms and Functional Impairment from Acute (Cross-Shift) Exposure to Welding Gases and Fumes." *The American Journal of the Medical Sciences* 298 (5): 314–19.
- Koh, D.-H., J.-I. Kim, K.-H. Kim, and S.-W. Yoo. 2015. "Welding Fume Exposure and Chronic Obstructive Pulmonary Disease in Welders." *Occupational Medicine* 65 (1): 72–77. <https://doi.org/10.1093/occmed/kqu136>.
- Koller, Daphne, Nir Friedman, Sašo Džeroski, Charles Sutton, Andrew McCallum, Avi Pfeffer, Pieter Abbeel, Ming-Fai Wong, David Heckerman, and Chris Meek. 2007. *Introduction to Statistical Relational Learning*. MIT press.
- Kou, Sindo. 2003. "Welding Metallurgy." *New Jersey, USA*, 431–46.
- Kroll, Andreas. 2000. "Grey-Box Models: Concepts and Application." *New Frontiers in Computational Intelligence and Its Applications* 57: 42–51.
- Kwak, Yong-Min, and Charalabos Doumanidis. 2002. "Geometry Regulation of Material Deposition in Near-Net Shape Manufacturing by Thermally Scanned Welding." *Journal of Manufacturing Processes* 4 (1).

- Lavoie, Marie, and James L. Addis. 2018. "Harnessing the Potential of Additive Manufacturing Technologies: Challenges and Opportunities for Entrepreneurial Strategies." *International Journal of Innovation Studies* 2 (4): 123–36. <https://doi.org/10.1016/j.ijis.2018.11.001>.
- Lewis, RW, and RS Ransing. 1997. "A Semantically Constrained Bayesian Network for Manufacturing Diagnosis." *International Journal of Production Research* 35 (8): 2171–88.
- Li, Guojun Jane, Long-Lian Zhang, Ling Lu, Ping Wu, and Wei Zheng. 2004. "Occupational Exposure to Welding Fume among Welders: Alterations of Manganese, Iron, Zinc, Copper, and Lead in Body Fluids and the Oxidative Stress Status." *Journal of Occupational and Environmental Medicine* 46 (3): 241–48. <https://doi.org/10.1097/01.jom.0000116900.49159.03>.
- Luo, Jiin-Chyuan John, Kuang-Hung Hsu, and Wu-Shiun Shen. 2009. "Inflammatory Responses and Oxidative Stress from Metal Fume Exposure in Automobile Welders." *Journal of Occupational and Environmental Medicine* 51 (1): 95–103.
- Magnier, Laurent, and Fariborz Haghghat. 2010. "Multiobjective Optimization of Building Design Using TRNSYS Simulations, Genetic Algorithm, and Artificial Neural Network." *Building and Environment* 45 (3): 739–46.
- Mashhadi, Ardeshir Raihanian, Behzad Esmacilian, and Sara Behdad. 2015. "Impact of Additive Manufacturing Adoption on Future of Supply Chains," June, V001T02A064. <https://doi.org/10.1115/MSEC2015-9392>.
- "Material Extrusion-Based Additive Manufacturing." 2022. In *Wikipedia*. https://en.wikipedia.org/w/index.php?title=Material_extrusion-based_additive_manufacturing&oldid=1067574041.
- Mazumder, J, D Dutta, N Kikuchi, and A Ghosh. 2000. "Closed Loop Direct Metal Deposition: Art to Part." *Optics and Lasers in Engineering, Laser Material Processing*, 34 (4–6): 397–414. [https://doi.org/10.1016/S0143-8166\(00\)00072-5](https://doi.org/10.1016/S0143-8166(00)00072-5).
- McCormick, Liam M, Martin Goddard, and Ravi Mahadeva. 2008. "Pulmonary Fibrosis Secondary to Siderosis Causing Symptomatic Respiratory Disease: A Case Report." *Journal of Medical Case Reports* 2 (1): 257.

- McMILLAN, Grant HG, and RJ Pethybridge. 1983. "The Health of Welders in Naval Dockyards: Proportional Mortality Study of Welders and Two Control Groups." *Occupational Medicine* 33 (2): 75–84.
- Mezrag, Bachir, Frédéric Deschaux-Beaume, and Mustapha Benachour. 2015. "Control of Mass and Heat Transfer for Steel/Aluminium Joining Using Cold Metal Transfer Process." *Science and Technology of Welding and Joining* 20 (3): 189–98.
- Mokhtarian, Hossein, Azarakhsh Hamed, Hari P. N. Nagarajan, Suraj Panicker, Eric Coatanéa, and Karl Haapala. 2019. "Probabilistic Modelling of Defects in Additive Manufacturing: A Case Study in Powder Bed Fusion Technology." *Procedia CIRP*, 52nd CIRP Conference on Manufacturing Systems (CMS), Ljubljana, Slovenia, June 12-14, 2019, 81 (January): 956–61. <https://doi.org/10.1016/j.procir.2019.03.234>.
- Monma, Clyde, Michael Paterson, Subhash Suri, and Frances Yao. 1990. "Computing Euclidean Maximum Spanning Trees." *Algorithmica* 5 (1): 407–19.
- Mur, JM, D Teculescu, QT Pham, M Gaertner, N Massin, C Meyer-Bisch, JJ Moulin, F Diebold, F Pierre, and B Meurou-Poncelet. 1985. "Lung Function and Clinical Findings in a Cross-Sectional Study of Arc Welders." *International Archives of Occupational and Environmental Health* 57 (1): 1–17.
- Nagarajan, Hari, Hossein Mokhtarian, Hessam Jafarian, Saoussen Dimassi, Shahriar Bakrani, Azarakhsh Hamed, Eric Coatanéa, G. Gary Wang, and Karl Haapala. 2019. "Knowledge-Based Design of Artificial Neural Network Topology for Additive Manufacturing Process Modeling: A New Approach and Case Study for Fused Deposition Modeling." *Journal of Mechanical Design* 141 (February): 02170501–12. <https://doi.org/10.1115/1.4042084>.
- Nagarajan, Hari P. N., and Karl R. Haapala. 2017. "Environmental Performance Evaluation of Direct Metal Laser Sintering through Exergy Analysis." *Procedia Manufacturing*, 45th SME North American Manufacturing Research Conference, NAMRC 45, Los Angeles, CA, USA, 10: 957–67. <https://doi.org/10.1016/j.promfg.2017.07.087>.
- Nagarajan, Hari P. N., Hossein Mokhtarian, Hesam Jafarian, Saoussen Dimassi, Shahriar Bakrani-Balani, Azarakhsh Hamed, Eric Coatanéa, G. Gary Wang, and Karl R. Haapala. 2018. "Knowledge-Based Design of Artificial Neural Network Topology for Additive Manufacturing Process Modeling: A New Approach and Case Study for Fused Deposition Modeling." *Journal of*

- Nagarajan, Hari P. N., Suraj Panicker, Hossein Mokhtarian, Théo Remy-Lorit, Eric Coatanéa, Romaric Prod'hon, Hesam Jafarian, Karl R. Haapala, and Ananda Chakraborti. 2019. "Graph-Based Metamodeling for Characterizing Cold Metal Transfer Process Performance." *Smart and Sustainable Manufacturing Systems* 3 (2): 20190026. <https://doi.org/10.1520/SSMS20190026>.
- Nakadate, Toshio, Yoshiharu Aizawa, Takashi Yagami, Yi-Qin Zheg, Makoto Kotani, and Kouichi Ishiwata. 1998. "Change in Obstructive Pulmonary Function as a Result of Cumulative Exposure to Welding Fumes as Determined by Magnetopneumography in Japanese Arc Welders." *Occupational and Environmental Medicine* 55 (10): 673–77.
- Näkki, Jonne. 2018. "Properties of Alloy 625 Claddings Made with Laser and CMT Methods."
- Nemery, B. 1990. "Metal Toxicity and the Respiratory Tract." *European Respiratory Journal* 3 (2): 202–19.
- Nguyen, N. 2004. "Thermal Analysis of Welds." *Applied Mechanics Reviews* 57: B34.
- Nielsen, Thomas Dyhre, and Finn Verner Jensen. 2009. *Bayesian Networks and Decision Graphs*. Springer Science & Business Media.
- Niemelä, Raimo, Hannu Koskela, and Kerstin Engström. 2001. "Stratification of Welding Fumes and Grinding Particles in a Large Factory Hall Equipped with Displacement Ventilation." *Annals of Occupational Hygiene* 45 (6): 467–71.
- Pal, Deepankar, Nachiket Patil, Kai Zeng, and Brent Stucker. 2014. "An Integrated Approach to Additive Manufacturing Simulations Using Physics Based, Coupled Multiscale Process Modeling." *Journal of Manufacturing Science and Engineering* 136 (6).
- Panchal, G., A. Ganatra, Y. P. Kosta, and D. Panchal. 2011. "Review on Methods of Selecting Number of Hidden Nodes in Artificial Neural Network." *International Journal of Computer Theory and Engineering* 3 (2): 332–37.

- Papadrakakis, Manolis, Nikos D Lagaros, and Yiannis Tsompanakis. 1998. "Structural Optimization Using Evolution Strategies and Neural Networks." *Computer Methods in Applied Mechanics and Engineering* 156 (1–4): 309–33.
- Paynter, Henry. 1961. *Analysis and Design of Engineering Systems*. Cambridge: MIT press.
- Pépe, Nuno, Stephan Egerland, Paul A Colegrove, David Yapp, Andreas Leonhartsberger, and Americo Scotti. 2011. "Measuring the Process Efficiency of Controlled Gas Metal Arc Welding Processes." *Science and Technology of Welding and Joining* 16 (5): 412–17.
- Pickin, C. G., and K. Young. 2006. "Evaluation of Cold Metal Transfer (CMT) Process for Welding Aluminium Alloy." *Science & Technology of Welding & Joining* 11 (5): 583–85. <https://doi.org/10.1179/174329306X120886>.
- Pradhan, Satyabrata, Rajveer Singh, Komal Kachru, and Srinivas Narasimhamurthy. 2007. "A Bayesian Network Based Approach for Root-Cause-Analysis in Manufacturing Process." In , 10–14. IEEE.
- Qin, Jingxiang, Wuzhong Liu, Jun Zhu, Wei Weng, Jiaming Xu, and Zisheng Ai. 2014. "Health Related Quality of Life and Influencing Factors among Welders." *PloS One* 9 (7): e101982.
- Rabinovich, Joshua E. 2000. "Rapid Manufacturing System for Metal, Metal Matrix Composite Materials and Ceramics," November.
- Ríos, Sergio, Paul A Colegrove, Filomeno Martina, and Stewart W Williams. 2018. "Analytical Process Model for Wire+ Arc Additive Manufacturing." *Additive Manufacturing* 21: 651–57.
- Rongo, LMB, FJMH Barten, GI Msamanga, D Heederik, and WMV Dolmans. 2004. "Occupational Exposure and Health Problems in Small-Scale Industry Workers in Dar Es Salaam, Tanzania: A Situation Analysis." *Occupational Medicine* 54 (1): 42–46.
- Rosenthal, Daniel. 1941. "Mathematical Theory of Heat Distribution during Welding and Cutting." *Welding Journal* 20: 220–34.
- Saito, Hiroyuki, Jun Ojima, Mitsutoshi Takaya, Takeshi Iwasaki, Naomi Hisanaga, Shigeru Tanaka, and Heihachiro Arito. 2000. "Laboratory Measurement of Hazardous Fumes and Gases at a Point Corresponding to Breathing Zone

- of Welder during a CO₂ Arc Welding.” *Industrial Health* 38 (1): 69–78.
<https://doi.org/10.2486/indhealth.38.69>.
- Schmidhuber, Jürgen. 2015. “Deep Learning in Neural Networks: An Overview.” *Neural Networks* 61: 85–117.
- Schoinochoritis, Babis, Dimitrios Chantzis, and Konstantinos Salonitis. 2017. “Simulation of Metallic Powder Bed Additive Manufacturing Processes with the Finite Element Method: A Critical Review.” *Proceedings of the Institution of Mechanical Engineers, Part B: Journal of Engineering Manufacture* 231 (1): 96–117.
<https://doi.org/10.1177/0954405414567522>.
- Sequeira Almeida, PM. 2012. “Process Control and Development in Wire and Arc Additive Manufacturing.”
- Shao, Tiefu. 2007. *Toward a Structured Approach to Simulation-Based Engineering Design under Uncertainty*. University of Massachusetts Amherst.
- Sharifian, Seyed Akbar, Ziba Loukzadeh, Ahmad Shojaoddiny-Ardekani, and Omid Aminian. 2011. “Pulmonary Adverse Effects of Welding Fume in Automobile Assembly Welders.” *Acta Medica Iranica*, 98–102.
- Shavlik, Jude W., Raymond J. Mooney, and Geoffrey G. Towell. 1991. “Symbolic and Neural Learning Algorithms: An Experimental Comparison.” *Machine Learning* 6 (2): 111–43.
- Shim, Taehyun. 2002. “Introduction to Physical System Modelling Using Bond Graphs.”
- Sjögren, Bengt, and Ulf Ulfvarson. 1985. “Respiratory Symptoms and Pulmonary Function among Welders Working with Aluminum, Stainless Steel and Railroad Tracks.” *Scandinavian Journal of Work, Environment & Health* 11 (1).
<http://www.jstor.org/stable/40965174>.
- Song, Lijun, and Jyoti Mazumder. 2011. “Feedback Control of Melt Pool Temperature during Laser Cladding Process.” *Control Systems Technology, IEEE Transactions On* 19 (6): 1349–56.
- Stănescu, Dan C, Laurentiu Pilat, Nicolae Gavrilăscu, Dan B Teculescu, and Iulia Cristescu. 1967. “Aspects of Pulmonary Mechanics in Arc Welders’ Siderosis.” *Occupational and Environmental Medicine* 24 (2): 143–47.

- Storaas, Torgeir, Jan-Paul Zock, Ana Espinosa Morano, Mathias Holm, Eythor Björnsson, Bertil Forsberg, Thorarinn Gislason, Christer Janson, Dan Norback, and Ernst Omenaas. 2015. "Incidence of Rhinitis and Asthma Related to Welding in Northern Europe." *European Respiratory Journal* 46 (5): 1290–97.
- Thomas, Douglas S., and Stanley W. Gilbert. 2014. "Costs and Cost Effectiveness of Additive Manufacturing." *Special Publication (NIST SP) - 1176*, December. <https://www.nist.gov/publications/costs-and-cost-effectiveness-additive-manufacturing>.
- Thompson, Mary Kathryn, Giovanni Moroni, Tom Vaneker, Georges Fadel, R Ian Campbell, Ian Gibson, Alain Bernard, Joachim Schulz, Patricia Graf, and Bhrihu Ahuja. 2016. "Design for Additive Manufacturing: Trends, Opportunities, Considerations, and Constraints." *CIRP Annals* 65 (2): 737–60.
- Topham, Nate, Mark Kalivoda, Yu-Mei Hsu, Chang-Yu Wu, Sewon Oh, and Kuk Cho. 2010. "Reducing Cr6+ Emissions from Gas Tungsten Arc Welding Using a Silica Precursor." *Journal of Aerosol Science* 41 (3): 326–30.
- Tsamardinos, Ioannis, Constantin F Aliferis, Alexander R Statnikov, and Er Statnikov. 2003. "Algorithms for Large Scale Markov Blanket Discovery." In , 2:376–80. St. Augustine, FL.
- Tu, Jack V. 1996. "Advantages and Disadvantages of Using Artificial Neural Networks versus Logistic Regression for Predicting Medical Outcomes." *Journal of Clinical Epidemiology* 49 (11): 1225–31.
- Välimäki, Emmi. 2017. "Modelling, Simulation and Validation of CMT Process: An Application for Additive Manufacturing."
- Varadarajan, Sriram, WEI CHEN*, and Chester J Pelka. 2000. "Robust Concept Exploration of Propulsion Systems with Enhanced Model Approximation Capabilities." *Engineering Optimization+ A35* 32 (3): 309–34.
- Vasinonta, Aditad, Jack L. Beuth, and Michelle L. Griffith. 2001. "A Process Map for Consistent Build Conditions in the Solid Freeform Fabrication of Thin-Walled Structures." *Journal of Manufacturing Science and Engineering* 123 (4): 615–22. <https://doi.org/10.1115/1.1370497>.

- Wang, G. Gary, and S. Shan. 2006. "Review of Metamodeling Techniques in Support of Engineering Design Optimization." *Journal of Mechanical Design* 129 (4): 370–80. <https://doi.org/10.1115/1.2429697>.
- Wang, X. L., Y. T. Tsai, J. R. Yang, Z. Q. Wang, X. C. Li, C. J. Shang, and R. D. K. Misra. 2017. "Effect of Interpass Temperature on the Microstructure and Mechanical Properties of Multi-Pass Weld Metal in a 550-MPa-Grade Offshore Engineering Steel." *Welding in the World* 61 (6): 1155–68. <https://doi.org/10.1007/s40194-017-0498-x>.
- Wang, Xin, Man Jiang, Zuowan Zhou, Jihua Gou, and David Hui. 2017. "3D Printing of Polymer Matrix Composites: A Review and Prospective." *Composites Part B: Engineering* 110: 442–58.
- Wang, Zhi Ping, Kjell Larsson, Per Malmberg, Bengt Sjögren, Bengt-Olov Hallberg, and Kent Wrangskog. 1994. "Asthma, Lung Function, and Bronchial Responsiveness in Welders." *American Journal of Industrial Medicine* 26 (6): 741–54.
- Werra, Dominique de, and Alain Hertz. 1989. "Tabu Search Techniques." *Operations-Research-Spektrum* 11 (3): 131–41.
- Witherell, Paul, Shaw Feng, Timothy W Simpson, David B Saint John, Pan Michaleris, Zi-Kui Liu, Long-Qing Chen, and Rich Martukanitz. 2014a. "Toward Metamodels for Composable and Reusable Additive Manufacturing Process Models." *Journal of Manufacturing Science and Engineering* 136 (6).
- Witherell, Paul, Shaw Feng, Timothy W. Simpson, David B. Saint John, Pan Michaleris, Zi-Kui Liu, Long-Qing Chen, and Rich Martukanitz. 2014b. "Toward Metamodels for Composable and Reusable Additive Manufacturing Process Models." *Journal of Manufacturing Science and Engineering* 136 (6): 061025–061025. <https://doi.org/10.1115/1.4028533>.
- Wohlers, Terry T, Ian Campbell, Olaf Diegel, Ray Huff, Joseph Kowen, and Wohlers Associates (Firm). 2021. *Woblers Report 2021: 3D Printing and Additive Manufacturing Global State of the Industry*.
- Wu, Bintaο, Zengxi Pan, Donghong Ding, Dominic Cuiuri, Huijun Li, Jing Xu, and John Norrish. 2018. "A Review of the Wire Arc Additive Manufacturing of Metals: Properties, Defects and Quality Improvement." *Journal of*

- Yang, Zhuo, Douglas Eddy, Sundar Krishnamurty, Ian Grosse, Peter Denno, Yan Lu, and Paul Witherell. 2017. “Investigating Grey-Box Modeling for Predictive Analytics in Smart Manufacturing.” In , V02BT03A024-V02BT03A024. American Society of Mechanical Engineers. <https://doi.org/10.1115/DETC2017-67794>.
- Yardimci, M Atif, Selcuk I Gucer, MK Agarwala, and Stephen C Danforth. 1996. “Part Quality Prediction Tools for Fused Deposition Processing.” In , 539–48.
- Yu, I. J. 2001. “Lung Fibrosis in Sprague-Dawley Rats, Induced by Exposure to Manual Metal Arc-Stainless Steel Welding Fumes.” *Toxicological Sciences* 63 (1): 99–106. <https://doi.org/10.1093/toxsci/63.1.99>.
- Yu, Il Je, Kyung Seuk Song, Hee Kyung Chang, Jeong Hee Han, Yong Hyun Chung, Kuy Tae Han, Kyu Hyuck Chung, and Ho Keun Chung. 2003. “Recovery from Manual Metal Arc-Stainless Steel Welding-Fume Exposure Induced Lung Fibrosis in Sprague–Dawley Rats.” *Toxicology Letters* 143 (3): 247–59. [https://doi.org/10.1016/S0378-4274\(03\)00154-1](https://doi.org/10.1016/S0378-4274(03)00154-1).

PUBLICATIONS

- Publication I **H.P.N. Nagarajan**, H. Mokhtarian, H. Jafarian, S. Dimassi, S. Bakrani, A. Hamedí, E. Coatanea, G. Wang, and K.R. Haapala, 2018 “Knowledge-Based Design of Artificial Neural Network Topology for Additive Manufacturing Process Modelling: A New Approach and Case Study of Fused Deposition Modelling,” *ASME Journal of Mechanical Design*, Volume 141(2), pp. 021705-12, Dec 2018. <https://doi.org/10.1115/1.4042084>
- Publication II **H.P.N. Nagarajan**, S. Panicker, H. Mokhtarian, E. Coatanea, and K.R. Haapala, “Improving Worker Health and Safety in Wire Arc Additive Manufacturing: A Graph-based Approach,” *Procedia CIRP*, 2020, Proceedings of the 27th CIRP International Conference on Life Cycle Engineering (LCE2020), May 13-15, Grenoble, France. <https://doi.org/10.1016/j.procir.2020.01.116>
- Publication III **H.P.N. Nagarajan**, S. Panicker, H. Mokhtarian, T. Remy-Lorit, E. Coatanea, R. Prod’hon, H. Jafarian, K.R. Haapala, and A. Chakraborti*, 2019 “Graph based Meta-modelling to Characterize Cold Metal Transfer Process Performance,” *Smart and Sustainable Manufacturing Systems* 3, no. 2 (2019): 169-189. doi:10.1520/SSMS20190026
- Publication IV S. Panicker, **H.P.N. Nagarajan**, J. Tuominen, M. Patnamsetty, E. Coatanea, and K.R. Haapala, 2022, “Investigation of Thermal Influence on Microstructure and Mechanical Properties in Wire Arc Additive Manufacturing of Steels, *Material Science and Engineering A*, 853 (2022): 143690. <https://doi.org/10.1016/j.msea.2022.143690>
- Publication V **H.P.N. Nagarajan**, S. Panicker, D. Wu, S. Bakrani, E. Coatanea, and K.R. Haapala, “Modelling the Geometrical and Mechanical Responses in Wire Arc Additive

Manufacturing: A Concept for Graph Metamodel based
Design Space Exploration. (Unpublished)

PUBLICATION

I

Knowledge-Based Design of Artificial Neural Network Topology for Additive Manufacturing Process Modelling: A New Approach and Case Study for Fused Deposition Modelling

Hari P.N. Nagarajan, Hossein Mokhtarian, Hesam Jafarian, Saoussen Dimassi, Shahriar Bakrani, Azarakhsh Hamed, Eric Coatanéa, Gary Wang, and Karl. R. Haapala

ASME Journal of Mechanical Design, 141(2), 021705-12, 2018

<https://doi.org/10.1115/1.4042084>

Publication reprinted with the permission of the copyright holders.

Knowledge-Based Design of Artificial Neural Network Topology for Additive Manufacturing Process Modeling: A New Approach and Case Study for Fused Deposition Modeling

Hari P.N. Nagarajan¹

Mechanical Engineering and Industrial Systems (MEI)
Tampere University of Technology
P.O. Box: 589, 33101, Tampere, Finland
hari.nagarajan@tut.fi

Hossein Mokhtarian

Mechanical Engineering and Industrial Systems (MEI)
Tampere University of Technology
Univ. Grenoble Alpes, CNRS, G-SCOP Laboratory, France
P.O. Box: 589, 33101, Tampere, Finland
Hossein.mokhtarian@tut.fi
ASME Membership: 100691564

Hesam Jafarian

Mechanical Engineering and Industrial Systems (MEI)
Tampere University of Technology
P.O. Box: 589, 33101, Tampere, Finland
hesam.jafarian@tut.fi

Saoussen Dimassi

Mechanical Engineering and Industrial Systems (MEI)
Tampere University of Technology
P.O. Box: 589, 33101, Tampere, Finland
swndimassi@gmail.com

Shahriar Bakrani-Balani

LGP-ENIT-INPT & Institut Clément Ader, CNRS UMR 5312
University of Toulouse, France
47th Avenue d'Azereix, BP1629-65016, Tarbes Cedex, France
sbakrani@enit.fr

¹ Corresponding author, Ph: +358-413668286.

Azarakhsh Hamedi

Mechanical Engineering and Industrial Systems (MEI)
Tampere University of Technology
P.O. Box: 589, 33101, Tampere, Finland
Azarakhsh.hamedi@tut.fi

Eric Coatanéa

Mechanical Engineering and Industrial Systems (MEI)
Tampere University of Technology
P.O. Box: 589, 33101, Tampere, Finland
eric.coatanea@tut.fi
ASME Membership: 102041102

G. Gary Wang

School of Mechatronics Systems Engineering
Simon Fraser University
250-13450 102 Ave, Surrey, British Columbia, Canada V3A0A3
gary_wang@sfu.ca
ASME Membership: 6375786

Karl R. Haapala

School of Mechanical, Industrial and Manufacturing Engineering (MIME)
Oregon State University
204 Rogers Hall, Corvallis, Oregon, USA 97331
karl.haapala@oregonstate.edu
ASME Membership: 8795155

ABSTRACT

Additive manufacturing (AM) continues to rise in popularity due to its various advantages over traditional manufacturing processes. AM interests industry, but achieving repeatable production quality remains problematic for many AM technologies. Thus, modeling different process variables in AM using machine learning can be highly beneficial in creating useful knowledge of the process. Such developed artificial neural network (ANN) models would aid designers and manufacturers to make informed decisions about their products and processes. However, it is challenging to define an appropriate ANN topology that captures the AM system behavior. Towards that goal, an approach combining dimensional analysis conceptual modeling (DACM) and classical ANNs is proposed to create a new type of knowledge-based

artificial neural network (KB-ANN). This approach integrates existing literature and expert knowledge of the AM process to define a topology for the KB-ANN model. The proposed KB-ANN is a hybrid learning network that encompasses topological zones derived from knowledge of the process and other zones where missing knowledge is modeled using classical ANNs. The usefulness of the method is demonstrated using a case study to model wall thickness, part height, and total part mass in a Fused Deposition Modeling (FDM) process. The KB-ANN based model for FDM has the same performance with better generalization capabilities using fewer weights trained, when compared to a classical ANN.

Keywords: *Additive manufacturing, fused deposition modeling, dimensional analysis, empirical learning, knowledge-based artificial neural networks*

INTRODUCTION

Major technological and industrial advancements in manufacturing (e.g., additive manufacturing, cloud computing, nano-manufacturing, and advanced materials) have brought about great paradigm shifts in the way products are designed and manufactured. Additive manufacturing (AM) research has enabled the growth of innovative techniques and functional products, framing AM as a feasible alternative to subtractive and formative techniques [1]. AM processes are being adopted at an ever-increasing pace for mainstream manufacturing. Particularly, polymer extrusion technology, such as fused deposition modeling (FDM) are among the most well researched and most widely used AM processes. The FDM process involves successive melting, extrusion, deposition, and solidification of thermoplastic polymer melts [2]. Typical FDM equipment consists of a material delivery system or extrusion system, heating system, build plate, and filament feeder. The process begins with the generation of layer profile information using a rapid prototyping (RP) software for any given 3D CAD

model. The FDM equipment then deposits semi-liquid molten polymer beads onto a heated build plate following the layer information provided from the RP software [2]. This process remains a source of innovation; new technologies are being developed using this approach for metal printing using a metal and polymer matrix, for example [3,4]. The FDM process involves storage of thermal energy in the molten material, distribution of this energy into the part through a thermal conduction process, and energy dissipation from the part by convection cooling. The redistribution of the thermal energy ensures the bonding between layers. Several methods exist for thermoplastic delivery in the process, namely, use of liquefiers for self-extruding filament, fluid metering rotary pumps, and high-pressure plunger systems [5,6]. The liquefier-based material delivery method is dominant in most FDM machines. In this research, material delivery using a liquefier, which employs a self-extruding filament, is modeled.

For FDM parts, the cross-section of a deposited layer is shaped through the direct flow of polymer melt between the previous layer and the printing nozzle. This results in shapes having the form of flattened ellipsoids. Since the 1980s, process models have been developed for understanding the complex phenomena taking place in FDM, such as thermal transfer, layer creation, and bonding processes [7,8]. Existing research on FDM modeling has focused on the cooling of single and multiple filaments, thermal behavior of the liquefier, analysis of melt front location, degree of cooling in the nozzle and impact of its design on operational stability, temperature distribution across different part design configurations, and impact of the build file [5,9,8]. This available

knowledge provides a set of dispersed sub-models supporting the understanding of localized phenomena, but does not provide an overall system perspective nor a global process model of FDM. Thus, it raises two main questions for qualification of FDM technology in mainstream manufacturing: i) Are the part requirements achievable with current FDM technology? and ii) What are the optimal manufacturing parameters that need to be selected to achieve required part specifications? Further, existing localized models cannot be used effectively in closed-loop control of FDM machines. Thus, metamodeling approaches can be evaluated for effective modeling and control of FDM processes [10].

Artificial neural networks (ANN) have been widely used as a modeling strategy to approximate complex functions. In this context, ANNs can be considered as one type of metamodeling approach [11–14]. ANNs are utilized in numerous domains and form the backbone of deep learning algorithms. The main challenge of developing and implementing an ANN is that it demands a large number of training data. Moreover, the architecture of an ANN is problem-dependent and it requires extra training to explore and progressively generate a suitable architecture via the weights allocated to each of the edges [15]. After training, ANNs are often difficult to interpret. Hence, ANNs have lost their lustre as a metamodeling approach over the past two decades [16]. This is specifically the case when a limited amount of training data is available or if the system to be modeled is subject to large variability due to its complexity. Deep learning approaches can be used for such large complex systems but the duration of the training can be extremely long (up to several years) and extremely costly [16–18]. The amount of

training data required sometimes implies the need of resources often only available in large companies. In addition to data challenges, an ANN topology has to be specified before the training, and available system knowledge is often not considered in designing such topologies. However, in engineering design and manufacturing, one needs to understand system behaviors in detail in order to produce better systems or products.

Towards this goal, a methodology to design a modular ANN topology by integrating existing knowledge is proposed in this research. The modular ANN is composed of zones where system-related knowledge is available and synapses/weights of neurons in the ANN can be precomputed without training. In addition, detected zones where knowledge about the system is insufficient to precompute weights, classical ANNs are trained using experimental data. This proposed methodology is applied to an FDM process to elucidate how the topology of a modular ANN is derived. The approach helps to understand how a modular ANN structure composed of a mixture of known zones with precomputed weights and unknown zones requiring training can improve the performance of ANNs compared to the classical ANN approach. The existing process knowledge is integrated into this research using the Dimensional Analysis Conceptual Modeling (DACM) framework [19]. The DACM framework recently has been applied in various engineering domains, including reverse engineering, early-stage design, multi-disciplinary optimization (MDO), and in this research is applied to artificial intelligence (AI). This conjoint modeling approach, combining DACM and classical ANNs, results in a new type of modular KB-ANN, differing greatly from existing KB-ANN methods. The expected outcome of this article is to benefit from the existing

knowledge of a system and encode this knowledge in the form of causal graphs linking different variables of a system. Specifically, in this research, variables are termed as neurons and causal graphs generated using DACM are considered as an ANN. Training datasets from experiments are required only for the zones in the KB-ANN where existing knowledge is limited, non-existent, or difficult to extract. For zones with sufficient pre-existing knowledge, the training process is replaced by pre-computed weights for neurons using the DACM methodology. This conjoint experimental and modeling approach using KB-ANN is used to predict wall thickness, height, and mass of a part produced using the FDM process. The developed KB-ANN model is compared to a classical, fully connected ANN model under prescribed performance metrics.

The research is organized as follows: Section 2 describes the experimental procedure used in the study and the approaches considered to encode knowledge for designing the ANN topology. Section 3 presents the case study and the application of the developed methodology for the case study. Section 4 discusses the key results of the study and Section 5 concludes the work and briefly describes future development efforts.

BACKGROUND

Design of Experiments

Performing experiments by varying one-factor-at-a-time is cost intensive. Thus, design of experiments (DOE) proposes a set of principles to maximize the efficiency of experiments by minimizing the number of experiments to be conducted. One of those

principles is the use of factorial experiments. Full factorial DOE explores all the possible combinations of factors and levels [20]. In AM, the number of factors influencing the part quality is potentially large, and it is impractical and difficult to explore all the potential combinations of these possible factors. Sampling, which is the use of a subset of the experimental space, is consequently required to explore this space at an acceptable cost [21,22]. Currently, there are multitude of sampling methods available to explore the experimental space, such as stratified sampling, probability sampling, and sequential sampling [20,22–25]. In this research, DOE plays a role in collecting training datasets for zones of non-existent knowledge. Thus, the sampling method must explore the experimental space in those zones to ensure good generalization for the ANN training. Plackett-Burman design or Taguchi's Orthogonal Arrays are proven to be useful in evaluating a small number of sample points considering interaction between the studied variables [20,26,27]. However, the Taguchi method has come under scrutiny due to its many weaknesses in terms of confusing signal-to-noise ratio statistics, non-adaptive and non-sequential approach to experimentation, and ignorance of randomization, and old data analytical approaches [28]. Hence, some of the classical Taguchi tools such as signal-to-noise ratio are not utilized in this study. Nevertheless, randomization is considered via the selection of Taguchi tables and the analytics are developed as part of the KB-ANN approach. The Taguchi method is employed in this study mainly for its simplicity. In addition, optimizing the experimental design for AM is not the central idea of the study, but such optimization could further improve the accuracy of the developed process models in this research.

Metamodeling using Artificial Neural Networks

Several metamodeling approaches, such as Kriging models, polynomial models, and neural network models, exist in literature for modeling complex systems. A metamodeling approach using ANNs can provide numerous advantages for the FDM process and AM, in general. ANN enables the development of global predictive models integrating numerous parameters. Furthermore, ANNs can support the implementation of a closed-loop control system to improve part quality and process repeatability. In other metamodeling approaches, such as Kriging or Gaussian process regression, modeling is performed as black boxes built over a designed set of experiments. This means that existing knowledge of the process or system (e.g., process physics) is not used. The current effort is using this untapped knowledge of the process or system to enable a grey box or white box metamodeling approach. The proposed approach differs from classical surrogate methods in using existing knowledge; thus, the number of required experiments is reduced. The experiments are not used to train the entire model, but to train only parts of the model. Through knowledge extraction and management, we can limit the need for experimental data sets by integrating the existing system knowledge available for the observed process into the ANN [19,29]. Nevertheless, existing knowledge in literature is represented in multiple forms and lacks interoperability [30]. For this reason, the DACM framework is utilized to integrate different knowledge to be coherent with each other, and to visualize the cause-effect relationships in the form of causal graphs.

Dimensional Analysis Conceptual Modeling Framework

Coatanea et al. [19] developed a method to extract and encode knowledge associated to system architectures, equations, and measuring units. The encoded knowledge is represented in the form of causal graphs. DACM can be an efficient approach to the creation of surrogate models and for adaptively training an ANN. Modeling starts with designation of the system boundary and definition of the model's objectives. Functional representation is used to represent the sequence of functions taking place in the system of interest. Those sequences of functions describe the different behavior of the observed system. DACM transforms the initial function model into a generic functional model formed around a limited set of fundamental functions and uses the causal rules extracted from bond graph theory [31–33]. The dimensional analysis is applied to each node of the graph to form behavioral equations. A color pattern is applied to different variables to highlight their design nature. The primary result of this modeling is a colored hypergraph with a list of governing equations for the system of interest. The model can then be used for qualitative or quantitative simulations, and to search for contradicting variables during optimization. Fig. 1 visualizes different steps in the DACM Framework; the process ends when a computable model of the system of interest is available with the required level of detail.

Generic functions represented by bond graph organs are used as an intermediate level between the classical functional models and the final causal graphs [32,33]. To facilitate the systematic assignment of variables to the generic functional representation, regardless of the energy domain, all variables are classified into five

generalized categories, namely, Flow, Effort, Momentum, Displacement, and Connecting [34].

Figure 1

The mathematical relationship between generic variables describes how the variables relate to each other. The sequence of functions in the functional model provides initial insight into the global causality. Mapping functions to the generic functional elements enables the extraction of the causality among the variables characterizing those functions. Table 1 summarizes the causal rules in the DACM approach. Fig. 2 represents a causal extraction algorithm used to automate the DACM modeling process. First, the algorithm checks if a generic functional organ is defined for each functional box. Then, the algorithm explores each functional box of the model from start to end, to verify that there is no conflict in the coherence of the generic functional representation in terms of causality.

Table 1

Finally, according to categories of assigned variables and using the causal rules (Table 1), the cause-effect relationships between variables are established [19,35]. The causal graph generated using DACM is used to define the topology of ANNs during process modeling.

Figure 2

Empirical Learning Using Artificial Neural Networks

Machine learning methods are empirical learning techniques. Empirical learning systems inductively generalize from specific examples. They usually require little theoretical knowledge about the problem domain. This advantage is compensated by the need for a large training data set. ANNs have proven to be equal, or superior, to other empirical learning systems over a wide range of domains, when evaluated in terms of their generalization ability [36,37]. ANNs are usually comprised of layers (k) with nodes (j), where each node sums up i weighted outputs of the nodes from the previous layer as per Eq. 1.

$$s_{j,k} = \sum_i w_{ij,k} x_{i,k-1} + w_{0,k} \quad (1)$$

In Eq. 1, $s_{j,k}$ represents the weighted sum of node j at layer k , w_{ij} represents the weight of i^{th} output at node j , $w_{0,k}$ represents the initial weight of layer k at the first node. This summation is passed through a non-linear activation function, the output of which acts as input for the next layer. A common choice for the activation function is the sigmoid function, which is also called the continuous unit step function (Eq. 2).

$$h(s_{j,k}) = \frac{1}{1 + \exp(-s_{j,k})} \quad (2)$$

The computational power attributed to these networks originates from these non-linear functions $h(s_{j,k})$ of the weighted sums. However, the non-linearity also makes it difficult to mathematically analyze these networks at a deeper level and requires a large set of training data to capture the desired relationship. In ANNs, a state p_i of a neural network can be uniquely described by $\{w_1 \dots w_n\}_p$ where w_i represents a weight

within the network. During the training process, the network goes through a subset of the state space (p) continuously improving the model performance. The hypothesis for the following investigation is that the total number of states p and the total number of weights n of an ANN can be reduced by incorporating prior knowledge about the system. Thus, this approach can increase the efficiency of the model, while reducing the computational cost.

The initial weights allocated to the network can greatly affect how well ANNs can learn [38]. The initial weights allocated is also the central source of the well-known vanishing gradient problem associated with ANNs [39], which is present when training ANNs with gradient-based learning methods and backpropagation. According to Hochreiter et al. [39], in such methods, each of the ANN's weights receives an update proportional to the gradient of the error function with respect to the current weight in each iteration of training. In some cases, the gradient will be vanishingly small, preventing the weight from changing its value. In the worst case, this may completely stop the ANN from training. This problem is more likely when too many hidden layers of neurons are used in an ANN. Some heuristic rules can be used to constrain the potential size of an ANN [40]. This implies that ANN designs must be small in terms of the number of inputs, number of outputs, size of hidden layers, and number of hidden layers.

ANN-based Process Modeling

ANNs with numerous architectures and training algorithms are utilized in process modeling and forecasting output variables. ANNs with the assistance of data

standardization, data preprocessing, and model performance optimization have become a key enabler in modeling different processes. The main advantages of ANNs in modeling when compared to other process modeling methods are, (i) its ability to handle noisy and ambiguous data, (ii) lower cost of implementation than other approaches, (iii) and their suitability for accurate representation of dynamic problems [41,42]. However, it is only possible to perform black box modeling using classical ANNs, resulting in limited information about the hidden layers and relations between the layers. This lack of process information during ANN topology design can result in overfitting models due to the empirical nature of ANNs [42]. Thus, research must be focused on designing ANN architectures that are transparent and require less computation to improve cost-effectiveness.

Relevance of Designing an Artificial Neural Network Topology for Manufacturing

In manufacturing, several problems are associated with capturing and using existing knowledge. This knowledge can be efficiently used to reduce the size and complexity of engineering models and be applied to the design of ANN topologies. Dimensional analysis offers a way to reduce problem dimensionality by combining variables. For example, inputs of an ANN can be combined into dimensionless groups. This transformation directly affects the number of weights to be trained and, intuitively, should have a positive effect on ANN performance. Similarly, the DACM method generates causal graphs that can be seen as elementary ANN topologies. Such ANNs can quickly grow in size and face the problems presented above, such as, vanishing gradient

issue and overfitting. For this reason, a modular approach to model the target variables is presented. For example, causal graphs such as the one presented in Appendix B can be seen as an ANN topology having multiple zones. For zones where sufficient process knowledge is available, weights can be pre-computed without the need for training datasets. A small portion of the causal graph in Appendix B is shown in Fig. 3 as an example of a knowledgeable zone. The bubbles in the figure represent different variables within a knowledgeable zone. The pre-computed weights are shown on the connectors between these variables.

For the zones where knowledge is non-existent, a combination of modules consisting of classical ANNs are modeled. The modules are smaller ANNs that can be trained separately. The intermediate blue nodes represent, in an explicit manner, the locations where sensors could be implemented in the AM process to collect data required to train the local ANNs. If sensing in these locations is not possible, the intermediate data will need to be simulated or otherwise predicted. The central concept of a knowledge-based ANN remains, i.e., to use existing knowledge of a specific problem to develop a topology supporting faster training and better performance using smaller datasets [43]. This approach is a “hybrid learning system” because it combines empirical learning and domain theory learning [44]. Experimental training examples are used for empirical learning and domain theory learning is completed by encoding existing knowledge.

Figure 3

As described above, a knowledge-based artificial neural network (KB-ANN) is a hybrid-learning network that uses both theoretical knowledge and empirical data to construct a model of a physical system. Knowledge extraction and encoding in a KB-ANN can enable superior interpolation and extrapolation to estimate unmeasurable parameters. The main aim of the KB-ANN is to apply, transfer, and translate pre-existing knowledge into a hybrid neural network [45]. This allows for consolidation of knowledge to develop a global model of the system. Traditional KB-ANN development algorithms for a system to learn from both existing knowledge and empirical examples are shown in Fig 4. The hybrid-learning approach starts with the conversion of existing knowledge to symbolic rules using the rules-to-network algorithm. These rules are used to construct and initialize a neural network that performs as a classifier that adheres to the rules upon which it is built. The next step involves using the network-training algorithm to train the classifier (initial ANN structure) using empirical examples to obtain a final trained ANN. Hence, the traditional KB-ANN method involves training all nodes within the developed ANN.

Figure 4

However, the KB-ANN approach developed herein follows one central objective: the significant reduction in the size of training data. The resulting approach is unique, because a significant portion of the KB-ANN produced using this approach does not require training. Training can be eliminated for portions of the network by using the DACM framework to encode existing knowledge in the form of an ANN architecture. This initial architecture, which forms the backbone of the KB-ANN structure, is

connected to smaller classical ANNs that represent the zones of the model where knowledge is non-existent. Thus, the proposed approach differs from existing KB-ANN methods in terms of initial structure development and training; however, the proposed approach is similar to classical ANNs in terms of training knowledge-limited zones. Hence, using the approach described in the foregoing, classical ANNs and a KB-ANN are developed to model an FDM process, as described next.

FUSED DEPOSITION MODELING CASE STUDY

In this section, it is demonstrated that exploration of the manufacturing space can be effectively performed using KB-ANN modeling to improve AM part quality, while keeping the number of required training data sets low. The printed FDM part used in this case study is shown in Fig. 5.

Figure 5

The FDM part has a wall thickness $e = 0.5 \pm 0.05$ mm and height $H_t = 12 \pm 0.05$ mm, constant for the entire profile. The concurrent modeling and experimental process applied in this study are decomposed into six steps summarized below (Fig. 6).

Step 1: Four initial printing tests are completed using pre-selected printing process parameters proposed by the slicing software (Repetier).

Step 2: The printing process parameters are analyzed and process parameters that will potentially affect the targets, namely, wall thickness (e), part height (H_t), and part mass (M_t) are extracted.

Step 3: A rapid evaluation of the effects of process parameters on the targets is performed with a few supplementary experiments, implying simultaneous variation of the parameters using orthogonal arrays. This evaluation is performed to find high latency variables that can later be fixed at a level minimizing their effect on the targets.

Step 4: The most significant parameters to achieve the expected thickness $e = 0.5 \pm 0.05$ mm and height $H_t = 12 \pm 0.05$ mm are selected for developing a predictive model.

Step 5: The prediction model for thickness, height, and mass are built for the remaining control factors: nozzle travel speed (TS), layer height (h_i), and extruder temperature (T_{set}). A colored causal graph is first developed using the DACM approach to encode the knowledge. The variables are classified into four main classes (i.e., colors). *Exogenous* variables (shown in black) are outside the system boundary and part of the surrounding environment of the system. They cannot be modified by the designer, but are imposed on the system. *Independent* design variables (shown in green) are not influenced by any other variables in the system, and their value can be modified by designers (examples include the nozzle travel speed, extruder temperature, and layer height). *Dependent* design variables (shown in blue) are influenced by other variables such as exogenous and independent variables, and are difficult to modify and control. *Performance* variables (shown in red) are the objective variables (selected by the designers to evaluate the performance of a system) and are usually dependent variables. In this case, wall thickness, part height, and mass are the dependent variables selected as the performance variables. Finally, the developed causal graph is translated

into an ANN topology, which is designed for maximum compactness to maintain all the connections in the causal graph. Three classical ANNs and a KB-ANN topology are evaluated in this study. The KB-ANN topology developed in the form of modular ANNs is shown in the causal graph in Appendix B.

Step 6: The three classical ANNs and the KB-ANN are compared for performance and prediction capability to evaluate the relative utility of the selected approaches.

RESULTS AND DISCUSSION

In Steps 1 and 2, initial experimental prints were created and the process parameters that could affect printed part quality were detected. In Step 3, the most influencing factors were taken into consideration, i.e., the layer height (h_i) in mm, the extruder temperature (T_{set}) in °C, the nozzle travel speed (TS) in mm/s, and the fan speed (Fan) in rpm. In Step 4, these four input parameters influencing the wall thickness, part height, and mass were analyzed at three possible levels. An L27 standard orthogonal array was adopted, and each of the necessary 27 experiments was replicated once to ensure repeatability of the FDM machine. In Step 4, fan speed variations were removed from the model because of the latency of its effects on the three performance variables. The fan speed parameter was fixed to a value of ON at 50%.

Figure 6

In Step 5, the prediction model for thickness, height, and mass was developed. The causal graph developed using the DACM framework for FDM is presented in Appendix A. The developed causal graph is simplified and represented in the form of

modular ANNs for designing the KB-ANN topology (Appendix B). In both causal graphs, the independent variables (TS , h_i , and T_{set}) are represented in green. The dependent variables of the system are represented in blue. The performance, or target, variables are represented in red. The nodes of the causal graph from DACM are connected using black leader lines, where the arrows represent the direction of causality and the numbers represent pre-computed weights for knowledgeable zones. Classical ANNs are presented in zones where knowledge is non-existent. From the developed causal graph structure, two types of ANNs are developed, namely, a classical fully-connected ANN and a KB-ANN.

Classical Artificial Neural Network

Three classical ANNs (Fig. 7) are designed to model the three outputs, namely, wall thickness, part height, and mass using three inputs: layer height, travel speed, and extruder temperature. The ANNs are designed with two hidden layers consisting of three (3) neurons each and one output layer with one (1) neuron. The performance of the network is measured in terms of mean squared error (MSE). The Levenberg-Marquardt algorithm was chosen as the training function and the tangent sigmoid function was chosen for the transfer function [46]. The input data for the ANN was divided, using 70% for training, 15% for validation, and 15% for testing.

Typical performance graphs contain three curves, namely, a training curve, a validation curve, and a test curve, which together indicate the mean square error of a training process. The performance curves indicate the quality of the training in terms of

error reduction, under-fitting (bad training), and overfitting. For a good fit performance, the three curves must follow a downward trend indicating low MSE. In addition, the curves must be smooth and must follow the pattern of training and testing curves at the very bottom, followed by a validation curve.

Figure 7

The performance curves (Figs 8a, 8b, and 8c) for the fully connected classical ANNs are shown in Fig 8. The MSE value for best performance was found to be $5.43e-04$ after nine iterations (Fig 8a), $1.15e-04$ after 10 iterations (Fig 8b), and $2.01e-03$ after 23 iterations (Fig 8c) for wall thickness, part height, and part mass respectively.

Figure 8a, 8b, 8c

The performance curves obtained from the classical ANN (Fig. 8a, 8b, 8c) are compared to the performance curve (Fig. 9) of a standard function, $z=\sin(x)\cos(y)$, modeled as a best fit performance using a classical ANN for 100 training samples. It is seen from Fig. 8a (wall thickness) and Fig. 8c (mass) that the training curve follows a downward trend, while the testing and validation curves follow a downward slope until the lowest MSE value achievable; it then trends slightly upwards, indicating a low generalization to inputs with values lying outside the range of the training data. In addition, the upward trend of the validation and testing curves against the continuous downward trend of the training curve indicate the possibility of overfitting. In Fig. 8b, curves are steady at a fixed MSE value with the validation curve trending below the testing curve, indicating a poor fit to the provided data samples and a low level of generalization for inputs that lie outside the training state.

Figure 9

All performance curves show MSE value at low number of iterations indicating that the ANNs could not find a better fit or any reduction in MSE past that iteration point. This is opposed to the best-fit scenario shown in Fig. 9, which obtained best performance MSE value at 1000 iterations.

Knowledge-Based Artificial Neural Network

The KB-ANN was designed as four modular ANNs following the simplified causal graph, as shown in Appendix B. The first modular ANN is designed for one output: ratio of viscosity (μ) of molten polymer at extrusion temperature to the viscosity (μ_i) of molten polymer at a reference temperature (175 °C). The filament feed rate (FFR) and extruder temperature (T_{set}) are used as inputs. Here, the output of the modular ANN 1 is an intermediate (blue) variable, which cannot be directly measured and, hence, has to be estimated using numerical simulations. A direct solution to the simulation of all the missing data is not provided in this study. In some cases, these data can be computed using the DACM method or numerical simulation, or can be directly measured using sensors. In this research, numerical simulation of viscosity was carried out using the CFD Module of COMSOL Multiphysics® software. The Navier-Stokes equation (Eq. 3) and continuity equation (Eq. 4) are solved for the conservation of the momentum and conservation of the mass [47].

$$\rho \frac{\partial u}{\partial t} = \nabla \cdot \left[-pI + \mu(\nabla u + (\nabla u)^T) \right] + \rho g + F_{st} + F \quad (3)$$

$$\rho(u \cdot \nabla u) = 0 \quad (4)$$

Viscosity of the fluid has been considered using the Carreau model in the numerical simulation (Eq. 5).

$$\mu = \mu_{inf} + (\mu_0 - \mu_{inf}) \left[1 + (\lambda \dot{\gamma})^a \right]^{\frac{n-1}{a}} \quad (5)$$

The viscosity of polylactic acid (PLA) has been previously determined by measurement from a parallel-plate rheometer for frequency range 100 s⁻¹ to 0.1 s⁻¹. Tests were carried out at four different temperatures: 175°C, 185°C, 195°C, and 205°C [48]. The viscosity curves were fitted with the Carreau-Yasuda equation using Origin software. The terms of the Carreau-Yasuda equation for the studied temperatures are shown in Table 2. These terms have been implemented in the Origin software in order to determine the flow properties in the liquefier.

Table 2

The second modular ANN is designed for the output, wall thickness. To reduce the dimensionality of the ANN, the inputs to predict wall thickness were represented in the form of Pi numbers (dimensionless primitives) using dimensional analysis (DA) [49]. A widely used theory in DA is the Vashy-Buckingham π theorem [50], which identifies the number of these independent dimensionless primitives (Pi numbers) that characterize a given physical problem. The dimensionless primitives are the invariants of the problem, where the term “invariant” is understood here as a relationship deeply connected with the behavior of certain aspects of a phenomenon. The DA method

offers a way to simplify complex problems by grouping variables into dimensionless primitives. Every law which takes the form $y_0 = f(x_1, x_2, x_3, \dots, x_n)$ can take the alternative form shown in Eq. 6, where π_i (for $i = 1$ to n) is the dimensionless product for the variable x_i and π_0 is the dimensionless product of variable y_0 .

$$\pi_0 = f(\pi_1, \pi_2, \dots, \pi_n) \quad (6)$$

Eq. 6 is the final form of the dimensional analysis and is the consequence of the Vaschy-Buckingham theorem for the variable x_i , which takes the form shown in Eq. 7.

$$\pi_y = y_i x_j^{\alpha_j} x_l^{\alpha_l} x_m^{\alpha_m} \quad (7)$$

Here, x_j , x_l , and x_m are called repeating variables, y_i is the performance variable, and the α values are exponents ensuring the dimensional homogeneity of the relation.

The third modular ANN was designed for part height (H_t) as the output, with layer height (h_i) and number of layers (n) as the inputs. The fourth modular ANN was designed for mass (M_t) as output, with wall thickness (e), height (H_t), and density of the material (ρ) used as the inputs. ANN performance was measured using mean squared error (MSE). The Levenberg-Marquardt algorithm was chosen as the training function and tangent sigmoid function was chosen for the transfer function [46]. The input data for the ANN was divided, using 70% for training, 15% for validation, and 15% for testing. The modular ANNs are designed with one hidden layer consisting of three (3) nodes each. The performance curves for the four modular ANNs are shown in Figs. 10a-d.

Figure 10a, 10b, 10c, 10d

Figure 10a shows that the modular ANN 1 was able to obtain the best validation performance at the 53rd iteration with an MSE of 7.7186e-05. The performance curves show training, testing, and validation following each other in a downward trend, indicating a good fit and good generalization capability. The downward trend also implies that a better model could be obtained by increasing the number of training samples. The results for modular ANN 2 for wall thickness (e) is shown in Fig. 10b. The observed MSE was found to be 9.30e-05 after 93 iterations. The curves show overlap during the first 10 iterations, but soon smoothen and follow a uniform trend. This shows that the ANN was able to train for 93 iterations without failure, indicating a good fit to the training data. The modular ANN 3 results for part height shown in Fig. 10c have best-fit performance with an MSE of 1.41e-04 after only four iterations. The curves are smooth and follow each other in the graph; however, the ANN achieved the best performance at four iterations, indicating a mediocre fit to the training data. Finally, the results of modular ANN 4 for part mass (M_t) are shown in Fig. 10d. The observed MSE is 2.54e-04 after 23 iterations. It was seen that the performance curves follow a downward trend with the validation curve below or at par with the testing curve. This indicates an average fit to the provided data samples, but with the possibility of overfitting.

Validation

The validation of the developed models was carried out with nine experimental tests. The values for the independent input variables (layer thickness, extruder

temperature, and travel speed) were chosen at random. The range of values for the independent variables are as follows, layer thickness (0.1 mm to 0.4 mm), extruder temperature (175 °C to 215 °C), and travel speed (5 mm/s to 19 mm/s). From validation, the standard prediction errors for thickness, height, and mass using the KB-ANN were found to be 0.1627, 0.3647, and 0.4621, respectively. Similarly, the prediction errors for the fully connected classical ANN were found as 0.1376 (thickness), 0.5898 (height), and 0.4667 (mass). The propagated global error of the KB-ANN model was found to be 0.5220.

Figure 11

It can be noted that the KB-ANN global model error is propagated due to the output of modular ANN 1 (viscosity) acting as input for modular ANN 2, and similarly, the output of modular ANN 2 (thickness) acting as input for modular ANN 3 (mass). The MSE and standard error calculated after validation for the two types of networks are compared in Fig. 11. It is seen that the errors for the KB-ANN are in the same range as the prediction error of the classical ANN.

Model Comparison

In the case presented above, the KB-ANN method performed better than the classical fully-connected ANN in terms of fit to the provided experimental data. Specifically, the prediction error for the KB-ANN method was found to be nearly the same as the classical approach for wall thickness and part mass, while lower for part height. This prediction error was largely the result of lost information when streamlining

the complete causal graph (Appendix B) to the simpler version (Appendix A). In particular, the regression fit for the height using the KB-ANN method was poor largely due to the absence of adequate knowledge or models to represent the phenomena that influence part height. For instance, the cooling effect of the fan may affect the solidification rate of the molten polymer, resulting in tight bonding or sparse bonding of layers, which would have a direct impact on part height. The addition of key variables to the study through simulation results or experimental estimates would improve the training and reduce the prediction error. The key difference between the classical ANN model and KB-ANN model lies in the total number of weights that define the state space for each model. In this example, the KB-ANN model had 12 fewer weights than its classical counterpart. Further, the hidden layer of the KB-ANN model operates within the dimensionally homogenous space. The combination of these factors (number of weights trained and dimensionally homogenous hidden layer) results in improved efficiency during fit to training and similar MSE performance for the same number of training (27) samples. This increase in efficiency is visible in the training and its robustness. The KB-ANN method provides more robust generalization compared with the classical ANN approach. Nevertheless, the small number of data in the training set used in this effort, limit the conclusions that can be drawn from the training, validation, and testing. The higher number of epochs required for training in the KB-ANN method demonstrate that the difference in training epochs will increase with bigger datasets. It also indicates that KB-ANN can provide better results for smaller datasets.

CONCLUSIONS

This research developed a knowledge-based artificial neural network (KB-ANN) approach to limit the amount of required experiments for training and validating ANNs for characterizing a manufacturing system. The approach was applied to develop a metamodel capable of dynamically predicting control factors of Fused Deposition Modeling. Benefits were gained from causal graph representation, which enabled the design of KB-ANN as modular ANNs with reduced dimensionality. The results demonstrated the superiority of the KB-ANN approach over classical full-connected ANNs in terms of fit and regularization for the same performance and same number of training samples. The case study was limited to the prediction of three target variables in comparison to the large number of target variables that essentially need to be modeled for a complex FDM system. In reality, more intermediate variables and phenomena (Appendix A) need to be modeled to represent the FDM process holistically. The work reported herein demonstrates an initial proof of concept for the techniques and approaches that can be used to combine knowledge in a modular manner and to reduce dimensionality of complex problems using knowledge extraction, representation, and integration techniques such as dimensional analysis.

FUTURE WORK

The authors are expanding the case study analysis to model a larger set of target variables for FDM using the current methodology to obtain a holistic FDM process model. The developed model will be usable for real production simulations and process

parameter tuning. In addition, the DACM method in this study generated causal graphs that were used to define elementary ANN topologies. Such elementary ANNs when expanded for a larger set of variables can grow quickly in size and be faced with problems such as, high training time, high training cost, requirement of large training data, high probability of model fitting issues (under-fitting or over-fitting), and vanishing gradient issue. Thus, a multi-level hierarchy approach to ANN topology creation as well as the use of regulators for the flow of values similar to long short-term memory neural networks is being investigated. This would allow for the development of a hierarchy of variables ranked based on importance and modular ANNs for variables in sequence following the hierarchy. This method could help in prioritizing variables and constrain the size of each modular ANN in the holistic KB-ANN model reducing training time and cost. The approach would also improve the accuracy of the ANN training and in turn reduce the prediction error of the holistic FDM model.

NOMENCLATURE

λ	Relaxation time index
A_f	Cross-sectional area of filament (mm^2)
a	Dimensionless parameter describing the transition between the first Newtonian plateau and the power law zone
c_p	Heat capacity (J/kg.K)
d_f	Diameter of filament (mm)

d_i	Diameter at i^{th} section of liquefier nozzle (mm)
dx/dt	Nozzle velocity in x direction for dx (mm/s)
dy/dt	Nozzle velocity in y direction for dy (mm/s)
e	Intended wall thickness (mm)
FFR	Filament flow rate (mm/s)
h_i	Layer height (mm)
H_t	Part height (mm)
k	Coefficient of conduction (W/m.K)
L_i	Length at i^{th} section of liquefier geometry (mm)
M_t	Part mass (g)
n	Power index
T_o	Output temperature ($^{\circ}\text{C}$)
T_i	Initial filament temperature ($^{\circ}\text{C}$)
T_{ref}	Reference temperature ($^{\circ}\text{C}$)
TS	Nozzle travel speed (mm/s)
T_w	Wall temperature ($^{\circ}\text{C}$)
VFR	Volumetric flow rate of filament (mm^3/s)
β	Conical angle of liquefier geometry
ΔP_i	Pressure drop (Pa) at i^{th} section of nozzle

ΔV	Change in nozzle travel velocity (mm/s)
θ	Dimensionless temperature
μ	Viscosity of polymer filament (Pa s)
μ_i	Kinematic viscosity (m^2/s) at reference temperature
μ_{inf}	Viscosity at the infinite shear rate (Pa s)
μ_0	Viscosity of fluid at zero shear rate (Pa s)
ρ	Filament density (kg/m^3)
γ	Shear rate (s^{-1})
F_{st}	Force resulting from surface tension (N)

REFERENCES

- [1] Bourell, D. L., Leu, M. C., and Rosen, D. W., 2009, "Roadmap for Additive Manufacturing: Identifying the Future of Freeform Processing," Univ. Tex. Austin Lab. Free. Fabr. Adv. Manuf. Cent.
- [2] Gibson, I., Rosen, D., and Stucker, B., 2014, *Additive Manufacturing Technologies: 3D Printing, Rapid Prototyping, and Direct Digital Manufacturing*, Springer New York.
- [3] Wang, X., Jiang, M., Zhou, Z., Gou, J., and Hui, D., 2017, "3D Printing of Polymer Matrix Composites: A Review and Prospective," *Compos. Part B Eng.*, **110**, pp. 442–458.
- [4] Rabinovich, J. E., 2000, "Rapid Manufacturing System for Metal, Metal Matrix Composite Materials and Ceramics."
- [5] Batchelder, J. S., Curtis, H. W., Goodman, D. S., Gracer, F., Jackson, R. R., Koppelman, G. M., and Mackay, J. D., 1994, "Model Generation System Having Closed-Loop Extrusion Nozzle Positioning."
- [6] Hilmas, G. E., Lombardi, J. L., Hoffman, R. A., and Stuffle, K., 1996, "Recent Developments in Extrusion Freeform Fabrication (EFF) Utilizing Non-Aqueous Gel Casting Formulations," pp. 443–450.
- [7] Bellehumeur, C., Li, L., Sun, Q., and Gu, P., 2004, "Modeling of Bond Formation between Polymer Filaments in the Fused Deposition Modeling Process," *J. Manuf. Process.*, **6**(2), pp. 170–178.
- [8] Atif Yardimci, M., and Güçeri, S., 1996, "Conceptual Framework for the Thermal Process Modelling of Fused Deposition," *Rapid Prototyp. J.*, **2**(2), pp. 26–31.
- [9] Yardimci, M. A., Guceri, S. I., Agarwala, M., and Danforth, S. C., 1996, "Part Quality Prediction Tools for Fused Deposition Processing," pp. 539–548.
- [10] Witherell, P., Narayanan, A., and Lee, J., 2011, "Using Metamodels to Improve Product Models and Facilitate Inferencing," *2011 Fifth IEEE International Conference on Semantic Computing (ICSC)*, pp. 506–513.
- [11] Papadrakakis, M., Lagaros, N. D., and Tsompanakis, Y., 1998, "Structural Optimization Using Evolution Strategies and Neural Networks," *Comput. Methods Appl. Mech. Eng.*, **156**(1–4), pp. 309–333.
- [12] Varadarajan, S., CHEN*, W., and Pelka, C. J., 2000, "Robust Concept Exploration of Propulsion Systems with Enhanced Model Approximation Capabilities," *Eng. Optim. A35*, **32**(3), pp. 309–334.
- [13] Atashkari, K., Nariman-Zadeh, N., Gölcü, M., Khalkhali, A., and Jamali, A., 2007, "Modelling and Multi-Objective Optimization of a Variable Valve-Timing Spark-Ignition Engine Using Polynomial Neural Networks and Evolutionary Algorithms," *Energy Convers. Manag.*, **48**(3), pp. 1029–1041.
- [14] Magnier, L., and Haghghat, F., 2010, "Multiobjective Optimization of Building Design Using TRNSYS Simulations, Genetic Algorithm, and Artificial Neural Network," *Build. Environ.*, **45**(3), pp. 739–746.
- [15] Yegnanarayana, B., 2009, *Artificial Neural Networks*, PHI Learning Pvt. Ltd.

- [16] Wang, G. G., and Shan, S., 2007, “Review of Metamodeling Techniques in Support of Engineering Design Optimization,” *J. Mech. Des.*, **129**(4), pp. 370–380.
- [17] Schmidhuber, J., 2015, “Deep Learning in Neural Networks: An Overview,” *Neural Netw.*, **61**, pp. 85–117.
- [18] Bengio, Y., Goodfellow, I. J., and Courville, A., 2015, “Deep Learning,” *Nature*, **521**, pp. 436–444.
- [19] Coatanéa, E., Roca, R., Mokhtarian, H., Mokammel, F., and Ikkala, K., 2016, “A Conceptual Modeling and Simulation Framework for System Design,” *Comput. Sci. Eng.*, **18**(4), pp. 42–52.
- [20] Montgomery, D. C., 2017, *Design and Analysis of Experiments*, John Wiley & Sons.
- [21] Dowdy, S., Wearden, S., and Chilko, D., 2011, *Statistics for Research*, John Wiley & Sons.
- [22] Levy, P. S., and Lemeshow, S., 2013, *Sampling of Populations: Methods and Applications*, John Wiley & Sons.
- [23] Schillewaert, N., Langerak, F., and Duharnel, T., 1998, “Non-Probability Sampling for WWW Surveys: A Comparison of Methods,” *Mark. Res. Soc. J.*, **40**(4), pp. 1–13.
- [24] Marshall, M. N., 1996, “Sampling for Qualitative Research,” *Fam. Pract.*, **13**(6), pp. 522–526.
- [25] Robbins, H., 1985, “Some Aspects of the Sequential Design of Experiments,” *Herbert Robbins Selected Papers*, Springer, pp. 169–177.
- [26] Plackett, R. L., and Burman, J. P., 1946, “The Design of Optimum Multifactorial Experiments,” *Biometrika*, **33**(4), pp. 305–325.
- [27] Roy, R. K., 2001, *Design of Experiments Using the Taguchi Approach: 16 Steps to Product and Process Improvement*, John Wiley & Sons.
- [28] Maghsoodloo, S., Ozdemir, G., Jordan, V., and Huang, C.-H., 2004, *Strengths and Limitations of Taguchi’s Contributions to Quality, Manufacturing, and Process Engineering*.
- [29] Efthymiou, K., Sipsas, K., Mourtzis, D., and Chryssolouris, G., 2015, “On Knowledge Reuse for Manufacturing Systems Design and Planning: A Semantic Technology Approach,” *CIRP J. Manuf. Sci. Technol.*, **8**, pp. 1–11.
- [30] Witherell, P., Feng, S., Simpson, T. W., Saint John, D. B., Michaleris, P., Liu, Z.-K., Chen, L.-Q., and Martukanitz, R., 2014, “Toward Metamodels for Composable and Reusable Additive Manufacturing Process Models,” *J. Manuf. Sci. Eng.*, **136**(6), pp. 061025–061025.
- [31] Hirtz, J., Stone, R. B., McAdams, D. A., Szykman, S., and Wood, K. L., 2002, “A Functional Basis for Engineering Design: Reconciling and Evolving Previous Efforts,” *Res. Eng. Des.*, **13**(2), pp. 65–82.
- [32] Karnopp, D., Margolis, D., and Rosemberg, R., 2000, “Analysis and Design of Engineering Systems.”
- [33] Shim, T., 2002, “Introduction to Physical System Modelling Using Bond Graphs.”

- [34] Coatanéa, E., 2005, *Conceptual Modelling of Life Cycle Design: A Modelling and Evaluation Method Based on Analogies and Dimensionless Numbers*, Helsinki University of Technology.
- [35] Coatanéa, E., 2005, “Conceptual Modelling of Life Cycle Design,” p. 205.
- [36] Shavlik, J. W., Mooney, R. J., and Towell, G. G., 1991, “Symbolic and Neural Learning Algorithms: An Experimental Comparison,” *Mach. Learn.*, **6**(2), pp. 111–143.
- [37] Atlas, L., Cole, R., Muthusamy, Y., Lippman, A., Connor, J., Park, D., El-Sharkawai, M., and Marks, R. J., 1990, “A Performance Comparison of Trained Multilayer Perceptrons and Trained Classification Trees,” *Proc. IEEE*, **78**(10), pp. 1614–1619.
- [38] Ahmad, S., and Tesauro, G., 1989, “Scaling and Generalization in Neural Networks: A Case Study,” pp. 160–168.
- [39] Hochreiter, S., Bengio, Y., Frasconi, P., and Schmidhuber, J., 2001, *Gradient Flow in Recurrent Nets: The Difficulty of Learning Long-Term Dependencies*, A field guide to dynamical recurrent neural networks. IEEE Press.
- [40] Panchal, G., Ganatra, A., Kosta, Y. P., and Panchal, D., 2011, “Review on Methods of Selecting Number of Hidden Nodes in Artificial Neural Network,” *Int. J. Comput. Theory Eng.*, **3**(2), pp. 332–337.
- [41] Dawson, C., and Wilby, R., 2001, “Hydrological Modelling Using Artificial Neural Networks,” *Prog. Phys. Geogr.*, **25**(1), pp. 80–108.
- [42] Tu, J. V., 1996, “Advantages and Disadvantages of Using Artificial Neural Networks versus Logistic Regression for Predicting Medical Outcomes,” *J. Clin. Epidemiol.*, **49**(11), pp. 1225–1231.
- [43] Ingrassia, S., and Morlini, I., 2005, “Neural Network Modeling for Small Datasets,” *Technometrics*, **47**(3), pp. 297–311.
- [44] Towell, G. G., and Shavlik, J. W., 1994, “Knowledge-Based Artificial Neural Networks,” *Artif. Intell.*, **70**(1–2), pp. 119–165.
- [45] Psychogios, D. C., and Ungar, L. H., 1992, “A Hybrid Neural Network-first Principles Approach to Process Modeling,” *AIChE J.*, **38**(10), pp. 1499–1511.
- [46] Moré, J. J., 1978, “The Levenberg-Marquardt Algorithm: Implementation and Theory,” *Numerical Analysis*, Springer, pp. 105–116.
- [47] Anderson, J. D., and Wendt, J., 1995, *Computational Fluid Dynamics*, Springer.
- [48] Bakrani Balani, S., Chabert, F., Valerie, N., Cantarel, A., and Christian, G., 2017, *Toward Improvement of the Properties of Parts Manufactured by FFF (Fused Filament Fabrication) through Understanding the Influence of Temperature and Rheological Behaviour on the Coalescence Phenomenon*.
- [49] Bridgman, P., “Dimensional Analysis, 1922,” *Phil Mag*, **2**(12), pp. 1263–1266.
- [50] Szirtes, T., 2007, *Applied Dimensional Analysis and Modeling*, Butterworth-Heinemann.
- [51] Mokhtarian, H., Coatanéa, E., Paris, H., Mbow, M. M., Pourroy, F., Marin, P. R., Vihinen, J., and Ellman, A., 2018, “A Conceptual Design and Modeling Framework for Integrated Additive Manufacturing,” *J. Mech. Des.*, **140**(8), p. 081101.

- [52] Mokhtarian, H., Coatanéa, E., and Paris, H., 2017, “Function Modeling Combined with Physics-Based Reasoning for Assessing Design Options and Supporting Innovative Ideation,” *AI EDAM*, **31**(4), pp. 476–500.

Figure Captions List

- Fig. 1 Visual representation of the DACM framework
- Fig. 2 The causal relationship extraction algorithm
- Fig. 3 Knowledgeable zone in the causal graph with pre-computed weights
- Fig. 4 Traditional KB-ANN development algorithm [44]
- Fig. 5 Solid model (left) and dimensions (right) for the sample part [51]
- Fig. 6 Concurrent experimental and modeling process
- Fig. 7 A classical ANN model for fused deposition modeling
- Fig. 8 Performance curves for classical fully-connected ANN to model: a) part wall thickness, b) part height, c) part mass
- Fig. 9 Performance curve for best-fit scenario (standard function $z=\sin(x).\cos(y)$)
- Fig. 10 Performance curves for: a) modular ANN 1 (viscosity) in the KB-ANN, b) modular ANN 2 (thickness) in the KB-ANN, c) modular ANN 3 (height) in the KB-ANN, and d) modular ANN 4 (mass) in the KB-ANN
- Fig. 11 Comparison of validation error for the fully-connected classical ANN and the developed KB-ANN
- Appendix A Detailed causal graph for fused deposition modeling using dimensional analysis conceptual modeling
- Appendix B Simplified causal graph with modular KB-ANN topology for fused

deposition modeling using dimensional analysis conceptual modeling

Table Caption List

Table 1	Causality for generic functions and associated bond graph elements [52]
Table 2	Values for Carreau-Yasuda viscosity curve fitting

Table 1: Causality for generic functions and associated bond graph elements [31]

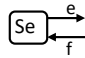
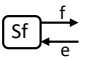
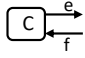
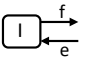
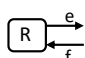
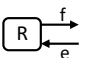
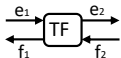
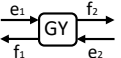
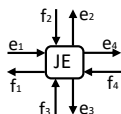
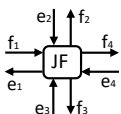
Bond Graph Element	Schematic View	Bond Graph Element	Schematic View
Source of effort (Se) Fixed effort-out causality		Source of flow (Sf) Fixed flow-out causality	
Capacitor (C) Fixed effort-out causality		Inertia (I) Fixed flow-out causality	
Resistor (R) Preferable effort-out causality (Resistive)		Resistor (R) Preferable flow-out causality (Conductive)	
Transformer (TF) Maintain incoming causality (two-port element)		Gyrator (GY) Switch incoming causality (two-port element)	
Effort Junction (JE) or (0) (Multiport element) $e_1=e_2=e_3=e_4$ $f_1+f_2+f_3+f_4=0$		Flow Junction (JF) or (1) (Multiport element) $f_1=f_2=f_3=f_4$ $e_1+e_2+e_3+e_4=0$	

Table 2: Values for Carreau-Yasuda viscosity curve fitting

	175°C	185°C	195°C	205°C
μ_0 (Pa.s)	5169 ± 5	2480 ± 14	1945 ± 16	726 ± 6
μ_{inf} (Pa.s)	0	0	0	0
λ	0.048 ± 0.02	0.09 ± 0.5	0.08 ± 0.02	0.05 ± 0.01
a	0.82 ± 0.3	1.6 ± 0.8	1.931 ± 0.5	2.60 ± 0.01
n	0.52 ± 0.3	0.7 ± 0.3	0.693 ± 0.2	0.79 ± 0.11

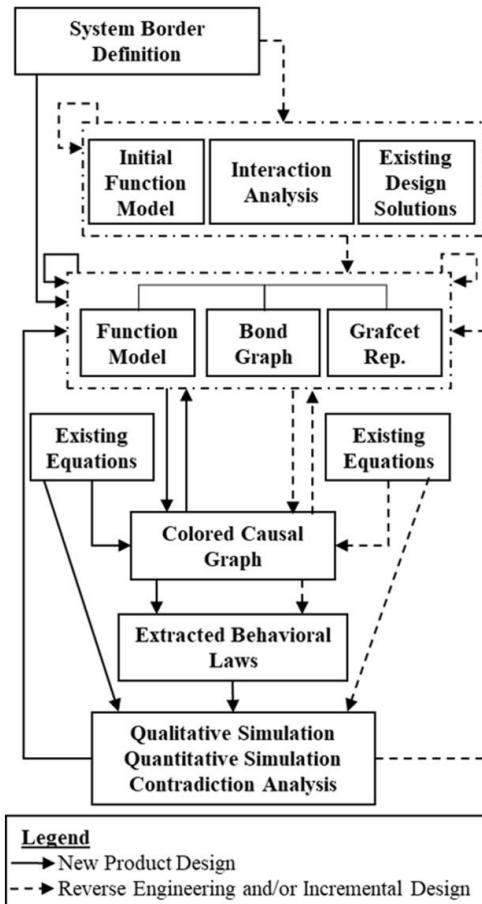


Figure 1: Visual representation of the DACM framework

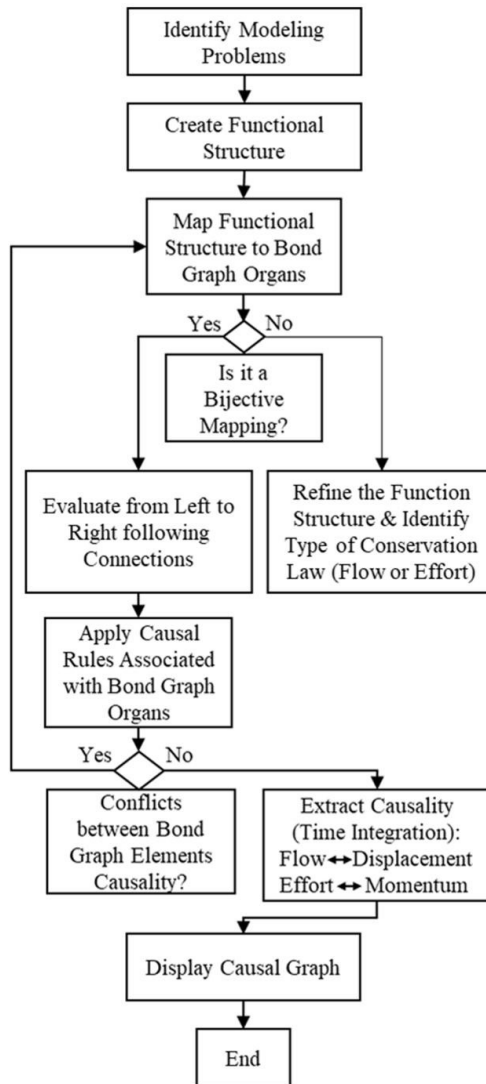


Figure 2: The causal relationship extraction algorithm

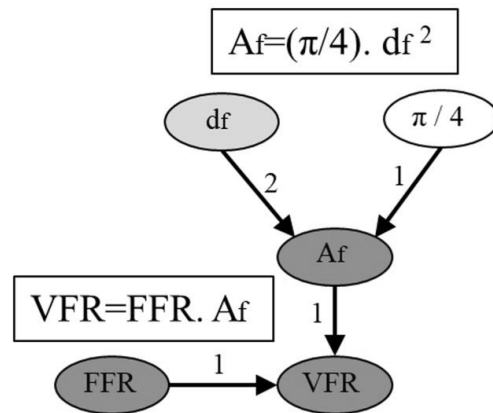


Figure 3: Knowledgeable zone in the causal graph with pre-computed weights

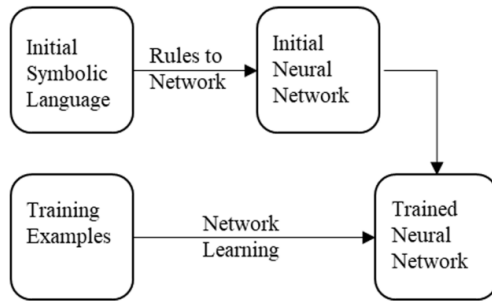


Figure 4: Traditional KB-ANN development algorithm [44]

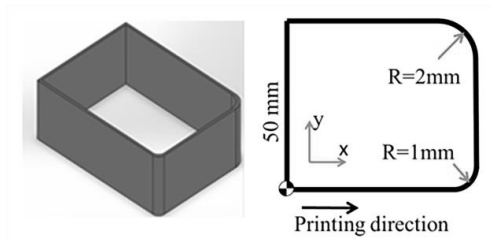


Figure 5: Solid model (left) and dimensions (right) for the sample part [51]

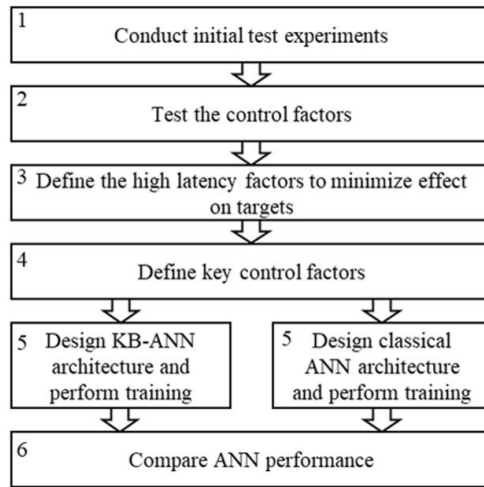


Figure 6: Concurrent experimental and modeling process

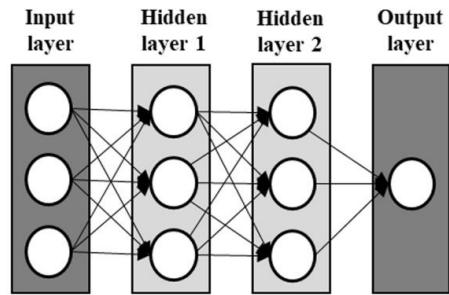


Figure 7: A classical ANN model for fused deposition modeling

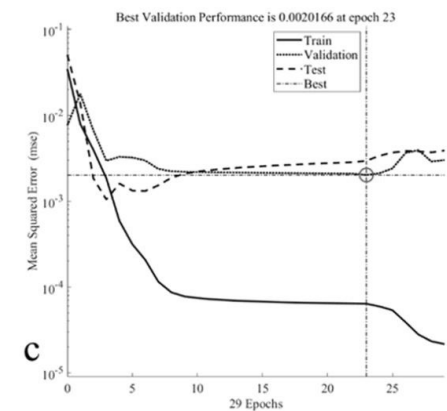
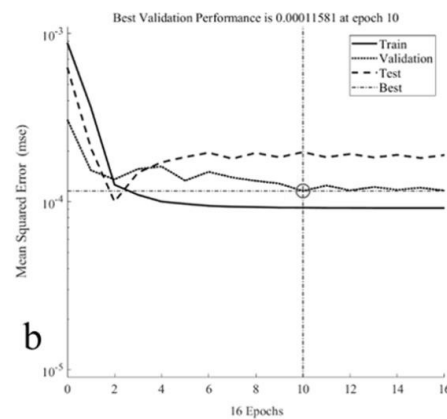
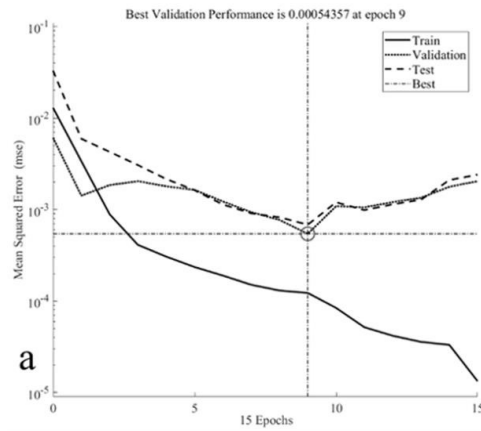


Figure 8: Performance curves for classical fully-connected ANN to model: a) part wall thickness, b) part height, c) part mass

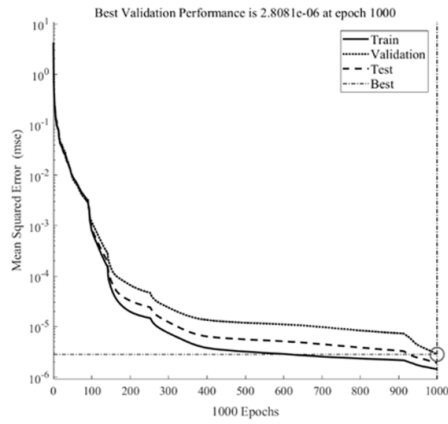


Figure 9: Performance curve for best-fit scenario (standard function $z=\sin(x).\cos(y)$)

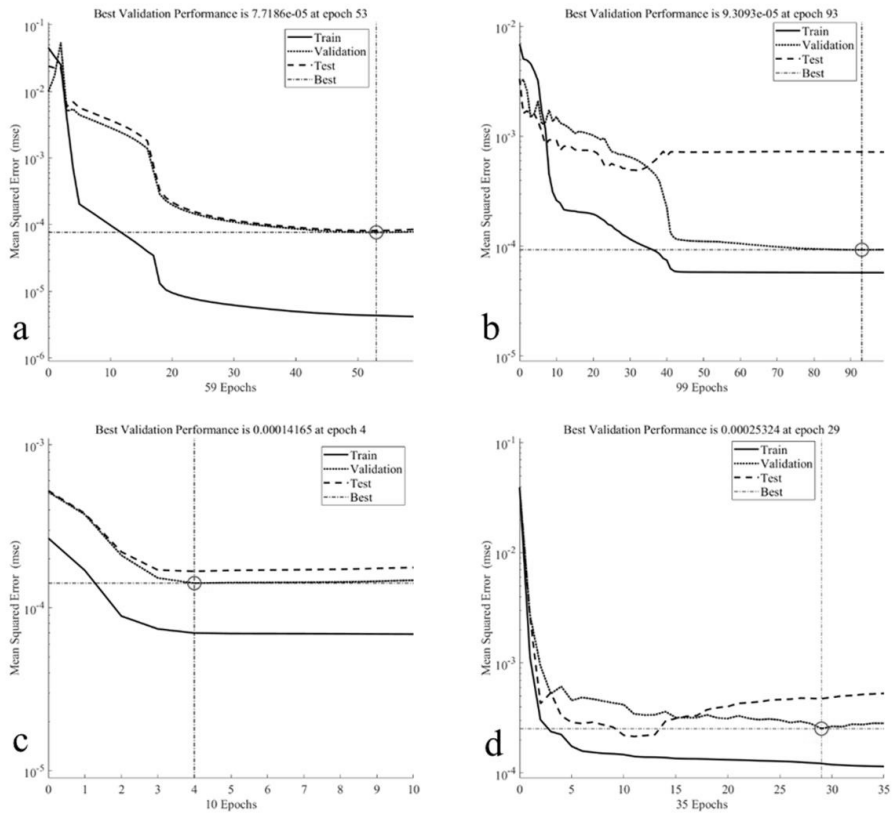


Figure 10: Performance curves for: a) modular ANN 1 (viscosity) in the KB-ANN, b) modular ANN 2 (thickness) in the KB-ANN, c) modular ANN 3 (height) in the KB-ANN, and d) modular ANN 4 (mass) in the KB-ANN

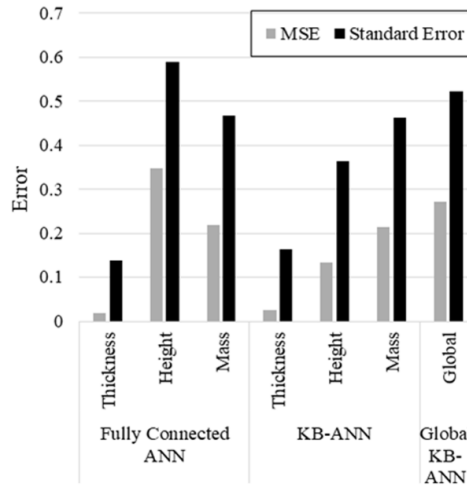
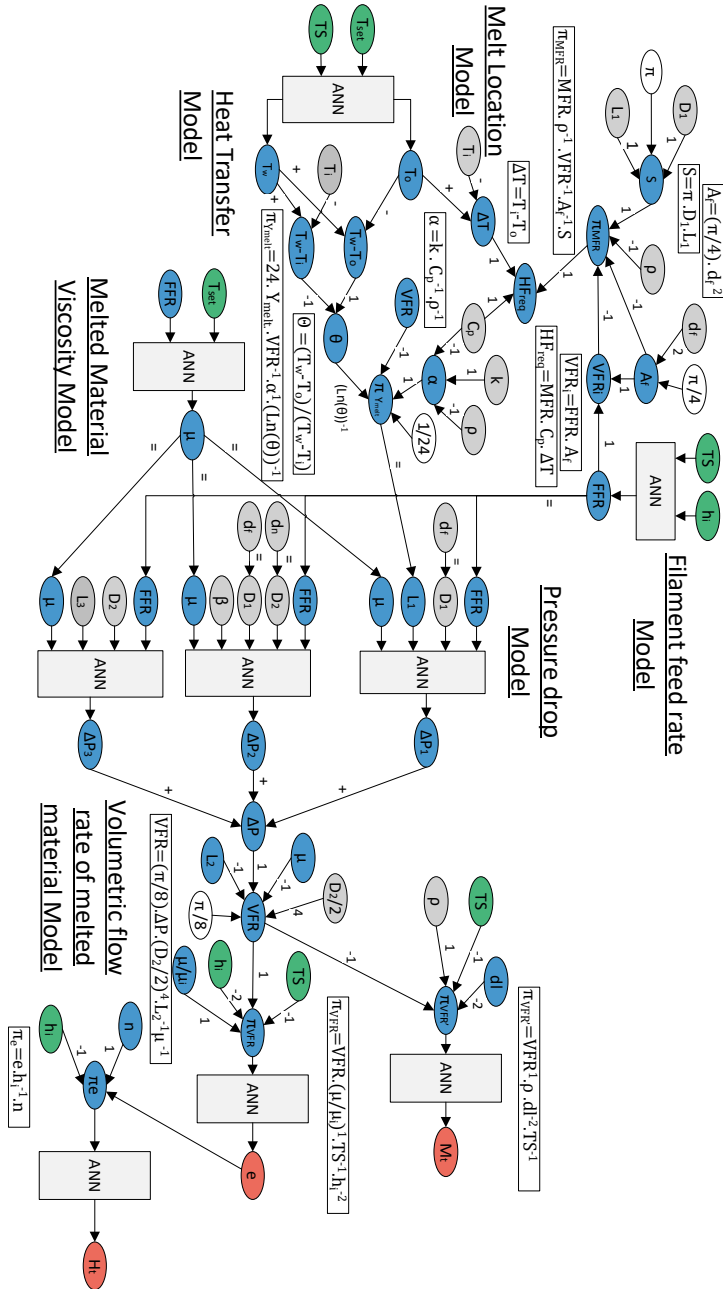
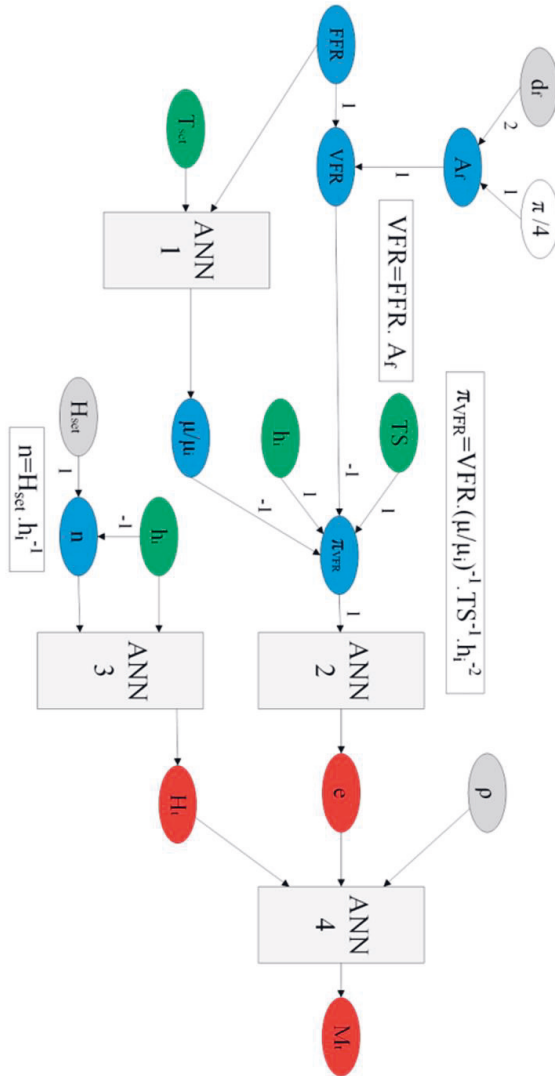


Figure 11: Comparison of validation error for the fully-connected classical ANN and the developed KB-ANN

APPENDIX A: Detailed causal graph for fused deposition modeling using dimensional analysis conceptual modeling



APPENDIX B: Simplified causal graph with modular KB-ANN topology for fused deposition modeling using dimensional analysis conceptual modeling



PUBLICATION
II

**Improving Worker Health and Safety in Wire Arc Additive Manufacturing: A
Graph-based Approach**

Hari P.N. Nagarajan, Suraj Panicker, Hossein Mokhtarian, Eric Coatanéa, and Karl
R. Haapala

Procedia CIRP, 90, 461-466
<https://doi.org/10.1016/j.procir.2020.01.116>

Publication reprinted with the permission of the copyright holders.



Improving worker health and safety in wire arc additive manufacturing: A graph-based approach

Hari P.N. Nagarajan^{a,*}, Suraj Panicker^a, Hossein Mokhtarian^a, Eric Coatanéa^a, Karl R. Haapala^b

^aFaculty of Engineering and Natural Sciences, Automation Technology and Mechanical Engineering Unit, Tampere University, Tampere 33720, Finland

^bSchool of Mechanical, Industrial, and Manufacturing Engineering, Oregon State University, Corvallis, OR 97331, USA

ARTICLE INFO

Keywords:

Additive manufacturing
Welding
Safety
Bayesian networks

ABSTRACT

Research on human health and safety impacts of wire arc additive manufacturing is often overshadowed by the need for weld quality and mechanical strength improvements. To address this gap, a review of research literature is conducted focusing on the influence of welding process parameters, welding fumes, and fume exposure on worker health. The review uses a causal graph to classify research literature into two domains: manufacturing technology and public health. The graph serves as a precursor to development of a Bayesian network model, whose expected benefits, steps for implementation, and likely challenges that would be encountered during implementation are discussed.

© 2020 The Author(s). Published by Elsevier B.V.
This is an open access article under the CC BY-NC-ND license.
(<http://creativecommons.org/licenses/by-nc-nd/4.0/>)

1. Introduction

Despite the confluence of new trends and technologies in manufacturing, the workforce remains pivotal in driving innovation and productivity. New advancements, such as those introduced by Industry 4.0, portend to be of great benefit to the dynamic workforce of the future. In particular, adaptive management cultures will ensure safe working environments that deliver broad societal and economic benefits. The rapid development of technology, coupled with reduced timelines for technology assimilation, makes it a challenge to perform holistic evaluation of related worker health and safety impacts. Production risk and reliability assessments often overshadow worker health and safety evaluations due to increasing demand for quick, seamless integration of new technologies on the shop floor. Existing safety procedures, such as those prescribed by the U.S. Occupational Safety and Health Administration (OSHA), are effective in reducing worker accidents and injuries (OSHA, 1970). However, the disruptive nature of advanced manufacturing technologies, such as additive manufacturing (AM), requires extensive characterization of emissions and wastes that can increase safety and health risks to operators and others. Further, characterizing worker health and safety requires expertise in manufacturing processes, and also delves into domains such as measurement science, environmental science, and public health and safety.

Metal AM systems operate as multi-physical-chemical-metallurgical processes, with myriad interrelated parameters that must be characterized to understand their functionality. Mapping the interrelationships between process variables (parameters), their influence on process emissions and waste, and associated worker impacts is crucial for making informed decisions on the safety equipment and procedures required by emerging metal AM technologies. Integration of pre-existing knowledge (e.g., models and expert knowledge) can hasten the development of meta-models for process characterization.

A causal graph-based approach is presented in this research as means for integrating pre-existing knowledge in modelling AM-related worker health and safety impacts. Operator safety in a directed energy deposition process, wire and arc additive manufacturing (WAAM), is discussed as an application case. Implementation of a Bayesian network (BN) that integrates process knowledge (process operation, emissions, and related impacts), worker habits and exposure pathways, health and safety factors (health risks and severity of risks), and suitable safety protocols from the developed causal graph is discussed. Simulation results using the developed BN could be used to evaluate potential health risks associated with WAAM and to prescribe potential corrective/preventative measures.

The remainder of the manuscript is organized as follows: Section 2 discusses literature reporting emissions and health risks associated with the WAAM process; Section 3 discusses development of the causal graph representing the factors and interconnections as well as possible BN implementation; and Section 4 dis-

* Corresponding author.

Nomenclature

BMC	blood mineral content
C.Filler	composition of filler weld
C.Fume	composition of fume
C.sgas	composition of shielding gas
CFE	cumulative fume exposure
<i>d</i>	filler wire diameter
FC	fume concentration in working space
FGR	fume generation rate
HI	heat input
<i>I</i>	arc current
<i>P</i>	arc power
PPY	packs per year
SGFR	shielding gas flow rate
<i>t_{exp}</i>	exposure time
<i>v</i>	welding speed
<i>V</i>	arc voltage
WFR	wire feed rate

discusses the findings of the presented work and opportunities for future research.

2. Background

AM processes can produce 3D objects in a layer-by-layer fashion using polymers, metals, and ceramics. The advantages provided by AM in terms of unhindered design freedom, higher material efficiency, faster product realization, and less constrained supply chain have accelerated the adoption of AM in high value industries such as medicine, automotive, and aerospace (Bourell et al., 2000). With the increased adoption of polymer and metal AM technologies in mainstream manufacturing, studies must be conducted to evaluate the potential health impact of operators exposed to emissions and other risks.

Stefaniak et al. (2019) explored the operator health impact of emissions and exposures from industrial scale machines for material extrusion and material jetting based AM technologies. They found that the emission rate for both technologies were in the range of 10^9 – 10^{11} particles per minute, with particle sizes predominantly below 300 nm. They concluded that exposure to released particles is prevalent in AM work settings, but that total exposure must take into consideration other contributing factors, such as pre- and post-processing activities. The health impacts from exposure to particle/vapor emissions were not studied, but it was reported that the inhalation of emissions from ABS filament could result in asthma in operators and hypertension in rodents. The authors suggested that evaluation of potential emission points in industrial-scale AM machines is required to adequately measure heavy metal and volatile organic compound (VOC) exposure levels.

Similarly, Graff et al. (2017) characterized the presence of nano-sized metal particles during metal AM. They studied different measurement techniques to characterize particles based on the number of particles, masses, sizes, and identities, focusing on alloys containing chromium, nickel, and cobalt. They found that a range of nanoparticles were present in the AM work environment. Specifically, exposure was greater for workers who directly handle metal powders. They suggested that improved material handling and measurement techniques for nanoparticles is essential; their development could provide useful knowledge that can be translated into workplace safety.

There is lack of information on emissions and related health impacts due to the infancy of WAAM technology and its mainstream use. However, WAAM functions similar to robot-assisted electric

arc welding, wherein the arc is used as a power source to melt filler metal wire onto a substrate. The arc welding process is modified to produce welds that overlap one another in the form of layers to build a 3D metal product. Thus, emissions from WAAM and their associated health impacts are similar to those of traditional welding processes.

Koh et al. (2015) measured the exposure of Korean shipyard welders to welding fumes and evaluated the potential of fume exposure to lead to chronic obstructive pulmonary disease (COPD). They studied 240 male subjects with an average age of 48 and exposure duration of 15 years. The study subjects' smoking habits, occupational history, and medical history were used to determine the number of packs per year (PPY) of cigarettes smoked and cumulative fume exposure (CFE). They found average fume exposure was 7.7 mg/m^3 -years, and reported a statistically significant excess risk of COPD for intermediate and high exposure groups. However, the authors concluded that a longitudinal study with more test subjects was required to confirm a causal relationship between welding fume exposure and risk of COPD.

Li et al. (2004) studied the effects of welding fumes on welders working in a vehicle manufacturing facility by using workers from a nearby food manufacturer as control subjects. It was found that welders had 4.3- and 1.9-times greater serum levels of manganese and iron, respectively, in comparison to the food industry workers. Based on linear regression analysis, no relation was found between the presence of the heavy metals in the blood with the age of the subjects. Of the 500 welders at the facility, thirty-seven who had frequent exposure to fumes from electric arc welding were selected for the study. The study included 22 males and 15 females in the age group of 38 ± 1.5 years, who worked 7–8 h shifts per day. Among the bodily fluid samples that were collected were 24-h urine specimens and blood samples. In addition, air samples from the breathing zone of the welding space were collected. Conclusions from the study reflected upon higher concentrations of manganese (above prescribed safety regulations) in the work atmosphere, and long-term, low-level exposure to fumes inducing oxidative stress in the welders.

Sjögren and Ulfvarson (1985) studied respiratory symptoms and pulmonary functions among aluminum, stainless steel, and railroad industry welders. Non-welding industrial and railroad workers were included in the study as referents. The study found that welders exhibited a higher frequency of chronic bronchitis symptoms than their respective referents. The authors reported that 80% of chromium concentration measurements exceeded the Swedish occupational exposure limit of $20 \mu\text{g/m}^3$ for hexavalent chromium in stainless steel welding, resulting in respiratory symptoms. More than 50% of ozone concentration measurements were above the allowable limit of 0.1 ppm for aluminum welders. However, pulmonary function did not appear to be affected for the welding group. The authors mentioned that smoking habits affected the frequency of chronic bronchitis more than welding.

A related study was conducted to investigate prevalence of respiratory symptoms, impairment of lung function, and occurrence of pulmonary radiography findings in 157 electric arc welders and 108 control subjects (Antti-Poika et al., 1977). In addition, air quality measurements were taken in the work environment for 88 of the welders. They found welders had simple chronic bronchitis more often than the unexposed workers (all men). However, no significant difference was found when accounting for time and level of exposure. In addition, no significant findings were reported for impairment of lung function or for pulmonary radiography measurements for all test and control subjects.

Saito et al. (2000) experimentally measured and verified the presence of hazardous welding fumes in the breathing zone of welders for a CO_2 shielded arc welding process. They used a welding robot and three kinds of welding wires. Shielding gas flow

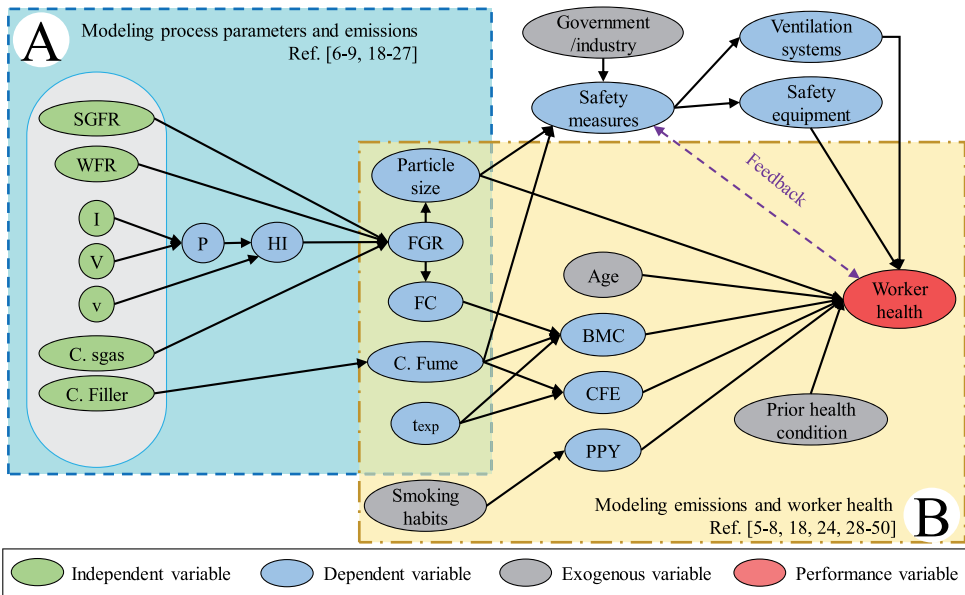


Fig. 1. Causal model of operator health impacts in wire arc additive manufacturing.

rate and the welding current were fixed at constant values. Experiments were conducted without local exhaust ventilation. Gas concentrations, fume concentrations, and particle size distributions were measured. Sampling involved synchronously moving and collecting data along a 200 mm horizontal and 300 mm vertical distance from the moving arc (the effective breathing zone for manual metal arc welding). It was found that fumes exceeded safe levels prescribed by safety standards; using half-face masks for protection was deemed to be insufficient. The authors suggested that use of supplied air respirators and/or use of half-face dust respirators along with a local exhaust ventilation system would be required to handle emission concentrations.

Popović et al. (2014) explored the influence of two types of filler materials, i.e., metal-covered wire and self-shielded wire, on the emission of toxic substances. They were able to detect and quantify the concentrations of dust, CO₂, CO, SO, Mn, Al, Ni, Cr, Cr (VI), Ca, and P. It was found that the concentrations of Mn and CO were high for metal-covered wires, while concentrations of P and Al were high for self-shielded wires. They suggested that the chemical composition of the shielding gas, filler material, and base metal determines the amount and composition of the welding fumes. These welding fumes are typically metal oxides formed when vaporized metal condenses rapidly on exposure to air. Other studies (i.e., Pires et al., 2006; Yoon and Kim, 2003) have established causality between fume generation rate and welding parameters such as electric current, arc voltage, wire diameter, shielding gas flow rate, welding speed, and the type of welding process (steady current or pulsed current welding). Welding fumes range from independent spherical particles less than 20 nm to conglomerated particles greater than 20 nm. Prior studies evaluated the health effects of short and long-term exposure to elemental metals in welding fumes, as shown in Table 1.

From the background literature study, we can infer that the body of research for modeling worker safety in welding falls into two domains: manufacturing technology (process) and public health. Findings from existing literature has been represented

as a graph (Fig. 1) that indicates the causal relationships between different variables in the process domain and in the public health domain.

The developed causal graph can be combined with a Bayesian inference system to predict the effects of individual variables on worker health and safety measures. Section 3 describes the developed causal graph model and discusses the requirements and challenges for the development and implementation of a Bayesian network.

3. Causal modeling of worker health impacts in WAAM

The background study reported in Section 2 is used to develop a graph-based model for worker health in WAAM. The developed graph-based model enables visualization of the potential cause-effect relationships and correlations between the different variables of the system based on the referenced literature, as shown in Fig. 1. At this stage, some of the relations can be considered to be causal, especially in area A, while in area B more efforts are needed to validate the causality of elements. This causal graph provides a unified structure to integrate the knowledge from the two identified domains. In the manufacturing technology domain, research has focused on characterizing the influence of the process and parameters on generation of emissions/fumes (Li et al., 2004; Sjögren and Ulfvarson, 1985; Antti-Poika et al., 1977; Saito et al., 2000; Jafari and Assari, 2004; Yu, 2001; Cole et al., 2007; Niemelä et al., 2001; Balkhyour and Goknil, 2010; Alfaro and Cayo, 2012; Topham et al., 2010; Yu et al., 2003; Heung et al., 2007; Keane et al., 2016). The public health domain has focused on characterizing the influence of emissions and components on worker health (Koh et al., 2015; Li et al., 2004; Sjögren and Ulfvarson, 1985; Antti-Poika et al., 1977; Jafari and Assari, 2004; Topham et al., 2010; Gube et al., 2013; Rongo et al., 2004; Hammond et al., 2005; Chinn et al., 1995; Cotes et al., 1989; Jayawardana and Abeysena, 2009; Bradshaw et al., 1998; Stănescu et al., 1967; Nakadate et al., 1998; Luo et al., 2009; Sharifian et al., 2011; Wang et al., 1994; Fogh et

Table 1
Effects of near and long-term exposure to welding fumes.

Fume component	Effects of long-term exposure	Immediate symptom(s)
Manganese(Mn)	Affects the central nervous system with symptoms similar to Parkinson's disease (Hamai and Bondy, 2004)	Chills and fever, dryness of throat, weakness and aching of head and body
Hexavalent chromium(Cr (VI))	Human carcinogen (specific to lungs) linked to DNA damage in welders (NTP (National Toxicology Program); Sellappa et al., 2010)	-
Nickel(Ni)	Linked to cancer of paranasal sinuses and lungs (List of Classifications – IARC Monographs on the Identification of Carcinogenic Hazards to Humans)	Itching pain, inflammation, redness
Aluminum(Al)	Associated with Alzheimer's disease (Kawahara and Kato-Negishi, 2011)	-
Phosphorous(P)	Linked to anemia, cachexia, necrosis of bone (Popović et al., 2014)	Abdominal pain, irritation to respiratory tract and eyes

al., 1969; Storaas et al., 2015; Qin et al., 2014; El-Zein et al., 2003; Nemery, 1990; Hjortsberg et al., 1992; McCormick et al., 2008; McMillan and Pethybridge, 1983; Barhad et al., 1975; Kilburn et al., 1989; Mur et al., 1985). Mathematical relationships linking process parameters to welding emissions have been documented in literature, while epidemiological studies related to health impacts are based on statistical analysis. From Fig. 1, the process parameters (welding current, voltage, speed, shielding gas flow rate, shielding gas composition, and filler wire composition) function as independent variables, represented as green nodes.

Any change in independent variables will affect intermediate variables (blue nodes), which are the variables associated with the fume emissions. Variables representing emissions, such as fume generation rate, fume composition, particle size, and cumulative exposure time, influence worker health (red target node). Intermediate variables are dependent variables whose values need to be monitored using sensors or, need to be simulated or predicted based on models. They also function as hubs within the graph model and provide a bridge for knowledge integration from the two domains.

In addition to the intermediate variables, worker health is affected by exogenous variables (grey nodes), such as smoking habits, age, and prior health condition. The causal relationships between these variables can be established using experimental data, equations, and/or functional models. Here, causal relationships between variables have been established using the dimensional analysis conceptual modeling (DACM) framework (Coatanéa et al., 2016). The DACM framework is a systems design approach that uses functional modeling, dimensional analysis, and bond graph theory to model the cause-effect relationship between variables in a system in the form of a causal graph. DACM can also be used to build a causal graph in a reverse engineering fashion when equations are known.

A causal graph can be used as a precursor to the development of machine learning models, such as BNs, for simulation (Nagarajan et al., 2018; Mokhtarian et al., 2019). BNs use Bayesian inference for computing conditional probabilities for variables represented in the graphical model. The BN satisfies the Markov chain, meaning that the conditional probability of a node is independent of its non-descendants, which simplifies the computation of the joint probability distribution of the whole network (Pearl, 2000). Causal relationships that exist between process parameters, machine specifications, measured emissions, prescribed safety measures, practiced safety measures, and worker health could be used to generate BN models. The BN model can be updated based on new information or knowledge that is obtained as evidence. The emphasis given to cause-effect relationships via the use of a causal graph provides an intuitive approach to explicitly evaluate the uncertainties in potential outcomes with the use of probability tables (Wade, 2000; Ascough et al., 2008). Thus, the BN can serve as an interactive multi-objective decision-making approach, wherein the computational losses can be minimized by using available knowledge, combined with a statistical framework, taking into account uncertainties in variables, decisions, and outputs of different domains.

Using this approach, the BN will comprise multiple nodes that represent the different variables of the system of interest. These nodes will be connected in the form of direct acyclic graphs (DAGs), developed based on their causal relationships. The causal relationships shown in Fig. 1 will help generate the DAG for worker health for the WAAM process. Apart from the parameter and dependent nodes, the network may also contain constraint nodes. Constraint nodes are Boolean (true/false) clauses that help restrict the network from generating conditional probabilities for certain interactions between nodes that do not exist in the physical world or that are inaccurate.

Simulation of the BN model can enable the following: (1) monitoring the effect of changes in process parameters on emissions and worker health, (2) suggesting safety equipment and procedures required based on exposure time, fume composition, and fume generation rate, and, conversely, and (3) prescribing optimal process parameters based on available safety equipment to control emissions rates and prevent adverse worker health effects. The implementation of such a model would allow engineers and managers to monitor shop floor processes and ensure the safety of workers a priori as conditions change.

4. Discussion and future work

Industries adopt new technologies in order to remain competitive in the marketplace. Effects of new technologies are often uncertain at the outset, and over time new information regarding their effects on workers becomes better known. Modeling new processes and systems must utilize the breadth of knowledge available at the earliest phases to develop models more quickly and efficiently. Pre-existing manufacturing knowledge is available in many different forms and spans across various science and engineering domains due to its multidisciplinary nature, especially for new manufacturing technologies (e.g., additive manufacturing processes).

Simulation of developed models must be flexible to enable use of new-found knowledge when making predictions. The graph-based modeling approach presented here enables cross-functional integration of knowledge of different forms, using causal relationships and correlations between the different variables in a system. The causal graph allows decision makers to bridge knowledge in different domains and acts as a precursor to the development of machine learning models, such as Bayesian networks (BNs), enabling rapid, system-wide simulation and scenario analysis.

Future work will develop and implement a BN model for monitoring worker health and safety in WAAM operations. Pre-existing knowledge and experimental data will be used to train and simulate the developed BN. The network will be trained and simulated using different sources of data, including pre-existing knowledge, sensor data for machine parameters and emissions, accident reports, machine-specific safety brochures, and standards from worker health and safety organizations. Finally, connecting the BN model to different sources of data that can be utilized by the network in the form of evidence during simulation will provide a basis for reinforced learning of the existing causal relationships.

CRedit authorship contribution statement

Hari P.N. Nagarajan: Conceptualization, Methodology, Investigation, Writing - original draft, Writing - review & editing. **Suraj Panicker:** Conceptualization, Methodology, Investigation, Writing - original draft. **Hossein Mokhtarian:** Methodology, Investigation, Writing - review & editing. **Eric Coatanéa:** Methodology, Investigation, Writing - review & editing, Supervision, Project administration, Funding acquisition. **Karl R. Haapala:** Writing - review & editing, Supervision, Project administration, Funding acquisition.

Acknowledgments

The authors would like to acknowledge Fulbright Finland Foundation for their support of this research.

References

Antti-Poika, M., Hassi, J., Pyy, L., 1977. Respiratory diseases in arc welders. *Int. Arch. Occup. Environ. Health* 40 (3), 225–230. doi:10.1007/BF01842087.
 Alfaro, S.C.A., Cayo, E.H., 2012. Sensing fusion data from the optic and acoustic emissions of electric arcs in the GMAW-S process for welding quality assessment. *Sensors* 12 (6), 6953–6966.

Ascough, J., Maier, H., Ravalico, J.K., Strudley, M., 2008. Future research challenges for incorporation of uncertainty in environmental and ecological decision-making. *Ecol. Model.* 219, 383–399. doi:10.1016/j.ecolmodel.2008.07.015.
 Balkhould, M.A., Goknil, M.K., 2010. Total fume and metal concentrations during welding in selected factories in Jeddah, Saudi Arabia. *Int. J. Environ. Res. Publ. Health* 7 (7), 2978–2987. doi:10.3390/ijerph7072978.
 Bourell, D.L., Leu, M.C., Rosen, D.W., 2000. Roadmap for Additive Manufacturing: Identifying the Future of Freeform Processing. Advanced Manufacturing Center, Laboratory for Freeform Fabrication. The University of Texas at Austin.
 Bradshaw, L.M., Fishwick, D., Slater, T., Pearce, N., 1998. Chronic bronchitis, work related respiratory symptoms, and pulmonary function in welders in New Zealand. *Occup. Environ. Med.* 55 (3), 150–154.
 Barhad, B., Teulescu, D., Crăciun, O., 1975. Respiratory symptoms, chronic bronchitis, and ventilatory function in shipyard welders. *Int. Arch. Occup. Environ. Health* 36 (2), 137–150.
 Cole, H., Epstein, S., Peace, J., 2007. Particulate and gaseous emissions when welding aluminum alloys. *J. Occup. Environ. Hyg.* 4 (9), 678–687.
 Chinn, D., Cotes, J., El Gamal, F., Wollaston, J., 1995. Respiratory health of young shipyard welders and other tradesmen studied cross sectionally and longitudinally. *Occup. Environ. Med.* 52 (1), 33–42.
 Cotes, J., Feinmann, E., Male, V., Rennie, F., Wickham, C., 1989. Respiratory symptoms and impairment in shipyard welders and caulker/burners. *Occup. Environ. Med.* 46 (5), 292–301.
 Coatanéa, E., Roca, R., Mokhtarian, H., Mokammel, F., Ikkala, K., 2016. A conceptual modeling and simulation framework for system design. *Comput. Sci. Eng.* 18 (4), 42–52. doi:10.1109/MCSE.2016.75.
 El-Zein, M., Malo, J., Infante-Rivard, C., Gauthrin, D., 2003. Prevalence and association of welding related systemic and respiratory symptoms in welders. *Occup. Environ. Med.* 60 (9), 655–661.
 Fogh, A., Frost, J., Georg, J., 1969. Respiratory symptoms and pulmonary function in welders. *Ann. Occup. Hyg.* 12 (4), 213–218.
 Graff, P., Ståhlbom, B., Nordenberg, E., Graichen, A., Johansson, P., Karlsson, H., 2017. Evaluating measuring techniques for occupational exposure during additive manufacturing of metals: a pilot study. *J. Ind. Ecol.* 21 (S1), S120–S129. doi:10.1111/jiec.12498.
 Gube, M., et al., 2013. Experimental exposure of healthy subjects with emissions from a gas metal arc welding process—part II: biomonitoring of chromium and nickel. *Int. Arch. Occup. Environ. Health* 86 (1), 31–37. doi:10.1007/s00420-012-0738-8.
 Hamai, D., Bondy, S.C., 2004. Oxidative basis of manganese neurotoxicity. *Ann. N. Y. Acad. Sci.* 1012 (1), 129–141. doi:10.1196/annals.1306.010.
 Hjortsberg, U., Orbaek, P., Arborelius, M., 1992. Small airways dysfunction among non-smoking shipyard arc welders. *Occup. Environ. Med.* 49 (6), 441–444.
 Heung, W., Yun, M.-J., Chang, D.P., Green, P.G., Halm, C., 2007. Emissions of chromium (VI) from arc welding. *J. Air Waste Manag. Assoc.* 57 (2), 252–260.
 Hammond, S.K., et al., 2005. Respiratory health effects related to occupational spray painting and welding. *J. Occup. Environ. Med.* 47 (7), 728–739.
 Jafari, A.J., Assari, M.J., 2004. Respiratory effects from work-related exposure to welding fumes in Hamadan, Iran. *Arch. Environ. Health: Int. J.* 59 (3), 116–120. doi:10.3200/AEOH.59.3.116-120.
 Jayawardana, P., Abeysena, C., 2009. Respiratory health of welders in a container yard, Sri Lanka. *Occup. Med.* 59 (4), 226–229.
 Kawahara, M., Kato-Negishi, M., 2011. Link between aluminum and the pathogenesis of Alzheimer's disease: the integration of the aluminum and amyloid cascade hypotheses. *Int. J. Alzheimer's Dis.* 1–17. doi:10.4061/2011/276393, 2011.
 Keane, M., Siert, A., Stone, S., Chen, B.T., 2016. Profiling stainless steel welding processes to reduce fume emissions, hexavalent chromium emissions and operating costs in the workplace. *J. Occup. Environ. Hyg.* 13 (1), 1–8. doi:10.1080/15459624.2015.1072634.
 Kilburn, K.H., Warshaw, R.H., Boylen, C.T., Thornton, J.C., 1989. Respiratory symptoms and functional impairment from acute (cross-shift) exposure to welding gases and fumes. *Am. J. Med. Sci.* 298 (5), 314–319.
 Koh, D.-H., Kim, J.-L., Kim, K.-H., Yoo, S.-W., 2015. Welding fume exposure and chronic obstructive pulmonary disease in welders. *Occup. Med.* 65 (1), 72–77. doi:10.1093/occmed/kqu136.
 Li, G.J., Zhang, L.-L., Lu, L., Wu, P., Zheng, W., 2004. Occupational exposure to welding fume among welders: alterations of manganese, iron, zinc, copper, and lead in body fluids and the oxidative stress status. *J. Occup. Environ. Med.* 46 (3), 241–248. doi:10.1097/01.jom.0000116900.49159.03.
 Luo, J.-C.J., Hsu, K.-H., Shen, W.-S., 2009. Inflammatory responses and oxidative stress from metal fume exposure in automobile welders. *J. Occup. Environ. Med.* 51 (1), 95–103.
 “List of Classifications – IARC Monographs on the Identification of Carcinogenic Hazards to Humans.” [Online]. Available: <https://monographs.iarc.fr/list-of-classifications>. [Accessed: 05-Sep-2019].
 McCormick, L.M., Goddard, M., Mahadeva, R., 2008. Pulmonary fibrosis secondary to siderosis causing symptomatic respiratory disease: a case report. *J. Med. Case Rep.* 2 (1), 257.
 McMILLAN, G.H., Pethybridge, R., 1983. The health of welders in naval dockyards: proportional mortality study of welders and two control groups. *Occup. Med.* 33 (2), 75–84.
 Mur, J., et al., 1985. Lung function and clinical findings in a cross-sectional study of arc welders. *Int. Arch. Occup. Environ. Health* 57 (1), 1–17.
 Mokhtarian, H., Hamed, A., Nagarajan, H.P.N., Panicker, S., Coatanéa, E., Haapala, K., 2019. Probabilistic modelling of defects in additive manufacturing: a case study

- in powder bed fusion technology. *Proc. CIRP* 81, 956–961. doi:10.1016/j.procir.2019.03.234.
- NTP (National Toxicology Program). "National Toxicology Program: 14th Report on Carcinogens," National Toxicology Program (NTP). [Online]. Available: <https://ntp.niehs.nih.gov/goj/roc14>. [Accessed: 05-Sep-2019].
- Niemelä, R., Koskela, H., Engström, K., 2001. Stratification of welding fumes and grinding particles in a large factory hall equipped with displacement ventilation. *Ann. Occup. Hyg.* 45 (6), 467–471.
- Nakadate, T., Aizawa, Y., Yagami, T., Zheg, Y.-Q., Kotani, M., Ishiwata, K., 1998. Change in obstructive pulmonary function as a result of cumulative exposure to welding fumes as determined by magnetopneumography in Japanese arc welders. *Occup. Environ. Med.* 55 (10), 673–677.
- Nemery, B., 1990. Metal toxicity and the respiratory tract. *Eur. Respir. J.* 3 (2), 202–219.
- Nagarajan, H.P.N., et al., 2018. Knowledge-based design of artificial neural network topology for additive manufacturing process modeling: a new approach and case study for fused deposition modeling. *J. Mech. Des.* 141 (2), 021705–021705–12. doi:10.1115/1.4042084.
- OSHA, 1970. "Regulations (Standards – 29 CFR) | Occupational Safety and Health Administration." [Online]. Available: <https://www.osha.gov/laws-regs/regulations/industry>. [Accessed: 27-Sep-2019].
- Popović, O., Prokić-Cvetković, R., Burzić, M., Lukić, U., Beljić, B., 2014. Fume and gas emission during arc welding: Hazards and recommendation. *Renew. Sustain. Energy Rev.* 37, 509–516. doi:10.1016/j.rser.2014.05.076.
- Pires, I., Quintino, L., Miranda, R.M., Gomes, J.F.P., 2006. Fume emissions during gas metal arc welding. *Toxicol. Environ. Chem.* 88 (3), 385–394. doi:10.1080/0272240600720472.
- Pearl, J., 2000. *Causality: Models, Reasoning and Inference*, 29. Springer.
- Qin, J., Liu, W., Zhu, J., Weng, W., Xu, J., Ai, Z., 2014. Health related quality of life and influencing factors among welders. *PLoS One* 9 (7), e101982.
- Rongo, L., Barten, F., Msamanga, G., Heederik, D., Dolmans, W., 2004. Occupational exposure and health problems in small-scale industry workers in Dar es Salaam, Tanzania: a situation analysis. *Occup. Med.* 54 (1), 42–46.
- Sjögren, B., Ulfvarson, U., 1985. Respiratory symptoms and pulmonary function among welders working with aluminum, stainless steel and railroad tracks. *Scand. J. Work Environ. Health* 11 (1), 27–32.
- Stefaniak, A.B., et al., 2019. Insights into emissions and exposures from use of industrial-scale additive manufacturing machines. *Saf. Health Work* 10 (2), 229–236. doi:10.1016/j.shaw.2018.10.003.
- Saito, H., et al., 2000. Laboratory measurement of hazardous fumes and gases at a point corresponding to breathing zone of welder during a CO₂ arc welding. *Ind. Health* 38 (1), 69–78. doi:10.2486/indhealth.38.69.
- Sellappa, S., Prathyumnan, S., Keyan, K.S., Joseph, S., Vasudevan, B.S.G., Sasikala, K., 2010. Evaluation of DNA damage induction and repair inhibition in welders exposed to hexavalent chromium. *Asian Pac. J. Cancer Prevent.* 11 (1), 95–100.
- Stănescu, D.C., Pilat, L., Gavrilescu, N., Teculescu, D.B., Cristescu, I., 1967. Aspects of pulmonary mechanics in arc welders' siderosis. *Occup. Environ. Med.* 24 (2), 143–147.
- Sharifian, S.A., Loukazadeh, Z., Shojaoddiny-Ardekani, A., Aminian, O., 2011. Pulmonary adverse effects of welding fume in automobile assembly welders. *Acta Med. Iran.* 39 (2), 98–102.
- Storaas, T., et al., 2015. Incidence of rhinitis and asthma related to welding in Northern Europe. *Eur. Respir. J.* 46 (5), 1290–1297.
- Topham, N., Kalivoda, M., Hsu, Y.-M., Wu, C.-Y., Oh, S., Cho, K., 2010. Reducing Cr₆₊ emissions from gas tungsten arc welding using a silica precursor. *J. Aerosol. Sci.* 41 (3), 326–330.
- Wang, Z.P., Larsson, K., Malmberg, P., Sjögren, B., Hallberg, B., Wrangskog, K., 1994. Asthma, lung function, and bronchial responsiveness in welders. *Am. J. Ind. Med.* 26 (6), 741–754.
- Wade, P.R., 2000. Bayesian methods in conservation biology. *Conserv. Biol.* 14 (5), 1308–1316. doi:10.1046/j.1523-1739.2000.99415.x.
- Yoon, C.S., Kim, J.H., 2003. Fume Generation and content of total chromium and hexavalent chromium in flux-cored arc welding. *Ann. Occup. Hyg.* 47 (8), 671–680. doi:10.1093/annhyg/meg063.
- Yu, I.J., Sep. 2001. Lung fibrosis in sprague-dawley rats, induced by exposure to manual metal arc-stainless steel welding fumes. *Toxicol. Sci.* 63 (1), 99–106. doi:10.1093/toxsci/63.1.99.
- Yu, I.J., et al., 2003. Recovery from manual metal arc-stainless steel welding-fume exposure induced lung fibrosis in Sprague-Dawley rats. *Toxicol. Lett.* 143 (3), 247–259. doi:10.1016/S0378-4274(03)00154-1.

PUBLICATION III

Graph-based Metamodelling for Characterizing Cold Metal Transfer Process Performance

Hari P.N. Nagarajan, Suraj Panicker, Hossein Mokhtarian, Theo Remy-Lorit, Eric Coatanéa, Romaric Prod'hon, Hesam Jafarian, Karl R. Haapala and Ananda Chakraborti

ASTM Smart and Sustainable Manufacturing Systems, 3(2), 169-189
doi:10.1520/SSMS20190026

Publication reprinted with the permission of the copyright holders.

PUBLICATION IV

Investigation of Thermal Influence on Weld Microstructure and Mechanical Properties in Wire and Arc Additive Manufacturing of Steels

Suraj Panicker, Hari P.N. Nagarajan, Jari Tuominen, Madan Patnamsetty, Eric Coatanéa, and Karl R. Haapala

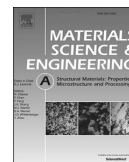
Materials Science and Engineering: A, 853 (2022), 143690
<https://doi.org/10.1016/j.msea.2022.143690>

Publication reprinted with the permission of the copyright holders.



Contents lists available at ScienceDirect

Materials Science & Engineering A

journal homepage: www.elsevier.com/locate/msea

Investigation of thermal influence on weld microstructure and mechanical properties in wire and arc additive manufacturing of steels

Suraj Panicker^{a,*}, Hari P.N. Nagarajan^a, Jari Tuominen^b, Madan Patnamsetty^b, Eric Coatanéa^a, Karl R. Haapala^c

^a Faculty of Engineering and Natural Sciences, Automation Technology and Mechanical Engineering, Tampere University, Tampere, 33720, Finland

^b Faculty of Engineering and Natural Sciences, Materials Science and Environmental Engineering, Tampere University, Tampere, 33720, Finland

^c School of Mechanical, Industrial, and Manufacturing Engineering, Oregon State University, Corvallis, OR, 97331, USA

ARTICLE INFO

Keywords:

Wire and arc additive manufacturing
Microstructure characterization
Mechanical properties
Steels

ABSTRACT

Alloy steels are commonly used in many industrial and consumer products to take advantage of their strength, ductility, and toughness properties. In addition, their machinability and weldability performance make alloy steels suitable for a range of manufacturing operations. The advent of additive manufacturing technologies, such as wire and arc additive manufacturing (WAAM), has enabled welding of alloy steels into complex and customized near net-shape products. However, the functional reliability of as-built WAAM products is often uncertain due to a lack of understanding of the effects of process parameters on the material microstructure and mechanical properties that develop during welding, primarily driven by thermal phenomena. This study investigated the influence of thermal phenomena in WAAM on the microstructure and mechanical properties of two alloy steels (G4Si1, a mild steel, and AM70, a high-strength, low-alloy steel). The interrelationships between process parameters, heating and cooling cycles of the welded part, and the resultant microstructure and mechanical properties were characterized. The welded part experienced multiple reheating cycles, a consequence of the layer-by-layer manufacturing approach. Thus, high temperature gradients at the start of the weld formed fine grain structure, while coarser grains were formed as the height of the part increases and the temperature gradient decreased. Microstructural analysis identified the presence of acicular ferrite and equiaxed ferrite structures in G4Si1 welds, as well as a small volume fraction of pearlite along the ferrite grain boundaries. Analysis of AM70 welds found acicular ferrite, martensite, and bainite structures. Mechanical testing for both materials found that the hardness of the material decreased with the increase in the height of the welded part as a result of the decrease in the temperature gradient and cooling rate. In addition, higher hardness and yield strength, and lower elongation at failure was observed for parts printed using process parameters with lower energy input. The findings from this work can support automated process parameter tuning to control thermal phenomena during welding and, in turn, control the microstructure and mechanical properties of printed parts.

1. Introduction

Directed energy deposition (DED) is a class of additive manufacturing technologies that fuse together powder or wire/filament material layer by layer as it is deposited using a heat source such as a laser, electron beam, or electric/plasma arc [1]. In particular, wire and arc additive manufacturing using cold metal transfer (WAAM-CMT) process, with its flexible material deposition rates (1–5 kg/h) and its ability to accommodate metallic materials with poor weldability, has enabled the timely and cost-effective production of large-scale metal

products without the need for costly manufacturing setups [2,3]. WAAM is an emerging DED process technology used to manufacture large metal components [3]. Specifically, welding of alloy steels has become more widespread with the use of WAAM [4]. With the increased development of functional steel components using additive manufacturing, it is important to understand the influence of process parameters on the evolution of microstructure and the resulting mechanical properties [5]. Broad research around WAAM is focused on qualification efforts for dimensional quality, mechanical strength, and welding path planning for different metal wire feedstocks, as summarized by Rodrigues et al.

* Corresponding author.

E-mail address: suraj.panicker@tuni.fi (S. Panicker).

[6] in their state-of-the-art review. They discussed the different types of welding technologies used in WAAM, common defects in WAAM printed parts, and stress relief strategies to improve mechanical strength. They found that residual stress buildup due to inhomogeneous heat distribution was a common occurrence in WAAM. Employing stress relief strategies such as cold interlayer rolling, machine hammer peening, or laser peening was found to help achieve grain growth refinement, providing better control of mechanical properties, path width, and surface finish.

In addition, Rodrigues and co-workers [6] found that interlayer temperature, or interpass temperature, had a high influence on final printed part quality and microstructure. A higher interpass temperature generally provides finer grain structure and improved toughness for high-strength steel. However, this characteristic reverses as interpass temperature exceeds 260 °C; increasing the interpass temperature beyond this limit causes the weld pool to puddle and collapse, affecting the quality of the part [7]. The wait time for cooling to the required interpass temperature is influenced by the cooling rate of the layer, which varies as a function of energy density and product height. Increasing part height influences conduction, convection, and radiation and, in turn, causes a reduction in the cooling rate of subsequent weld layers. Thus, controlling the thermal cycles during the process to maintain stable interpass temperatures is essential for achieving high quality welds (and parts). While their in-depth review provides an overview of WAAM part quality, Rodrigues and co-workers in Ref. [6] did not provide information on the microstructure and mechanical properties of alloys used in WAAM. Thus, several studies are detailed below that are relevant to the experimental work presented in this manuscript. These studies examine the microstructure and mechanical properties of similar steel alloys printed using a range of WAAM technologies.

Sun et al. [8] investigated the microstructure and mechanical properties of low-carbon, high-strength steel fabricated using WAAM. A 907-steel alloy plate substrate and an A-Fe-W-86 welding alloy wire feedstock were used. They found the microhardness values varied from 290 HV to 260 HV along the build direction of the welded part. In addition, the average UTS of longitudinal specimens (976.53 MPa) was significantly lower than transverse specimens (1017.8 MPa), confirming anisotropic behavior. The inclusion of more interlayer zones in the microstructure resulted in higher stress concentrations in the longitudinal specimens. Electron back-scatter diffraction (EBSD) revealed a higher Taylor factor (0.907) for interlayer zones compared to the deposited weld (0.865), which indicates the presence of non-uniform deformation and local stress concentrations in the interlayer zones. Phase transformation analysis revealed that the bottom zone of the printed part was comprised of tempered bainite and sorbite, while the middle zone was comprised of tempered bainite and the top zone was comprised of tempered bainite, tempered sorbite, and ferrite. The order of occurrence of the phases also corresponded with the microhardness results, where hardness decreased along the build direction. Additionally, two crucial control parameters were found to influence the microstructure formation: temperature gradient (G) and solidification velocity (SV). Based on solidification theory, the G/SV ratio determines the microstructure formation. When G/SV is extremely high (approaching infinity), planar grains form, when G/SV is relatively high, columnar grains form, and when G/SV is small, equiaxed grains form.

Lu et al. [9] investigated the microstructure and mechanical properties of copper-coated mild steel welding wire (0.8 mm diameter) deposited on an ASTM 1045 steel substrate using an open-source GMAW-AM process. In their study, forced cooling of the weld zone facilitated a successful deposition of a thin-walled structure with 150 layers. The YS and UTS values of horizontal specimens (519.5 ± 8.3 MPa and 693.5 ± 8.5 MPa) were higher than for specimens from the vertical build direction (461.5 ± 6.3 MPa and 618.5 ± 10.8 MPa). Elongation along the horizontal and vertical directions were found to be $36.8 \pm 0.2\%$ and $28.2 \pm 0.5\%$, respectively. The microstructural evolution

shows the presence of primary austenite dendrites along the building direction. In addition, acicular ferrite and reticular ferrite intergranular structures were observed in the bottom zone, due to continued air cooling and conduction.

While the prior study focused on mild steel, Rodrigues et al. [10] investigated the thermal influence of WAAM on microstructure and mechanical properties of high-strength, low-alloy steel using a commercial-grade wire electrode (AWS A5.28 ER110S-G) deposited onto a mild steel substrate. Two samples were printed at two levels of heat input (P1 at 511 J/mm and P2 at 221 J/mm). The voltage (21 V), current (95 A), and wire feed rate (3 m/min) were maintained constant for both samples, while travel speed and shielding gas flowrate was maintained at two different levels for the experiments. Sample P1 used a travel speed of 3.9 mm/s and a shielding gas flowrate of 8 L/min, while sample P2 used 9 mm/s and 16 L/min, respectively.

The microstructural analysis in the above study found that ferrite, bainite, martensite, and retained austenite were present for both levels of heat input. Further, it was reported that heat input directly affected the cooling rates, interlayer temperatures, and residence times in the 800 °C–500 °C cooling interval. These findings align with well-established knowledge that cooling rate has a significant impact on the microstructure obtained for steels [11]. Two primary cooling intervals (1300 °C–800 °C and 800 °C–500 °C) are known to promote phase transformations and grain growth development. Austenite grain growth occurs in the 1300 °C–800 °C range, while in the 800 °C–500 °C range, a phase transformation from austenite to distinct ferrite morphologies and bainite can be observed. Oxide inclusions, weld metal hardenability, and cooling conditions are known to be associated with acicular ferrite formation. Also, cooldown to room temperature can cause full or partial transformation of the remaining austenite to martensite, depending on the carbon content of the weld.

In the experiments reported by Rodrigues et al. [10], martensite-austenite (MA) microstructures were observed for cooling rates in the range of 10–40 °C/s. Bainite formed under intermediate cooling rates (between martensite and pearlite phases), and its presence increased the UTS of the printed parts. The presence of bainite has been reported to play a critical role in crack initiation and propagation [12]. Rodrigues and co-workers found that the welds deposited with the higher heat input had a smoother, less bumpy top surface, which was credited to improving the weldability of subsequent layers. For both heat input levels, it was observed that overall part temperature increased with part height, while cooling rates and temperature gradients decreased through the weld. For the higher heat input level, higher residence times were observed in the 800 °C–500 °C temperature range at higher layer numbers (as part height increases). Despite using different heat inputs for the two samples, no significant difference was observed in the microstructure of the parts. Both samples had the same phase constituents (i.e., ferrite, bainite, and MA). Uniaxial tensile tests and Charpy impact tests found the mechanical properties in the build and travel directions to be similar, exhibiting isotropic behavior. Sample P1 (higher heat input) was found to have slightly higher UTS (by ~50 MPa) than sample P2 (lower heat input). Consequently, for sample P2, lower and more uniform microhardness values were measured along the part height compared to sample P1.

The above studies have characterized the microstructure and mechanical properties of metal alloys printed using WAAM and found that the thermal cycles of the layer-by-layer fabrication process influence the microstructural evolution of the part material. Specifically, controlling the cooling rates and maintaining stable interpass temperatures in the build can aid in controlling microstructure phase evolution, hence improving the mechanical properties of the final part. Process parameters directly influence welding energy density and part temperature gradients, which in turn affect cooling rates of printed parts. Thus, characterizing the influence of WAAM process parameters on part microstructures and mechanical properties can support qualification efforts for different metal alloys, and enable product quality improvement

and repeatability in production. Towards that goal, this research investigates the influence of two sets of process parameters on thermal cycles during WAAM as well as the resultant microstructures and mechanical properties for two alloy steels: G4Si1, a mild steel, and AM 70, a high-strength, low-alloy steel. This research adds to the state of the art by qualifying the WAAM-CMT process for two alloy steel wires and enables the development of material models for simulation and optimization purposes. The remainder of the manuscript is organized as follows: Section 2 describes the experimental study undertaken, and Section 3 presents the experimental study results characterizing the interconnections of WAAM process parameters and thermal and mechanical properties. Section 4 provides a discussion on the mechanisms influencing the microstructure of WAAM printed components, and Section 5 discusses the findings and opportunities for future work.

2. Materials and methods

2.1. Materials and equipment

For the WAAM-CMT experimental work, G4Si1 and AM70 alloy steel wire feedstock (1.2 mm diameter) is used; their chemical compositions are presented in Table 1. An S355 mild steel plate (300 × 200 × 20 mm) was used as a substrate for the fabrication of a thin wall. The WAAM-CMT setup (Fig. 1) consists of a welding unit (Fronius CMT Advanced 4000), a 6-axis industrial robot with a 3-axis worktable (ABB 4600 40/2.55), a wire feeder, and an inert gas supply. The welding torch is mounted on the industrial robot arm such that the travel direction is in the X axis, build direction is in the Z axis, and traverse direction is in the Y axis.

The robot path program was generated using Robot Studio 6. An infrared pyrometer (Micro Epsilon w/max temperature 1000 °C) in tandem with temperature measurement software (Compact Connect v1.9) was used to measure and record the temperature of the weld during fabrication. In addition, a contact-type digital thermal probe (Center 314 humidity temperature meter with a K-Type thermocouple) was used to monitor the interpass temperature between consecutive weld passes.

Welding was performed with CMT technology, which alters arc length and thermal input during welding by controlling material transfer (droplet removal) to the melt pool through a short-circuiting phase [15]. During this phase, the wire feeder dips the molten droplet into the weld pool and retracts the wire at a specific frequency (50–120 Hz) to detach the droplet through surface tension. The controlled wire oscillating motion in the nozzle is carried out at zero current, lowering heat input to the weld. The fast-retracting motion results in near spatter-free droplet transfer. Further, the lowering of heat input enables the fabrication of thin-walled structures (a few millimeters in thickness).

2.2. Product and process parameters

A schematic of the thin wall structure built using WAAM-CMT is shown in Fig. 2. The steel baseplate was sandblasted and cleaned with ethanol before the first print and cleaned using a wire brush for each

subsequent wall to remove residual spatter from the print area. Wire feed rate (WFR) and interpass temperature (T_0) parameters were chosen for Material 1 (G4Si1) and Material 2 (AM70) to achieve low-heat input and high-heat input levels, resulting in four printed wall structures. The travel speed and shielding gas flow rate were kept constant at 10 mm/s and 15 L/min, respectively, for all experiments. The process parameters chosen for the experiments are shown in Table 2. A WFR of 6 m/min was used in printing the first layer to avoid incomplete deposition of subsequent layers.

This higher WFR provides a thicker base layer and preheats the baseplate, resulting in better bonding between subsequent layers. A two-directional travel strategy was implemented for the weld nozzle during deposition to aid in maintaining a constant printed wall height along its length. Samples were taken from the deposited walls to investigate the microstructure evolution (optical microscopy specimens) and mechanical properties (tensile and microhardness specimens) under the different weld conditions explored, as shown in the figure.

2.3. Thermal profile during welding

As discussed in Section 1, the thermal profile during welding influences solid state transformations and grain formation during cooling, which affect the microstructure and mechanical properties of the welded part. The ratio of wire feed rate to travel speed influences the amount of heat input to the weld, with higher wire feed rates increasing heat input for a fixed travel speed. Thus, WFR was varied for the different wall specimens to investigate the effect of heat input on the weld microstructure.

A wait time was introduced before depositing each layer to allow the previously deposited layer to cool to the desired interpass temperature (150 °C or 250 °C). The interpass temperature was measured at the middle of each layer before depositing the next layer, as shown in Fig. 2 using the contact-type digital thermal probe. From literature [16], it is seen that the thermal profile of a layer changes as new material is deposited, impacting microstructure evolution. Initially, the heat input to the weld is dissipated by conduction to the baseplate, forced convection through the shielding gas, and radiation to the surroundings. The increase in the number of layers affects the heat accumulation in the part, resulting in varying thermal cycles in the deposited layers. Thus, the pyrometer was used to measure the thermal profile of every 10th layer of material deposited. This data is used to characterize the effect of successive heating and cooling of one weld layer on associated microstructure evolution and mechanical properties.

2.4. Mechanical characterization

A total of four walls were printed for the different process parameter settings. The walls printed using the higher energy input setting (M1E2 and M2E2) resulted in thicker walls (~1–2 mm thicker) than their lower energy counterparts. Thus, post-process machining (face milling) was performed to ensure uniform thickness (~2.5 mm) for all walls. Following the initial machining, hardness test specimens were cut along the build direction from the bottom, middle, and top of each wall using a CNC mill (Fig. 2). For the tensile tests, specimens were cut along the build direction (wall height) and along the travel direction (wall length). Microhardness tests were performed in accordance with ASTM test standard E92-17 using a Vickers microhardness tester (Matsuzawa MMT-X7) with a test load of 9.8 N and dwell time of 10 s. Tensile properties (i.e., YS, UTS, and percent elongation) were investigated according to EN ISO 6892-1:2019 (Annex B) with tests conducted using an Instron 8800. A crosshead speed of 0.01 mm/s and an initial strain rate of 0.00025/s were set, based on the test standard.

2.5. Microstructure characterization

Five samples for optical measurement (metallographic analysis)

Table 1
Wire feedstock chemical composition [13,14].

Elements	G4Si1 (wt. %)	AM70 (wt. %)
C	0.090%	0.08%
Mn	1.670%	1.700%
Si	0.87%	0.60%
S	0.006–0.010%	0.000%
P	0.004–0.010%	0.000%
Cr	0.000%	0.200%
Mo	0.000%	0.500%
Ni	0.000%	1.500%
Fe	98.133–98.143%	95.42%

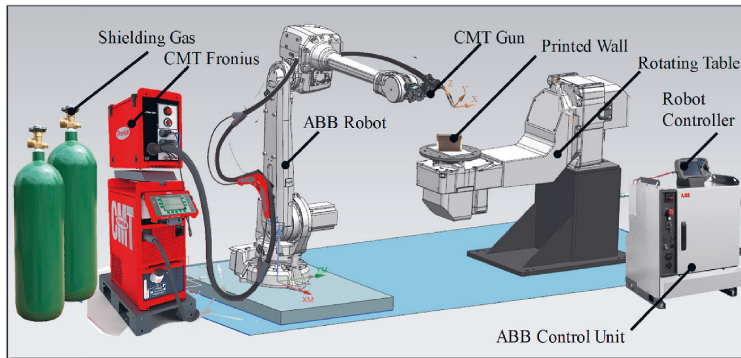


Fig. 1. WAAM equipment setup.

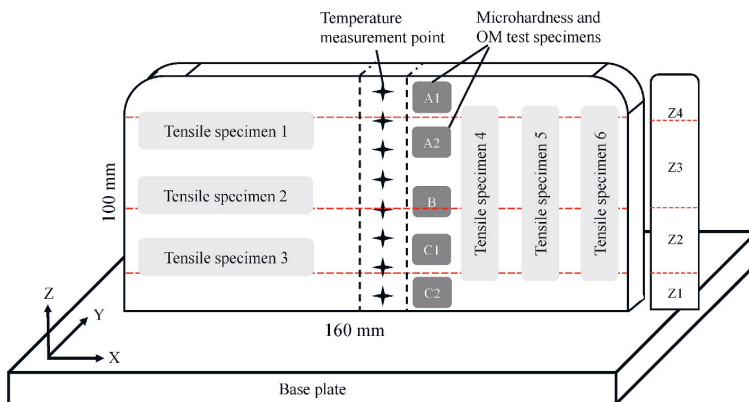


Fig. 2. Schematic of the deposited wall with locations of temperature measurement and mechanical samples marked along build direction.

Table 2
Description of experimental setup and process parameters.

Study Material and Equipment	Material 1	Material 2
Base Plate Size (Material)	300*200*20 mm (S355 steel)	
Wire Material (Diameter)	G4Si1 (1.2 mm)	AM70 (1.2 mm)
Wall Length	160 mm	
Wall Height	100 mm	
Robot	ABB 4600 40/2.55	
Shielding Gas Type (Composition)	Mison 8 (Ar + 8% CO ₂ + 0.03% NO)	
Study Parameter		
F - Ignition Time	0.2 s	
F - Ignition Current	80%	
Wire Feed Rate (Level)	2 m/min (M1E1), 4 m/min (M1E2)	3 m/min (M2E1), 6 m/min (M2E2)
Interpass Temperature (Level)	150 °C (M1E1), 250 °C (M1E2)	150 °C (M2E1), 250 °C (M2E2)
Step Height	1.2 mm (M1E1), 1.5 mm (M1E2)	1.5 mm (M2E1 and M2E2)
F - Travel Speed	10 mm/s	
F - Shielding Gas Flow Rate	15 L/min	
F - Arc Ending Time	0.2 s	
F - Arc Ending Current	80%	
F - Wire Stick Out	15 mm	

Note: F- Fixed Parameter.

were selected at different heights along the build direction of each wall with a sample cross section length of 15 mm. These specimens were mechanically polished and etched using 4% Nital solution. The microstructures of the prepared specimens were observed and recorded using a Leica DMi8 optical microscope. The microstructural images obtained for G4Si1 were used to estimate grain size in Leica Application Suite X (LAS X version 5) software following the ASTM E112 standard using the Jeffries planimetric method [17]. Image analysis for grain size estimation was not conducted using LAS X for AM70 due to lack of equiaxed grains in the specimen. Instead, grain size estimation for AM70 was performed manually following the Jeffries planimetric method.

Electron back-scatter diffraction (EBSD) was used to analyze the prior austenite grain structure of the evaluated metallographic specimens for AM70. EBSD was not conducted for G4Si1 due to the lack of prior austenite grains in the microstructure. Following OM, the metallographic samples were polished further using a 0.02 μm colloidal silica suspension to enable EBSD analysis. Data acquisition for EBSD was done using a Zeiss Ultra Plus field emission scanning electron microscope (FESEM) equipped with a Symmetry® EBSD detector (Oxford Instruments). Data was acquired with a step size of 0.7 μm over a 300 μm \times 1500 μm area using an acceleration voltage of 20 kV. The collected data was analyzed using Channel 5 EBSD software. The grain boundaries were categorized based on a minimum cut-off misorientation angle of 15°, and only the grains above 10 pixels (at 2048 \times 1536 resolution) were considered for noise reduction.

3. Results and analysis

The wall temperature data, hardness and tensile strength properties, and microstructure images were used to characterize the effect of different process parameters (i.e., filler wire material, WFR, TS, and T_0) on the weld properties.

3.1. Thermal analysis

Using the collected temperature data, four zones of interest from the bottom to the top of the wall, labeled Z1, Z2, Z3, and Z4 in Fig. 2 were identified. The cooling rate of the weld tends to decrease moving from zone Z1 to Z4. This trend has the effect of increasing the wait time to reach the specified interpass temperature between successive depositions. It was observed that the cooling rate reaches a steady state value as the height of the part and number of layers deposited increases; this value appears to be dependent on the material type and energy input. This phenomenon was not examined further in this study.

At the bottom of the wall (Z1), for one to ten layers (up to ~10–15 mm wall height), the weld experiences the fastest cooling rate, with wait times between subsequent weld passes of 10–15 s. In the lower middle section of the wall (Z2), for ten to thirty layers (~15–45 mm wall height), the weld experiences a much slower cooling rate, with wait times of 20–48 s per layer, increasing with layer number. At the start of the upper middle section of the wall (Z3, >45 mm), the cooling rate sees a slight decrease from zone Z2. However, the rate of decrease of cooling rate is comparatively slower for zone Z3 than Z2. For example, in the wall printed using parameter set M1E1, the average interpass wait time at layer 10 (~12 mm) was found to be 12s, while at layers 20 (~24 mm) and 30 (~36 mm) the wait time increased to 26s and 48s between deposition, respectively. We can see that the cooling rate reduces ~50% between layers 10–20, and ~75% between layers 10–30. However, in zone Z3 of this wall (M1E1), the average wait time at layers 40, 50, and 60 were found to be 58s, 62s, and 64s, respectively.

From this data, it is evident that the rate of decrease in the cooling rate is not uniform as the height of the part increases. The decrease in cooling rate appears to reach a steady state in zone Z3, which was also observed for other prints in this study and is maintained through printing of zone Z4. A key difference in thermal phenomena between zones Z3–Z4 is a decrease in the number of heating and cooling cycles that each subsequent layer undergoes in this metal additive process.

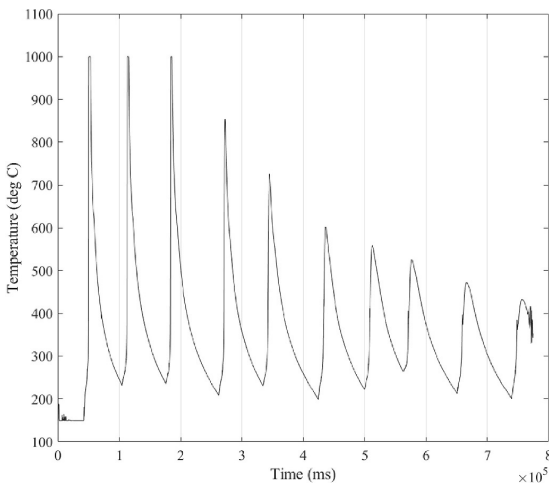


Fig. 3. Temperature profile of layer 40 (M1E1) extracted from infrared pyrometer showing reheating and cooling cycles.

Fig. 3 presents the temperature profile for the 40th layer (M1E1) to show the reheating and cooling cycles undergone by a single layer. In WAAM, arc energy is used to melt the filler material and substrate to temperatures above 1000 °C. Thus, as a new layer is deposited, a number of previously deposited layers undergo conductive heating to temperatures above 1000 °C. This successive heating and cooling of the part highly influences the resultant material microstructure (e.g., grain sizes and shape, and microstructural phase constituents) and its mechanical properties.

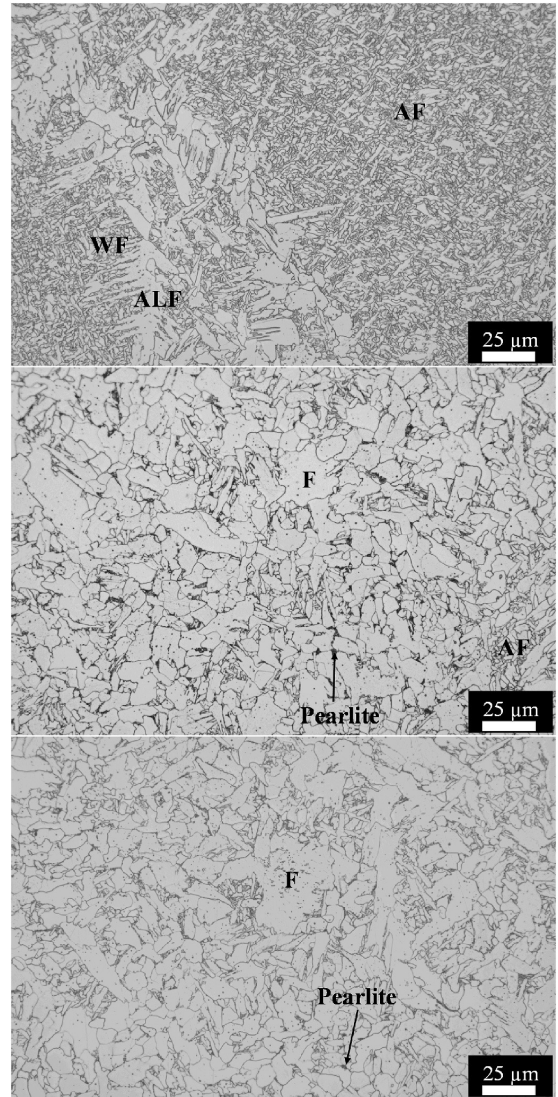


Fig. 4a. Optical micrographs (25 μm scale) of WAAM built parts using G4Si1 welding wire for M1E1. Micrographs reported along wall height from top to bottom (sample A1, A2, and B). Phases identified: AF – Acicular ferrite, ALF – Allotriomorphic ferrite, WF – Widmanstätten ferrite, and F – Equiaxed ferrite.

3.2. Microstructure and mechanical properties

Image analysis was used to identify the material grain sizes and microstructure phase constituents of the printed specimens. Fig. 4a–d shows the microstructural variation along the height of the WAAM-built walls for the two parameter sets (M1E1 and M1E2) using G4Si1. As shown in Fig. 2, sample A1 was taken from zone Z4 and sample A2 from zone Z3, sample B overlaps zones Z2 and Z3, sample C1 was taken from zone Z2, and sample C2 was taken from zone Z1 adjacent to the base plate. For the G4Si1 alloy, both welded walls exhibit distinctive microstructural (grain size) variations resulting from layer-by-layer deposition. For M1E1, sample C2 (Fig. 4b) experiences the highest cooling rate due to the large temperature difference between the new weld layers and the non-preheated baseplate, resulting in faster heat dissipation from the weld. In addition, a higher WFR for the first layer results in a higher heat input and contributes to the temperature difference between the base plate and the weld. This thermal phenomenon results in small grain sizes ($2.46 \pm 1.95 \mu\text{m}$) in zone Z1 with the microstructure largely composed of bainite and acicular ferrite with traces of Widmanstätten and allotriomorphic ferrite. The hardness at the bottom of the wall was measured to be $248.25 \pm 28.27 \text{ HV1}$. The large variability in the hardness at this location is due to the rapidly changing cooling rate at the bottom of the wall. As the height of the wall increases to the lower middle zone Z2, the cooling rate decreases to less than half of the cooling rate at the bottom of the wall. The microstructure of sample C1 (Fig. 4b) consists of equiaxed ferrite, allotriomorphic ferrite, and with small regions exhibiting bainite, pearlite islands, and remnant acicular ferrite with average grain size of $2.96 \pm 3.15 \mu\text{m}$ and hardness of $173.55 \pm$

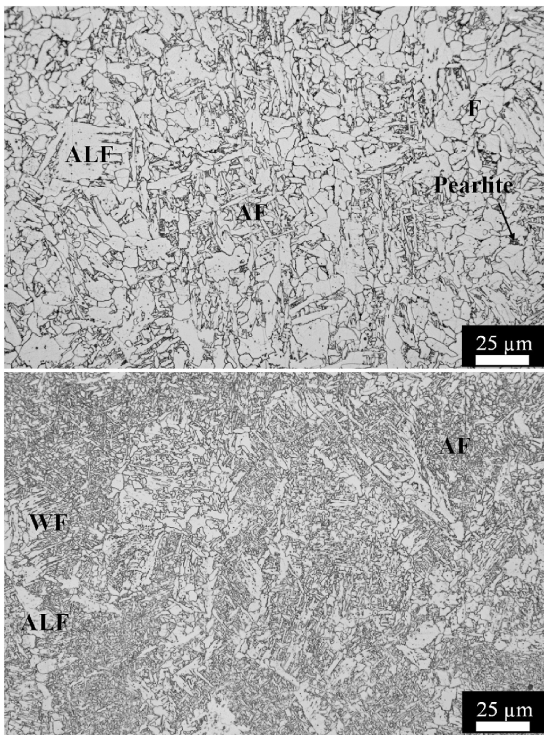


Fig. 4b. Optical micrographs (25 μm scale) of WAAM built parts using G4Si1 welding wire for M1E1. Micrographs reported along wall height from top to bottom (sample C1 and C2). Phases identified: AF – Acicular ferrite, ALF – Allotriomorphic ferrite, WF – Widmanstätten ferrite, and F – Equiaxed ferrite.

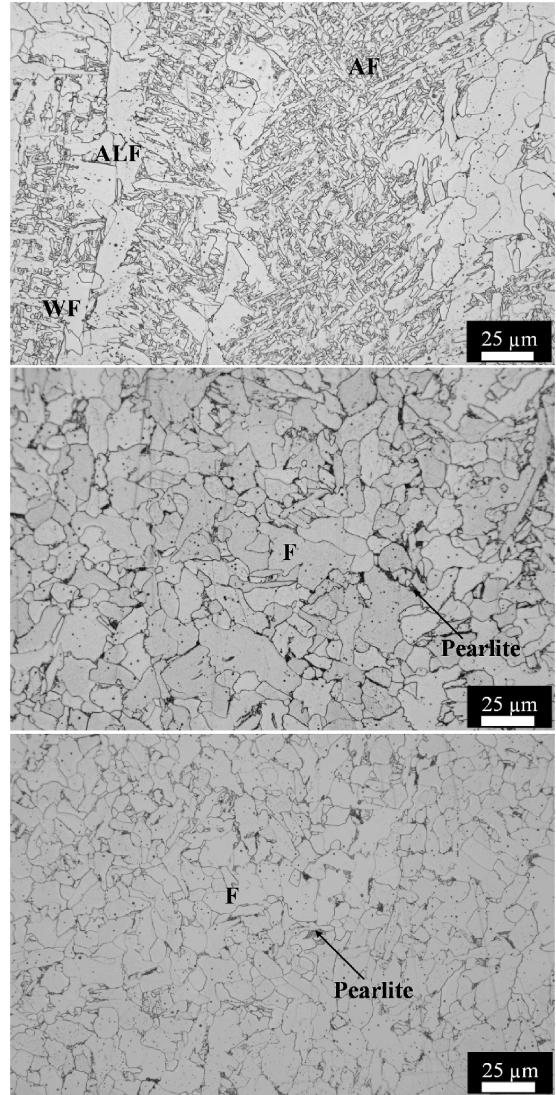


Fig. 4c. Optical micrographs (25 μm scale) of WAAM built parts using G4Si1 welding wire for M1E2. Micrographs reported along wall height from top to bottom (samples A1, A2, and B). Phases identified: AF – Acicular ferrite, ALF – Allotriomorphic ferrite, WF – Widmanstätten ferrite, and F – Equiaxed ferrite.

4.10 HV1. Sample B (Fig. 4a) is largely comprised of equiaxed ferritic grains with trace amounts of pearlite at the grain boundaries. The average grain size and hardness at this location were found to be $4.03 \pm 4.30 \mu\text{m}$ and $168.60 \pm 4.85 \text{ HV1}$, respectively. Sample A2 (Fig. 4a) was similar in microstructure to sample B, with remnant acicular ferrite grains also observed, indicating a lack of transformation time during welding.

The average grain size and hardness at this location were found to be $5.39 \pm 4.21 \mu\text{m}$ and $168.65 \pm 5.39 \text{ HV1}$, respectively. Sample A1 (Fig. 4a), taken from zone Z4 of the weld, was largely comprised of acicular ferrite with allotriomorphic ferrite found along the prior austenitic grain boundaries.

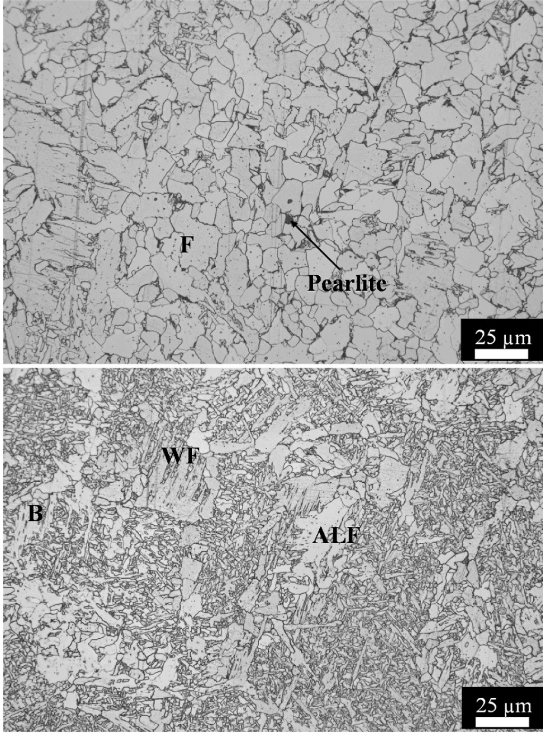


Fig. 4d. Optical micrographs (25 μm scale) of WAAM built parts using G4Si1 welding wire for M1E2. Micrographs reported along wall height from top to bottom (sample C1 and C2). Phases identified: AF – Acicular ferrite, ALF – Allotriomorphic ferrite, WF – Widmanstätten ferrite, and F – Equiaxed ferrite.

In addition, Widmanstätten ferritic grains were observed at the grain boundaries of allotriomorphic ferrite as shown in Fig. 4b. The grains in this region have an average hardness value of 191.90 ± 9.45 HV1 and average grain size of 3.21 ± 2.90 μm.

The hardness of the material increases (~20 HV1) as we move from zone Z3 to zone Z4. The increase in hardness at the top of the wall (sample A1) can be associated with the variation in constituent phases and smaller grain sizes compared to sample A2. In addition, the top of the wall experiences fewer reheating and cooling cycles, limiting recrystallization and the number of phase transformations in the region. From the microstructure and hardness characterization for experimental wall M1E1, it was seen that the material becomes softer as we move from zone Z1 to zone Z3, with an increase in average grain size. The microstructure phase analysis (Fig. 4c and d) for wall M1E2 showed a similar phase structure to that of M1E1, but with increased ferritic grain sizes. It was seen that the higher energy printing parameters (M1E2) resulted in a wall with lower hardness than M1E1. Though the trends for cooling rate, hardness, and grain size for M1E2 were similar to M1E1, microstructure analysis found a small fraction of bainitic structures in the C2 (Fig. 4d) sample close to the base plate. The resulting microstructure phases, grain sizes, and mechanical properties for the experiments are presented in Table 3.

Similar to G4Si1, the walls printed using AM70 steel alloy exhibit distinctive microstructural variations as a result of layer-by-layer deposition (Fig. 5a–d). The walls produced using AM70 (M2E1 and M2E2), resulted in a fine-grained steel consisting of ferrite, martensite, and bainite, along with trace amounts of oxide inclusions. The grain sizes of walls printed using AM70 were smaller than their G4Si1

Table 3

Microstructure and mechanical property results for G4Si1 and AM70 deposits.

Tested Sample	HV1	Grain Size (μm)	YS (MPa)	UTS (MPa)	% e	Phase
M1E1-A1	191.90 ± 9.45	3.21 ± 2.90	447.20 ± 0.78	628.35 ± 17.78	31%	Acicular ferrite with traces of Widmanstätten and allotriomorphic ferrite
M1E1-A2	168.65 ± 5.39	4.21 ± 3.92				Equiaxed ferrite, remanent acicular ferrite, traces of pearlite and bainite
M1E1-B	168.60 ± 4.85	4.03 ± 4.30				Equiaxed ferrite and traces of pearlite
M1E1-C1	173.55 ± 4.10	5.61 ± 3.15				Equiaxed ferrite and pearlite, allotriomorphic ferrite, remanent acicular ferrite, and traces of bainite
M1E1-C2	248.25 ± 28.27	2.46 ± 1.95				Acicular ferrite and traces of Widmanstätten, allotriomorphic ferrite and bainite
M1E2-A1	165.25 ± 11.92	4.55 ± 4.83	395.55 ± 1.62	605.00 ± 10.60	41%	Acicular ferrite with traces of Widmanstätten and allotriomorphic ferrite
M1E2-A2	155.10 ± 3.26	5.40 ± 4.78				Equiaxed ferrite, remanent acicular ferrite, traces of pearlite and bainite
M1E2-B	155.15 ± 2.16	5.38 ± 4.58				Equiaxed ferrite with trace amounts of pearlite
M1E2-C1	170.45 ± 6.00	3.92 ± 2.34				Equiaxed ferrite and pearlite, allotriomorphic ferrite, remanent acicular ferrite, and traces of bainite
M1E2-C2	190.5 ± 10.63	2.79 ± 2.07				Bainite, acicular ferrite and traces of Widmanstätten and allotriomorphic ferrite
M2E1-A1	311.00 ± 26.18	2 ^a	771.82 ± 0.84	932.96 ± 28.67	25%	Acicular ferrite and bainite
M2E1-A2	271.55 ± 7.58					Bainite and acicular ferrite
M2E1-B	271.45 ± 9.56					Bainite, acicular ferrite, and martensite
M2E1-C1	286.90 ± 11.03					Bainite and acicular ferrite
M2E1-C2	339.17 ± 15.34					Bainite and martensite
M2E2-A1	305.30 ± 9.30	2-3 ^a	707.58 ± 3.53	943.34 ± 9.98	28%	Acicular ferrite and bainite

(continued on next page)

Table 3 (continued)

Tested Sample	HV1	Grain Size (μm)	YS (MPa)	UTS (MPa)	% e	Phase
M2E2-A2	266.50 \pm 10.62					Bainite and acicular ferrite
M2E2-B	244.95 \pm 7.96					Bainite, acicular ferrite, and martensite
M2E2-C1	281.95 \pm 12.45					Bainite and acicular ferrite
M2E2-C2	346.25 \pm 24.07					Bainite and martensite

^a Obtained using manual measurement following ASTM E112.

counterparts, averaging at 2–3 μm throughout the part.

AM70 material showed overall higher hardness and strength compared to G4Si1. For sample C2 (Fig. 5b) in M2E1, the microstructure was largely composed of bainite and martensite. The hardness at the bottom of the wall was measured to be 339.17 ± 15.34 HV1. The large variability in the hardness at this location is due to the rapidly changing cooling rate at the bottom of the wall.

As the height of the wall increases to zone Z2, the microstructure of sample C1 (Fig. 5b) is similar to that of C2, comprised of bainite and acicular ferrite in a weave basket pattern with average hardness of 286.90 ± 11.03 HV1. Sample B (Fig. 5a) taken at the intersection of zones Z2 and Z3 is largely comprised of lower bainite, upper bainite, acicular ferrite, and martensite with an average hardness of 271.45 ± 9.56 HV1. Sample A2 (Fig. 5a) was comprised of bainite and acicular ferrite, exhibiting an average hardness of 271.55 ± 7.58 HV1. Sample A1 (Fig. 5a) was found to be largely comprised of acicular ferrite and bainite. The hardness in this region was 311.00 ± 26.18 HV1. The increase in hardness at the top of the wall can be associated with fewer heating and cooling cycles resulting in more harder phases in the microstructure, as observed in the experiments using G4Si1 steel alloy.

The microstructure analysis for M2E2 (Fig. 5c and d) showed a similar phase structure to M2E1. It was seen that the higher energy printing parameters (M2E2) resulted in a wall with lower hardness than M2E1. The trends for cooling rate, hardness, and grain size were observed to be the same for M2E1 and M2E2. The only difference in microstructural phases was seen in prior austenite grains observed through EBSD analysis. It was observed that prior austenite grains were polygonal with parameter set M2E1, while prior austenite grains were columnar using parameter set M2E2, as shown in Fig. 6a and b, respectively.

The higher energy parameter set (M2E2) normalized the columnar grains and increased the sub-grain size. The variation of hardness along the build direction for both materials (all parameter combinations) is shown in Fig. 7. From the figure, it is seen that the hardness is uniform through the part, with a slight increase at the bottom and top of the printed walls.

Following the optical microscopy of the hardness samples, tensile specimens cut along the build direction (vertical) and nozzle travel direction (horizontal) were tested. For both materials, the strength did not vary with orientation of the tensile specimen (horizontal and vertical) implying that mechanical properties favor isotropy in WAAM-CMT. The wall with parameter combination M1E1 showed higher YS (447.20 MPa), UTS (628.35 MPa), and lower elongation at failure (31%) than the wall built using parameter set M1E2 (395.55 MPa, 605 MPa, and 41%, respectively). The samples from wall M1E2 experienced greater elongation (~5% higher strain) than M1E1. The M1E2 specimens experienced higher heat input per layer and a slower cooling rate than M1E1, resulting in specimens with lower hardness and higher ductility, but with slightly lower strength. The difference in average UTS between the

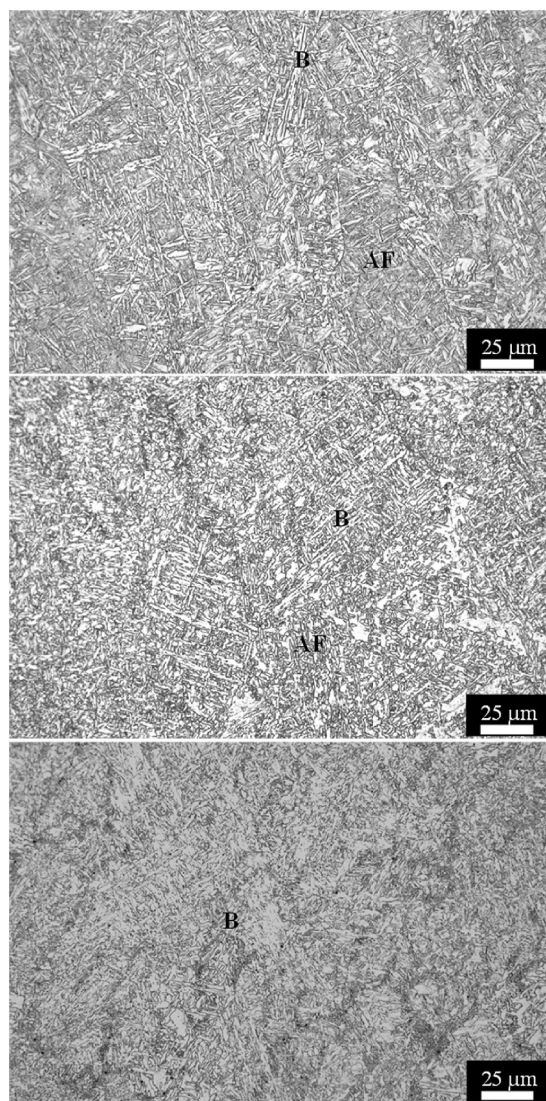


Fig. 5a. Optical micrographs (25 μm scale) of WAAM built parts using AM70 welding wire for M2E1. Micrographs reported along wall height from top to bottom (samples A1, A2, and B). Phases identified: AF – Acicular ferrite, and B – Bainite.

two parameter sets (M1E1 and M1E2) was found to be 15 MPa.

The measured YS, UTS, and % elongation values for parameter sets M1E1 and M1E2 are reported in Table 3, and the true stress strain curves for the two parameter sets tested for material G4Si1 in shown in Fig. 8. For the AM70 alloy, specimens from the lower weld energy parameter set M2E1 exhibited higher YS (771.82 MPa), lower UTS (932.96 MPa), and lower elongation (25%) than the wall using parameter set M2E2 (707.58 MPa, 943.34 MPa, and 28%, respectively).

The measured YS, UTS, and % elongation values for parameter sets M2E1 and M2E2 are shown in Table 3, and the true stress strain curves for the two parameter sets tested for material AM70 in shown in Fig. 8. The findings indicate that lower energy input results in higher YS and

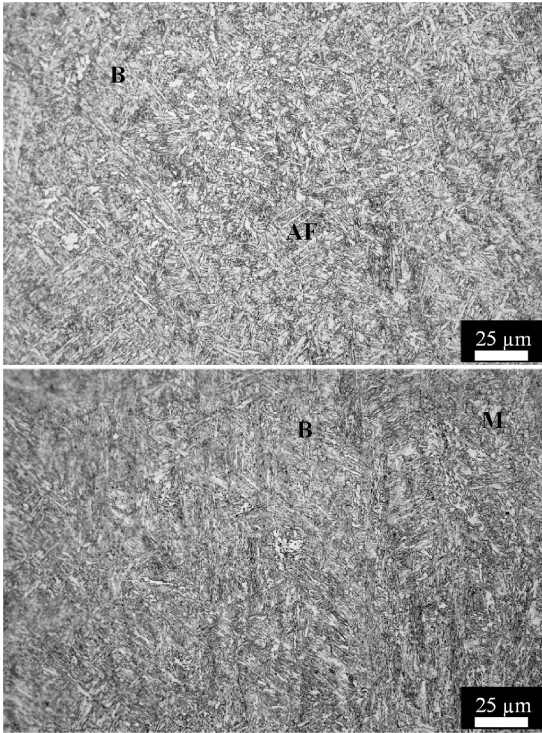


Fig. 5b. Optical micrographs (25 μm scale) of WAAM built parts using AM70 welding wire for M2E1. Micrographs reported along wall height from top to bottom (samples C1 and C2). Phases identified: AF – Acicular ferrite, B – Bainite, and M – Martensite.

UTS for both materials. However, the ductility of both materials increased when printing using the higher energy input parameters.

4. Discussion and validation

Microstructural characterization for the two steel alloys (G4Si1 and AM70) showed presence of acicular ferrite, bainite, equiaxed ferrite, Widmanstätten ferrite, allotriomorphic ferrite phases, and pearlite. In addition, martensite was also formed in the AM70 welds. The fraction of each of these microstructure phases identified influences the mechanical properties observed during testing of the welds. Acicular ferrite is a desired phase in inoculated steels due to its influence on the overall toughness of the material. Acicular ferrite grains are usually formed at intragranular nucleation sites formed at inclusions. Similar to bainite, which nucleates at austenite grain boundaries and grow inwards as sheaves or plates, transformation to acicular ferrite occurs below the bainite start temperature. The growth of acicular ferrite phase over bainite may be favored based on the prior austenite grain size and inclusion density in the alloy used for printing [18]. In addition, the presence of Widmanstätten ferrite and allotriomorphic ferrite along prior austenite grain boundaries have been seen to favor acicular ferrite growth over bainite. The increased amount of acicular ferrite grains may be favored in applications where higher ductility is warranted. Similar to acicular ferrite, the presence of bainite may also bring good strength to ductility performance but with higher hardness. Widmanstätten ferrite structures generally possess higher hardness due to a higher phase boundary area where dislocations at short distances may be hindered resulting in an increase in the hardness. In addition, microcracks

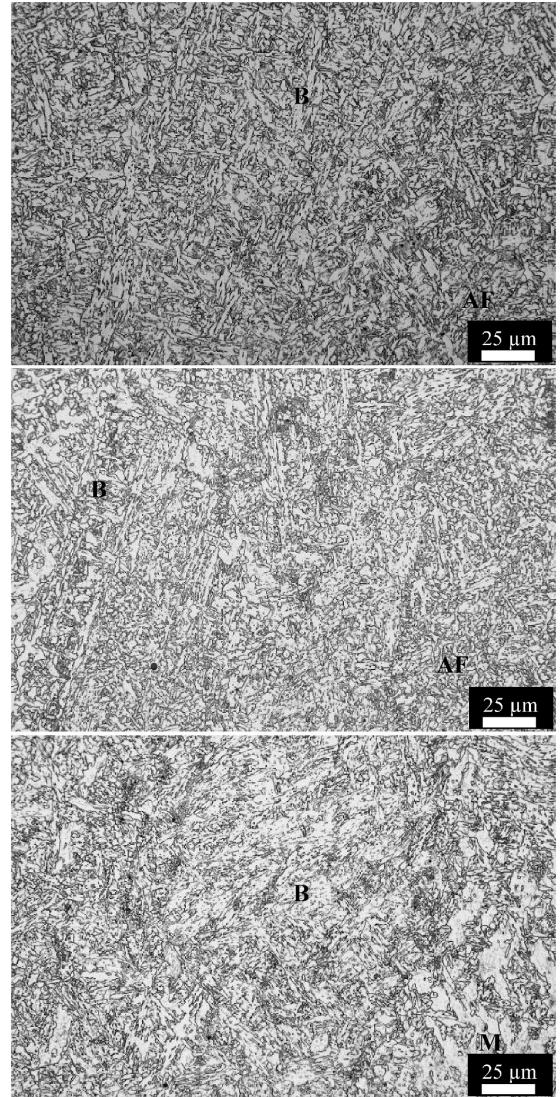


Fig. 5c. Optical micrographs (25 μm scale) of WAAM built parts using AM70 welding wire for M2E2. Micrographs reported along wall height from top to bottom (samples A1, A2, and B). Phases identified: AF – Acicular ferrite, B – Bainite, and M – Martensite.

are common in Widmanstätten ferrite which can limit the impact strength of the material and thus, only preferable in select applications. A high cooling rate can result in an increase in Widmanstätten ferrite since it provides less time for ferrite nucleation sites. Pearlite on the other hand forms when the material is slowly cooled from the austenitizing temperature for steels. Pearlites are generally lamellar with alternating layers of ferrite and cementite and are formed in steels with lower than eutectoid carbon content ($\sim 0.75\text{--}0.85$ wt % of carbon). The presence of pearlite can increase hardness, strength, and ductility of steels, but can have a detrimental effect on the toughness properties of the material. Finally, martensite structures are generally the hardest and strongest phase in steel alloys but also constitute the most brittle

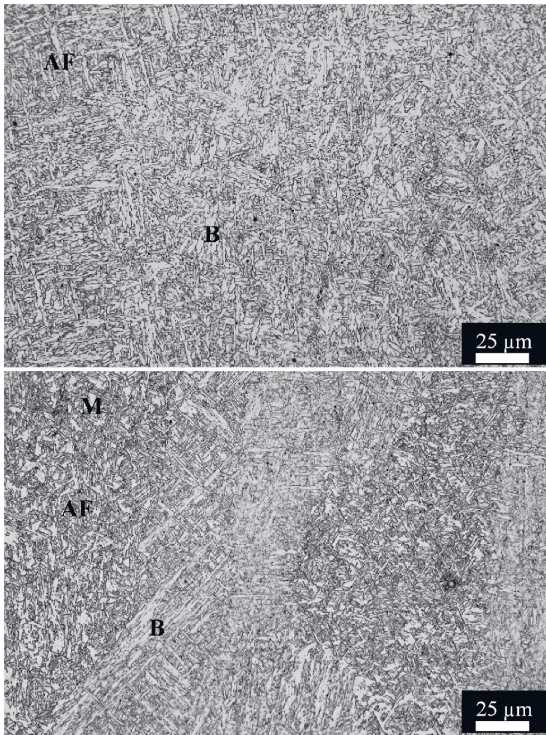


Fig. 5d. Optical micrographs (25 μm scale) of WAAM built parts using AM70 welding wire for M2E2. Micrographs reported along wall height from top to bottom (samples C1 and C2). Phases identified: AF – Acicular ferrite, B – Bainite, and M – Martensite.

structure [18].

The SEM micrographs for G4Si1 welds (both process parameter settings) indicated the presence of allotriomorphic ferrite and Widmanstätten ferrite phases along the prior austenite grain boundaries at the bottom (Zone Z4) and top (Zone Z1) zones of the part as shown in Fig. 9a. Thus, G4Si1 welds exhibited a higher percentage of acicular ferrite phase in their microstructure than bainite. Additionally, the higher energy input parameters (M1E2) resulted in an increase in the percentage of equiaxed ferrite, acicular ferrite, and pearlite phases and also increased the grain sizes in the microstructure (Fig. 9b). The combination of the phases as well as the larger grain sizes resulted in decreasing the hardness, while increasing the ductility of the high

energy input G4Si1 welds without a considerable loss in strength (UTS for M1E2 was 23 MPa less than M1E1). On the other hand, AM70 is a bainitic steel with chromium, manganese, and molybdenum concentrations which may lower the formation of allotriomorphic ferrite in the final microstructure [18]. Hence, the resulting microstructure saw a decrease in the presence of acicular ferrite.

However, it is important to note that, the concentration of acicular ferrite in AM70 was significantly higher than the G4Si1 welds. All four temperature zones in AM70 samples exhibited largely bainitic grains (mean grain size of 2–3 μm) with smaller regions of acicular and martensitic phases.

Martensitic laths were identified in the microstructure of AM70 deposits at the top of the wall and near the base plate (A1 and C2 zones) as shown in Fig. 10. The formation of martensitic laths along the prior austenite grain boundaries can be attributed to the high cooling rates near the base plate and lack of remelting (due to addition of layers of top) at the top of the wall. Acicular ferrite phases can be linked to the

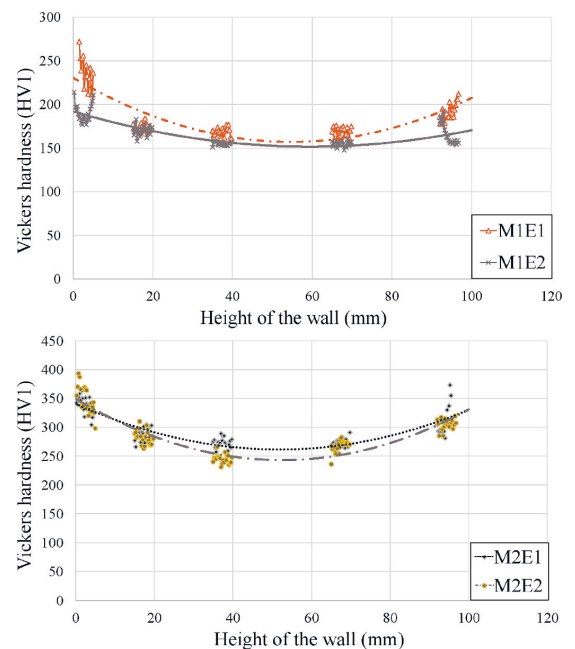


Fig. 7. Microhardness values for G4Si1 (top) and AM70 (bottom) deposits measured along build direction.

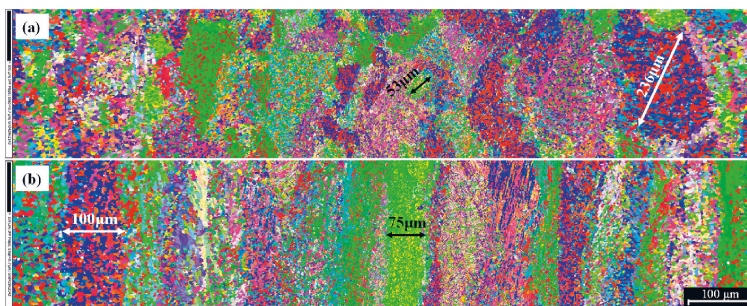


Fig. 6. EBSD scans of AM70 welds with parameter set a) M2E1 and b) M2E2.

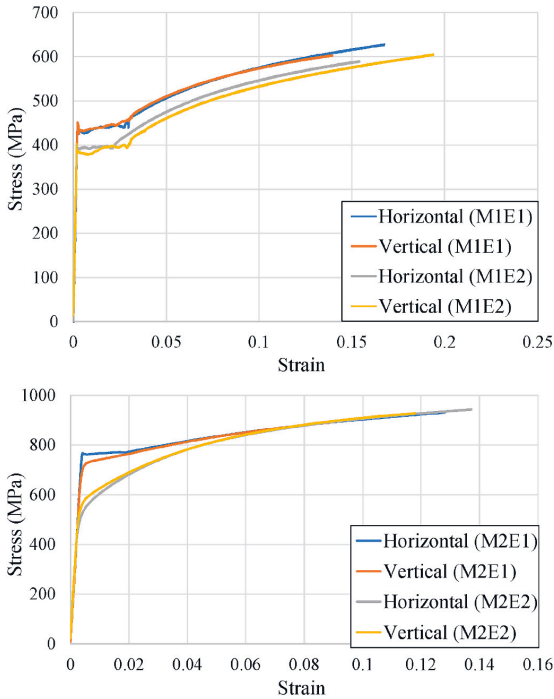


Fig. 8. Stress-strain curve for G4Si1 deposits (top) and AM70 deposits (bottom) characterized in the build (vertical) and travel (horizontal) direction.

presence of microscopic inclusions as seen in the micrographs of AM70 welds (Fig. 4). Similar to G4Si1, the AM70 micrographs show an increase in the fraction of acicular ferrite phase when using higher energy input parameters (M2E2) compared to M2E1, which slightly increased ductility and strength.

This performance improvement can be associated with the largely bainitic microstructure of AM70 welds. Specimens for both process parameter settings (M2E1 and M2E2) resulted in similar UTS (~930 MPa for M2E1 and ~940 MPa for M2E2). However, despite having similar UTS, the YS for M2E1 and M2E2 have a difference of 70 MPa (~10%), indicating that M2E1 is more brittle. The microstructural phases obtained for AM70 are in accordance with prior research investigating HSLA steels, where in the major constituents were ferrite and bainite phases [10,19]. Further, the small grain size and presence of bainite (Fig. 11) and acicular ferrite throughout the sample contributed to higher hardness, UTS, and YS, but lower ductility than G4Si1 samples. The relative lower ductility of AM70 may be associated with the large number of fine inclusions found throughout the welded microstructure which can aggravate microcracks and their propagation in the weld. The hardness and strength of fully bainitic microstructures decrease during tempering; this change is more evident in high strength steels. The repeated heating and cooling cycles in the WAAM process results in a non-uniform tempering of the printed part. Consequently, a clear variation in the microstructure and mechanical properties can be seen due to the layer-by-layer building approach. For printing WAAM parts with uniform microstructure, reducing or eliminating the need for stress relief heat treatment requires understanding the variation in microstructure caused by process-related thermal phenomena. Capturing data related to changes in cooling rates and wait times as a function of part height can help create computational models which can enable process tuning and optimization.

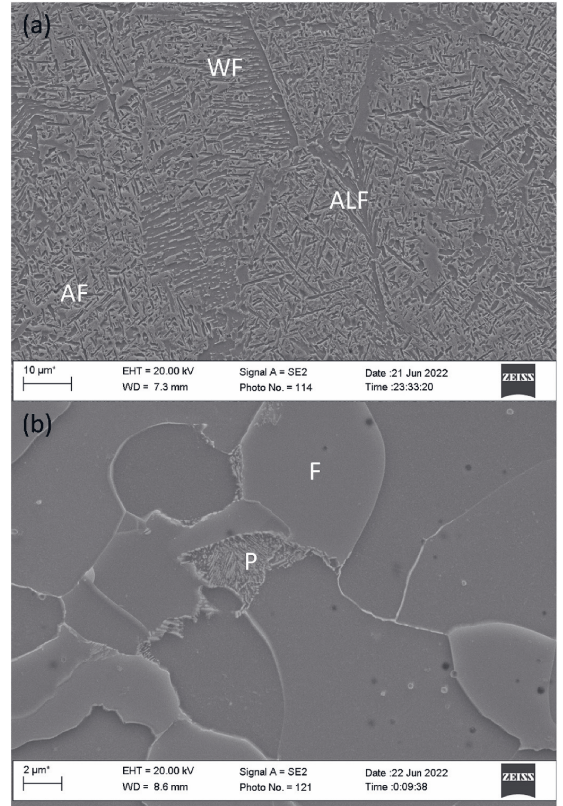


Fig. 9. SEM micrographs of G4Si1 deposits for M1E1 (top) and M1E2 (bottom); (a) AF- acicular ferrite, WF- Widmanstätten ferrite, and ALF- allotriomorphic ferrite, (b) P- pearlite and F- equiaxed ferrite.

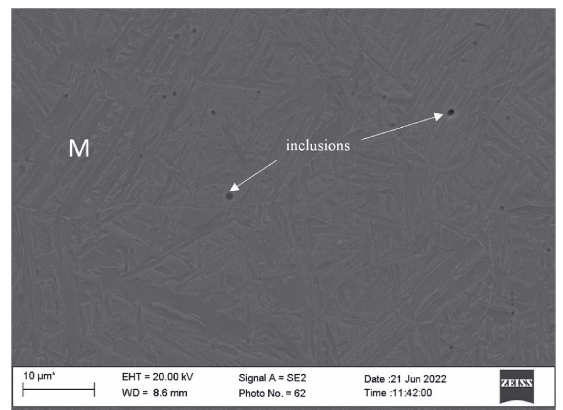


Fig. 10. SEM micrographs of AM70 deposits for M2E1 with martensite (M) laths.

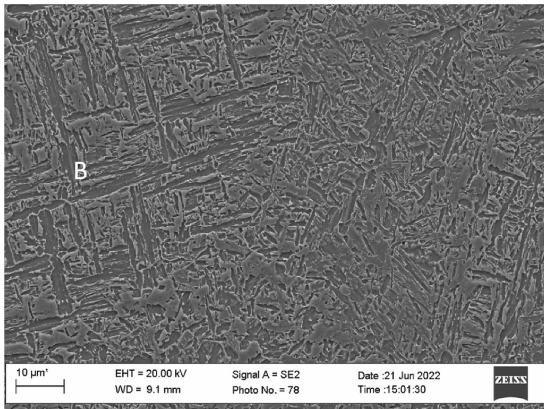


Fig. 11. SEM micrographs of AM70 deposits for M2E1 with bainite (B).

5. Conclusions and future work

Thin walls ($160 \times 100 \times 5$ mm) of mild steel (G4Si1) and high-strength, low-alloy steel (AM70) were fabricated using WAAM-CMT. A fixed travel speed and two different sets of wire feed rates and interpass temperatures were employed, resulting in four walls for subsequent microstructural analysis and mechanical testing. Microstructural evolution (using an optical microscope, SEM, and EBSD scans) and mechanical properties (i.e., YS, UTS, and %e) were investigated (in the horizontal and vertical directions of material deposition) to better understand the associated influence of thermal cycles of layer-by-layer deposition.

From these investigations, the following observations were made:

- Based on observed phenomena, four different temperature zones were identified, which are characterized by differences in cooling rate, wait time between layers, and number of reheating cycles.
- Cooling rate decreases as the height of the part increases until it reaches a steady state value. The decrease in cooling rate leads to an increase in wait time between layers as the height of the part increases.
- Lower heat input resulted in higher YS and UTS and lower uniform strain.
 - YS and UTS increased by 13% and 3.8%, respectively, in G4Si1 steel deposits with the lower energy input parameters (M1E1) than with higher energy input parameters (M1E2).
 - YS increased by 9% in AM70 steel deposits with the lower energy input parameters (M2E1) than with higher energy input parameters (M2E2). However, in case of UTS the lower energy input parameters (M2E1) saw a 1% decrease compared to high energy input parameter (M2E2).
 - Percentage elongation at failure was 10% and 3% lower in G4Si1 and AM70 deposits respectively, for printing with lower energy input parameters (M1E1 and M2E1) than with higher energy input parameters (M1E2 and M2E2).
- Higher energy input parameters resulted in increased ductility and reduced hardness for both materials.
- Owing to a lack of significant anisotropy in G4Si1 deposits due to an equiaxed grain structure, the mechanical properties in the travel direction showed negligibly higher UTS (0.38%) than the samples taken in the build direction. A similar trend was observed for AM70 (increases of 2.7% and 0.24% in YS and UTS, respectively).
- Even though energy input varied for both materials for the different parameter sets, no significant microstructural changes were observed across the parameter sets for G4Si1, though energy input

variation had a significant influence on the material microstructure for AM70. Prior austenite grains were equiaxed/polygonal for M2E1, while they were columnar for M2E2. Higher heat input settings normalized the columnar grains, increasing the sub-grain size. The observed microstructures for M2E1 and M2E2 were comprised of similar phases (i.e., ferrite + bainite + martensite + inclusions).

- Smaller grain sizes due to higher solidification rates and limited grain growth in lower energy input parameter sets (M1E1 and M2E1) resulted in higher YS and hardness in both alloys. Since grain boundaries play an essential role in resisting dislocation movement in polycrystalline materials, the observed mechanical property trends are attributed to the presence of more grain boundaries in samples printed using lower energy input parameters.

The work herein will support development of models capable of characterizing the process parameter-process physics-property relationships for a family of steels. Specifically, graph-based modeling and machine learning approaches are being investigated to combine knowledge from different domains into one integrated system model.

CRedit authorship contribution statement

Suraj Panicker: Conceptualization, Methodology, Software, Validation, Formal analysis, Investigation, Writing – original draft, Writing – review & editing. **Hari P.N. Nagarajan:** Methodology, Validation, Formal analysis, Investigation, Data curation, Writing – original draft, Writing – review & editing, Visualization. **Jari Tuominen:** Validation, Formal analysis, Investigation, Resources, Writing – review & editing. **Madan Patnamsetty:** Validation, Formal analysis, Investigation, Writing – review & editing. **Eric Coatanéa:** Writing – review & editing, Supervision, Project administration. **Karl R. Haapala:** Writing – review & editing, Visualization, Supervision.

Declaration of competing interest

The authors declare that they have no known competing financial interests or personal relationships that could have appeared to influence the work reported in this paper.

Data availability

Data will be made available on request.

Acknowledgements

The authors acknowledge the support from Jaakko Kotiranta and Merja Ritola from the Automation Technology and Mechanical Engineering Lab at Tampere University for their assistance in the machining and preparation of metallographic and mechanical specimens for material testing.

References

- [1] F42 Committee, Standard Guide for Directed Energy Deposition of Metals, ASTM International, Sep. 2016, <https://doi.org/10.1520/F3187-16>.
- [2] D. Ding, Z. Pan, D. Cuiuri, H. Li, Wire-feed additive manufacturing of metal components: technologies, developments and future interests, *Int. J. Adv. Manuf. Technol.* 81 (1–4) (Oct. 2015) 465–481, <https://doi.org/10.1007/s00170-015-7077-3>.
- [3] B. Wu, et al., A review of the wire arc additive manufacturing of metals: properties, defects and quality improvement, *J. Manuf. Process.* 35 (Oct. 2018) 127–139, <https://doi.org/10.1016/j.jmapro.2018.08.001>.
- [4] W. Jin, C. Zhang, S. Jin, Y. Tian, D. Wellmann, W. Liu, Wire arc additive manufacturing of stainless steels: a review, *Appl. Sci.* 10 (5) (Jan. 2020), <https://doi.org/10.3390/app10051563>. Art. no. 5.
- [5] M.R. Jandaghi, A. Saboori, L. Iuliano, M. Pavese, On the effect of rapid annealing on the microstructure and mechanical behavior of additively manufactured stainless steel by Laser Powder Bed Fusion, *Mater. Sci. Eng. A* 828 (Nov. 2021) 142109, <https://doi.org/10.1016/j.msea.2021.142109>.

- [6] T.A. Rodrigues, V. Duarte, R. Miranda, T.G. Santos, J. Oliveira, Current status and perspectives on wire and arc additive manufacturing (WAAM), *Materials* 12 (7) (2019) 1121.
- [7] X.L. Wang, et al., Effect of interpass temperature on the microstructure and mechanical properties of multi-pass weld metal in a 550-MPa-grade offshore engineering steel, *Weld. World* 61 (6) (Nov. 2017) 1155–1168, <https://doi.org/10.1007/s40194-017-0498-x>.
- [8] L. Sun, F. Jiang, R. Huang, D. Yuan, C. Guo, J. Wang, Microstructure and mechanical properties of low-carbon high-strength steel fabricated by wire and arc additive manufacturing, *Metals* 10 (2) (Feb. 2020), <https://doi.org/10.3390/met10020216>. Art. no. 2.
- [9] X. Lu, Y.F. Zhou, X.L. Xing, L.Y. Shao, Q.X. Yang, S.Y. Gao, Open-source wire and arc additive manufacturing system: formability, microstructures, and mechanical properties, *Int. J. Adv. Manuf. Technol.* 93 (5) (Nov. 2017) 2145–2154, <https://doi.org/10.1007/s00170-017-0636-z>.
- [10] T.A. Rodrigues, V. Duarte, J.A. Avila, T.G. Santos, R.M. Miranda, J.P. Oliveira, Wire and arc additive manufacturing of HSLA steel: effect of thermal cycles on microstructure and mechanical properties, *Addit. Manuf.* 27 (May 2019) 440–450, <https://doi.org/10.1016/j.addma.2019.03.029>.
- [11] V.N. Lazić, et al., Theoretical-experimental determining of cooling time ($t_{8/5}$) in hard facing of steels for forging dies, *Therm. Sci.* 14 (1) (2010) 235–246.
- [12] A. Lambert-Perlade, T. Sturel, A.F. Gourgues, J. Besson, A. Pineau, Mechanisms and modeling of cleavage fracture in simulated heat-affected zone microstructures of a high-strength low alloy steel, *Metall. Mater. Trans. A* 35 (3) (Mar. 2004) 1039–1053, <https://doi.org/10.1007/s11661-004-0030-y>.
- [13] Lincoln Electric, “G4Si1, Mild Steel, Material Safety Data Sheet.” https://www.lincolnelectric.com/assets/global/Products/Consumable_MIGGMAWires-SuperArc-SuperArcG4Si1/c41025.pdf.
- [14] Böhrler, “3D PrintAM70, low-alloyed, high strength steel, Material Safety Data Sheet.” [https://www.vabw-service.com/documents/boehler/datenblaetter/en/L1_34551_en_3Dprint_AM_70_1H43C006_3367515_EN%20\(1\).pdf?cache=1639059520](https://www.vabw-service.com/documents/boehler/datenblaetter/en/L1_34551_en_3Dprint_AM_70_1H43C006_3367515_EN%20(1).pdf?cache=1639059520).
- [15] B. Mezrag, F. Deschoux-Beaume, M. Benachour, Control of mass and heat transfer for steel/aluminium joining using cold metal transfer process, *Sci. Technol. Weld. Join.* 20 (3) (2015) 189–198.
- [16] S. Ríos, P.A. Colegrove, F. Martina, S.W. Williams, Analytical process model for wire+ arc additive manufacturing, *Addit. Manuf.* 21 (2018) 651–657.
- [17] “Standard Test Methods for Determining Average Grain Size.” <https://www.astm.org/e0112-96e02.html> (accessed Mar. 01, 2022).
- [18] H.K.D.H. Bhadeshia, J. Christian, Bainite in steels, *Metall. Trans. A* 21 (3) (1990) 767–797.
- [19] P. Dirisu, S. Ganguly, A. Mehmanparast, F. Martina, S. Williams, Analysis of fracture toughness properties of wire+ arc additive manufactured high strength low alloy structural steel components, *Mater. Sci. Eng. A* 765 (2019), 138285.

PUBLICATION
V

**Modelling the Geometrical and Mechanical Responses in Wire Arc Additive
Manufacturing: A Concept for Graph Metamodel based Design Space
Exploration**

Hari P.N. Nagarajan, Suraj Panicker, Inigo Flores Ituarte, Eric Coatanéa. and Karl
R. Haapala

Unpublished

Publication reprinted with the permission of the copyright holders.

